Your Guide

FOP 2010
Sept 16 -19

Neotectonics, active faults, fluvial processes, soils, ancient lakes, paleoseismology, tectonic geomorphology, and other stuff in the central Walker Lane....

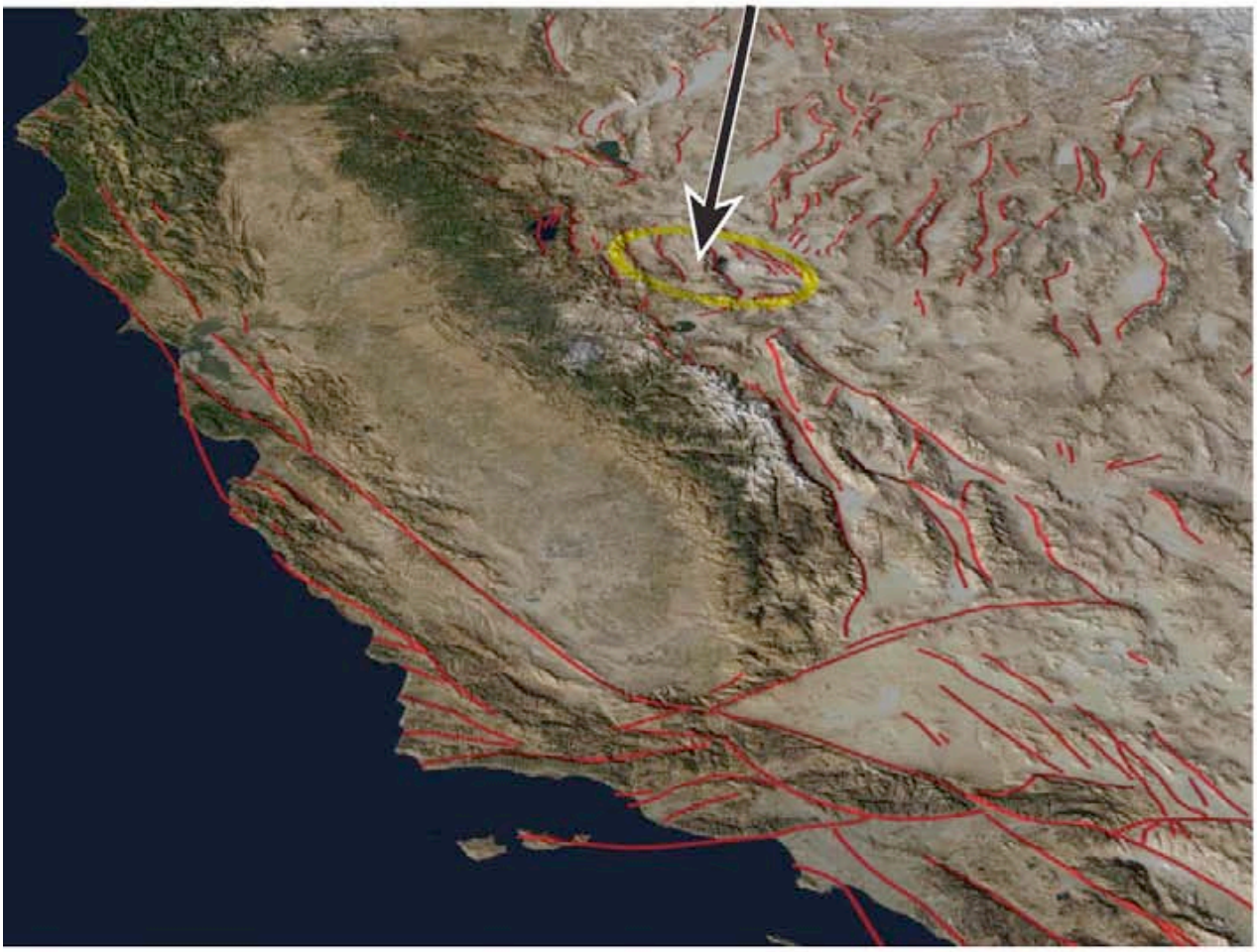

Wassook to Wabooska

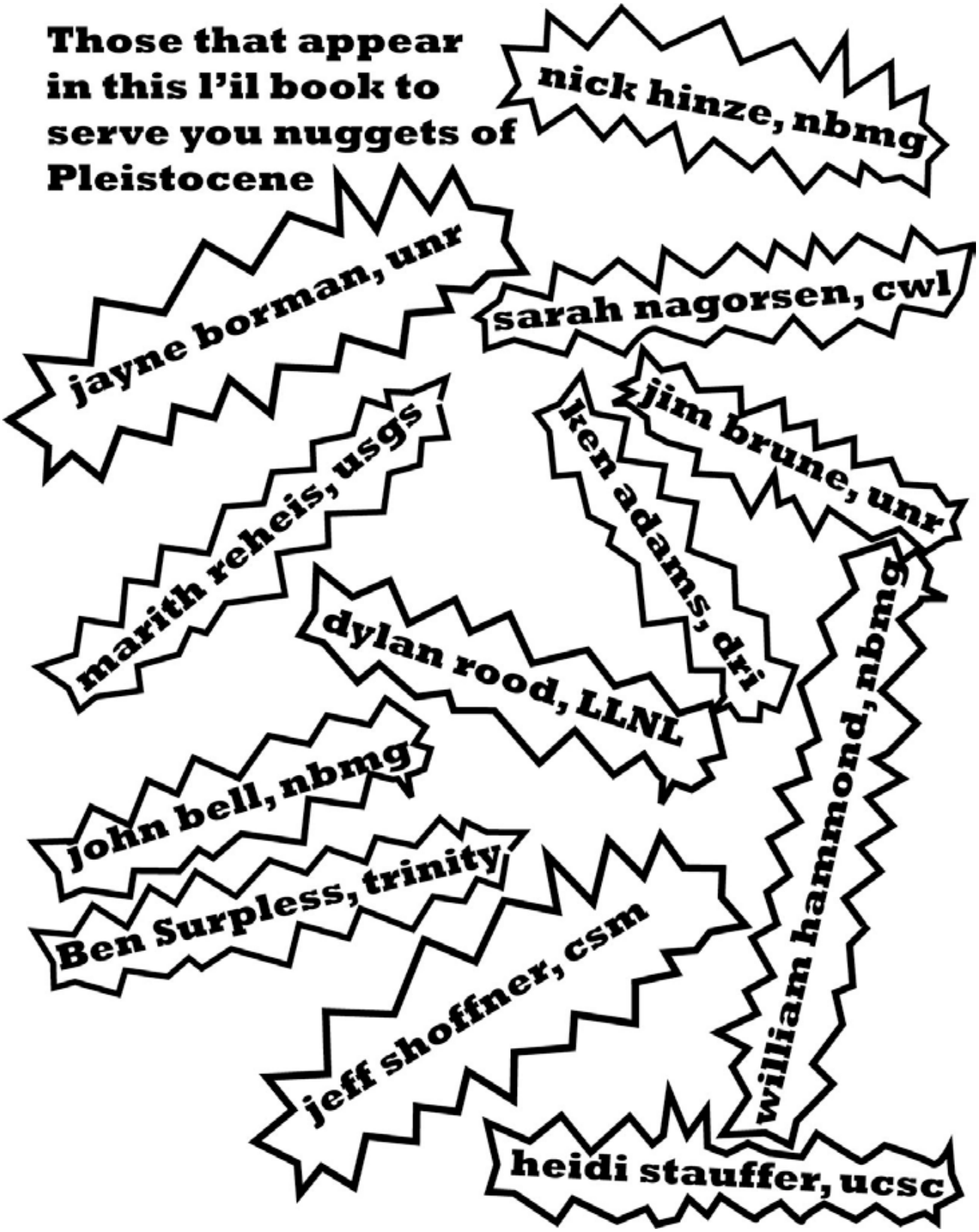
Those that appear in this l'il book to serve you nuggets of Pleistocene
nick hinze, nbmg
jayne borman, unr
sarah nagorsen, cwl
marith reheis, usgs
ken adams, dri
jim brune, unr
dylan rood, LLNL
william hammond, nbmg
john bell, nbmg
Ben Surpless, trinity
jeff shoffner, csm
heidi stauffer, ucsc

Please be sure...

This guide is not proofed

This guide is not edited

This guide does not have a complete reference list

This guide does not have a table of contents

This guide does not exist

This guide will not be televised

This guide does not want to deal with this anymore...

Here's the deal.

Alright everybody. FOP 2010. From Wassook to Wabooska. Got a nice little trip lined up. In a nutshell, we'll meet up on the 16th near the little town of Gabbs which is wouldn't y'know in Gabbs Valley, Nevada. Gabbs is a place; golf course, bar open most of the time, a little grocery whose hours I don't recall, and a restaurant if your are there at the right time (between 8am to 2pm but not on Sun or Mon mind you). We'll awake on the 17th along the Petrified Springs fault, take a look at the boundary of the Walker Lane and Basin and Range, put the place in some geodetic perspective, look at some of the best right-lateral strike-slip tectonic geomorphology to be seen in the central Walker Lane, have the opportunity to put your head in a soil pit, and get started talking about the tectonics of the Walker Lane. From there we'll move on to a midday stop along the Benton Springs fault, another right-lateral one, where you'll all get to do more of the same, and talk a bit about how it all relates to geodetic measures of strain accumulation in the area. Then we'll continue our journey westward through the metropolis of Mina to the north flank of the Excelsior Mtns and Rattlesnake Flat which is pretty much nowhere. Things get flipped there a bit and we'll switch to looking at what the world looks like when it moves left-laterally and conversation will drift toward the dizzying topic of how this particular part of the planet might be spinning around on a vertical axis, whichever one that is. After that, it;'s time to park our butts and get ready for outdoor dinner theatre where we will have the pleasure to see one of the young, well maybe not so young, and upcoming film directors screen his newest hits in the famous Tsunami Ball series including though not limited to 'Tahoe Tsunamis', 'The Jokulaup Destruction of Reno (or thereabouts)', 'The Great Johnstown Flood', and the newest but not least 'Rise and Fall of Lake Wellington' -move over Spielberg.

Waking up from that excitement on the 18th morning we'll take a little drive north to the west flank of the Wassuk Range, start up things with a beautiful view of Walker Lake, continue with a trench across the rangebounding normal fault to view ancient earthquakes, and follow with discussions of ancient Lakes that once was, the uplifting experience of the Wassuk Range, and neotectonics as the new divining rod for finding geothermal energy and solving the world's energy problems (perhaps I exaggerate). Moving north and down to the Walker river delta for a second stop, we'll take an autumnal stroll along the riverbank and through the cottonwoods talking about how to figger how and when the dirt on which one is walking got there, and the ebb and flow of Holocene lake levels. With that, a drive westward across the Wassuks, through Mason Valley, and into Smith Valley will bring us to the home of another rangebounding normal fault and pluvial Lake Wellington, where you'll get a chance to touch those ancient lacustrine muds, crawl around on fault scarps that cross them, think about how and when the ancient Lake got there, postulate how fast the fault is moving, and conjecture in the context of neotectonics and geodesy the role of these normal fault basins in the evolution of the Pacific-North American plate boundary. After that, it is time to call it quits for the day, and as it is my understanding, the evenings festivities will include a small campfire and 3 hours of silent meditation. Of course, there might be an alternative to that too...

Now, for Sunday the 19, we've got a brief little stop to observe some things that might hold clues for folks to ponder regardng the genesis of Lake Wellington, and then move north to Carson City where we will see rocks that may well hold the future of our nations nuclear energy and storage in precarious balance. That's it.

Before You Get There:

There are likely to be some rough sections of road during this endeavor. Though 4-wheel drive isn't a must, GOOD TIRES are and high clearance will lead to a less stressful and uninterrupted drive. It's September, the weather can be anything, but we'll hope for clear warm days and evenings cool enough to warrant a fire. It's a desert. Bring fluids. We'll try and help on that too.

Sept 16 - Getting there:

You can come at this problem from a number of directions. The attached map comes with a few suggestions. Loading up the waypoints on to a handheld GPS could be most useful (download them from the FOP2010 website), particularly if you are arriving in darkness. And as well, like Motel 6, we'll try to keep the light on.

For those coming from the north, you want to gas up in either Hawthorne or Fallon before you get there. There are restaurants and grocery stores in those places as well - they'll be your last chance for awhile. From the south, well, whose coming from the south anyway? But if you must, Mina works, though it's a tad more expensive and the word grocery store is a bit of an exaggeration.

Waypoints can be downloaded directly from the CNS/FOP website in txt format, and should readily be imported into a handheld GPS.

The tab delimited file can be imported into EXCEL or other spreadsheet.

Specific format is that of MacGPS software, so most simple if you own it.

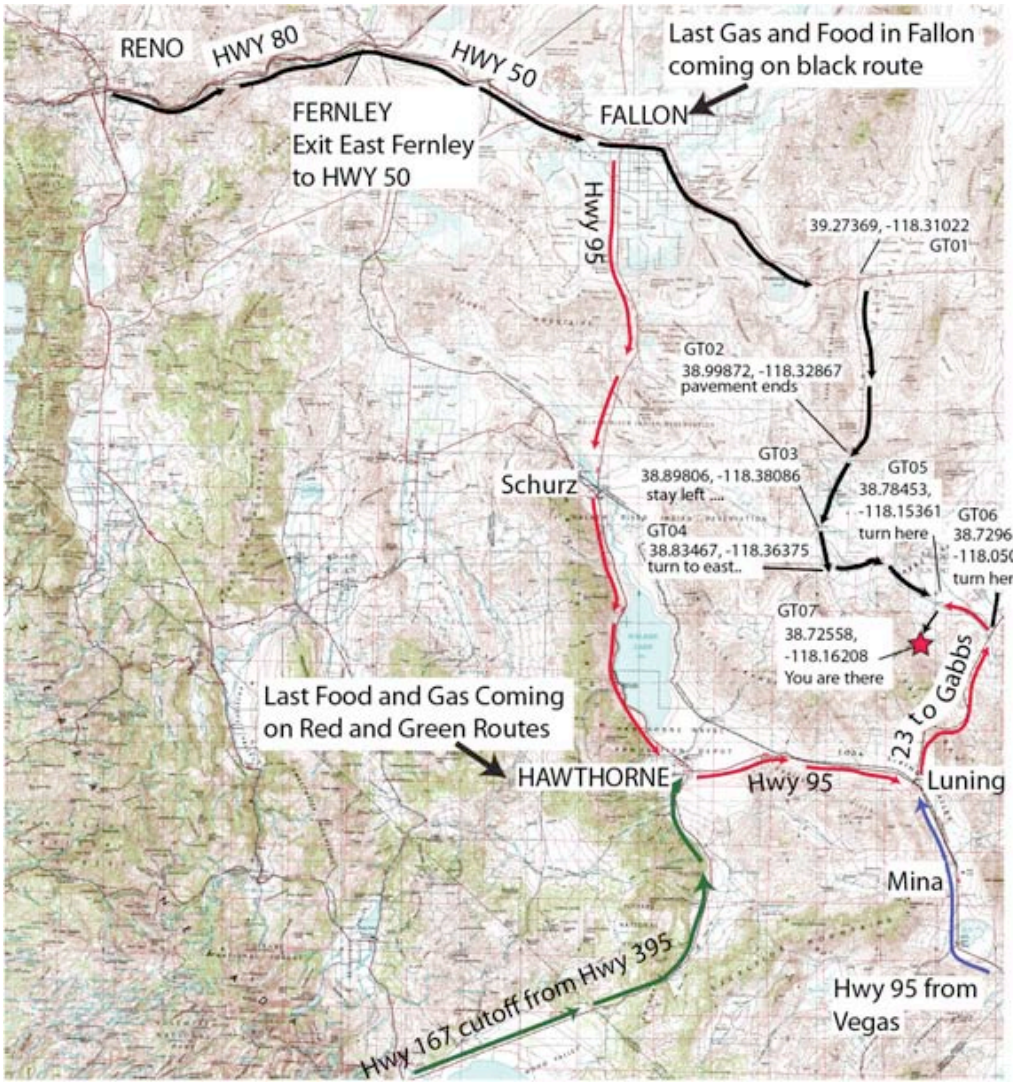

Figure 0-1.

Sept 17 - Friday

The Path to be trodden

Easy, this is where you **wake** up. We'll get started at 4 am to see the sunrise. Well, probably not. But when we do get up we should be standing just about on the Petrified Springs fault. The fault, if you're not a purest and don't get hung up in minutiae (we will later), the fault pretty much marks the contact of the Walker Lane and Basin and Range physiographic provinces. But perhaps it is good to backtrack a bit here and first lay out the path of the day first **(Figure 1-1)** and place our whereabouts in the grander scale of things.

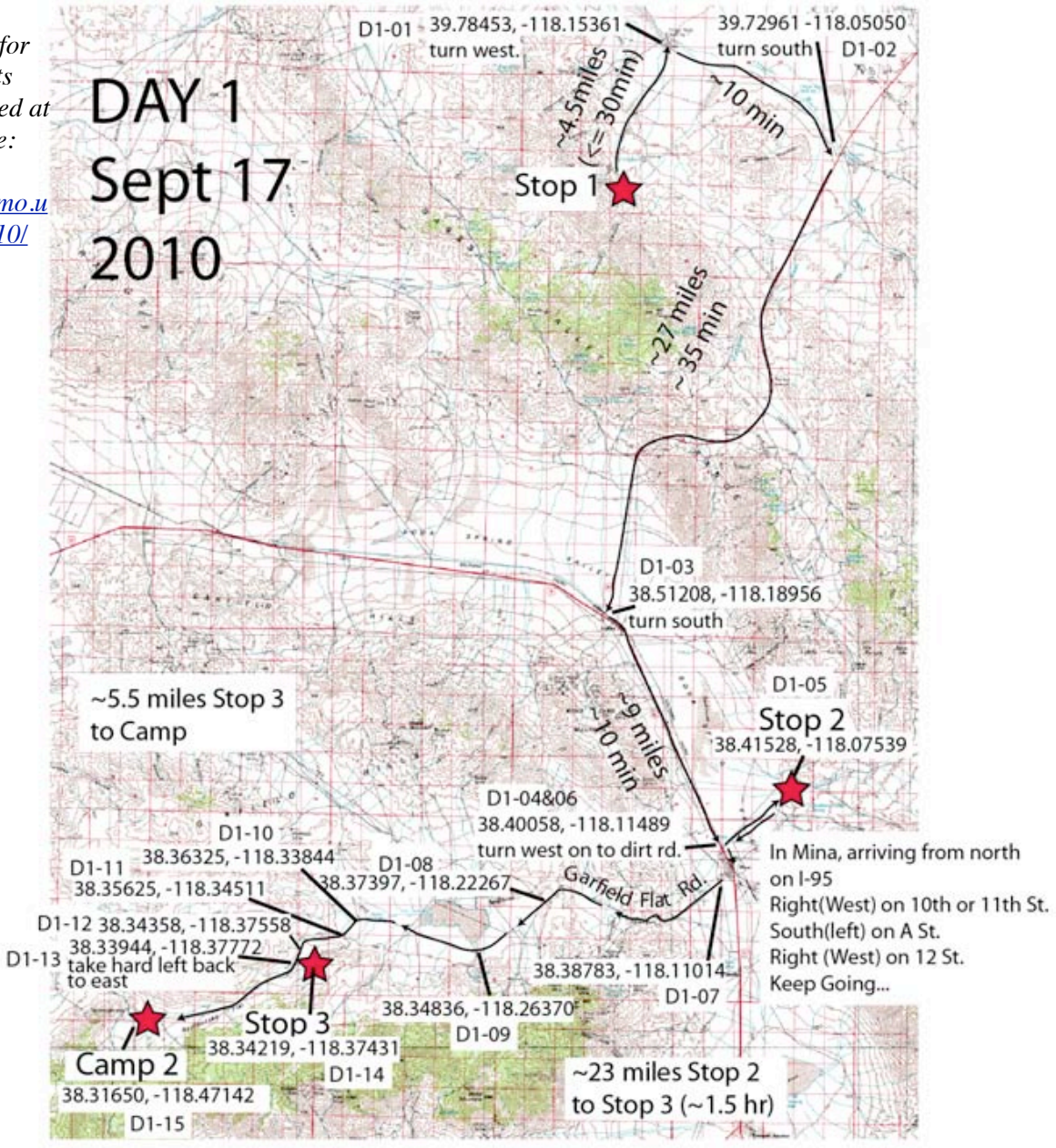

Fig 1-1. Options for arrival. Waypoints can be downloaded at FOP2010 website: http://neotectonics.seismo.unr.edu/0_FOP2010/FOP2010.html

A little Background - The grander scale

Pacific-North American relative right-lateral plate motion of about 50 mm/yr is distributed on faults across the western United States (**Figure 1-2**; , Bennett et al. 2003, Minster & Jordan 1987). Northwest-striking right-lateral faults of the San Andreas fault system take up about 2/3 of the motion, about 33 mm/yr . Most of the remaining transform motion (~10 mm/ry occurs on a similarly trending zone of faults that strikes through the Mojave Desert and bounds the east flank of the Sierra Nevada, which at our latitude is generally referred to around here as the Walker Lane. (Deformation Rates: Bennett et al. 2003, Dixon et al. 1995, Dokka & Travis 1990b, Sauber et al. 1986, Thatcher et al. 1999. Nomenclature: Locke et al. 1940, Billingsley & Locke; 1941, Stewart 1980, Carr 1984, Dokka & Travis 1990b). A yet smaller amount (2-3 mm/yr) is taken up by north-northeast striking normal faults in the Basin and Range, a province that extends about 800 km from the Walker Lane to the Salt Lake city and the Wasatch. **X marks the spot we are standing in Figure 1-2, smack dab on the the boundary between the Walker Lane and the Basin and Range physiographic and structural provinces.**

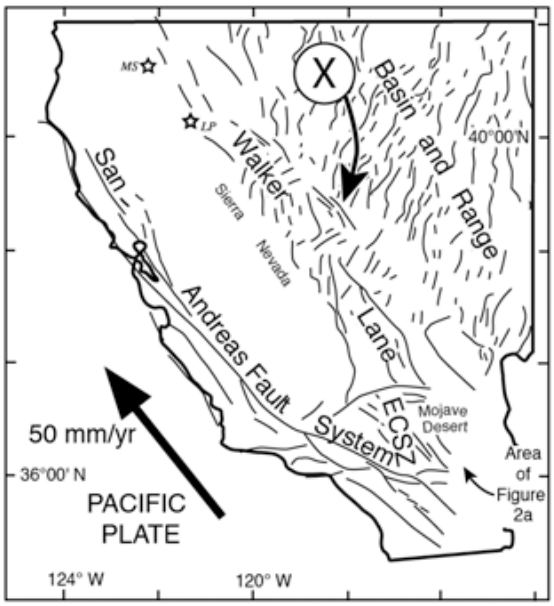

Figure 1-2. X marks the spot (adapted from Wesnousky, 2005).

For history buffs, the earliest accounts of strike-slip faulting east of the Sierra Nevada include Gilberts' (1907) recount of his observations along the 1872 Owens' Valley earthquake fault, Gianella and Callaghan's (1934) description of the 1932 Cedar Mountain earthquake and the mapping of Ferguson and Muller (1949) and Nielsen (1965).

Measures of cumulative right-slip of basement terranes range from about 300 km to 450 km along the southern and northern reaches of the San Andreas fault system, respectively (e.g., Dillon and Ehlig, 1993; James et al., 1993). Cumulative right-slip across the Walker Lane is less, with best estimates ranging around 75-85 km in the south and apparently decreasing to about 30 km in the northern latitudes beyond Reno (Wesnousky, 2005a provides a long-winded, uhmmmm I mean elegant, review of all this) (**Figure 1-3**).

The San Andreas and Walker Lane fault systems also look different (**Figure 1-4)**. The San Andreas system is composed of relatively smooth, curvilinear, and anastomosing fault traces. The Walker Lane is marked by a generally broader and discontinuous set of strike-slip faults. Observations such as these have led to the suggestion that the Walker Lane fault system might provide some insights or analogs to the early structural development of the San Andreas fault system, that the locus of San Andreas plate motion is shifting eastward to the Walker Lane, and that by golly we might even be viewing the birth of a new Transform system (Faulds et al, 2005). Imagine that. And if you were to read the newspapers, you'd might be maybe expect'n it to be happenin' as early as next week!

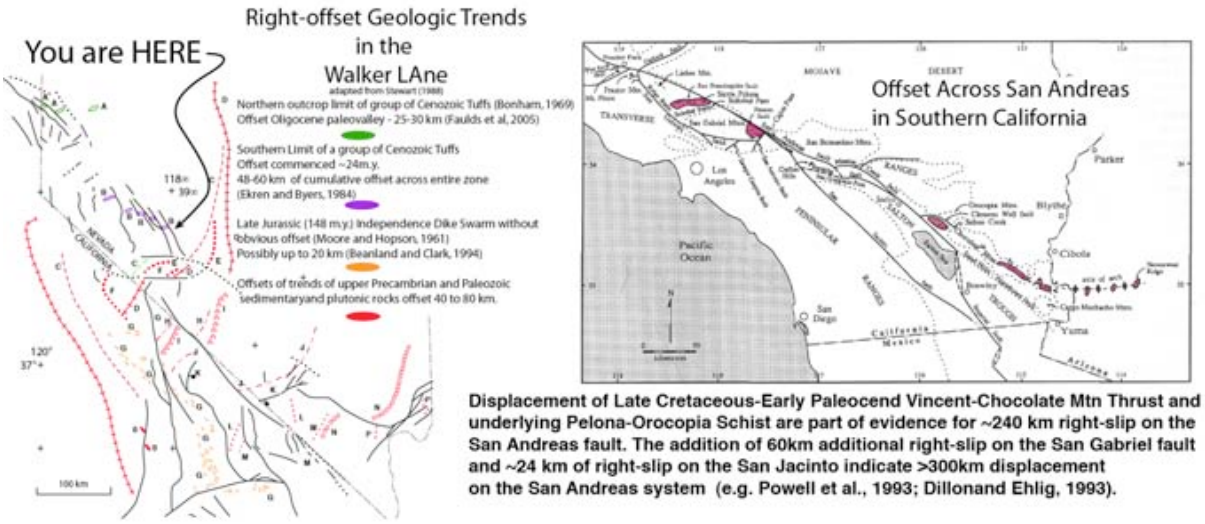

Figure 1-3. Offset rocks and geologic trends across the Walker Lane and San Andreas fault systems.

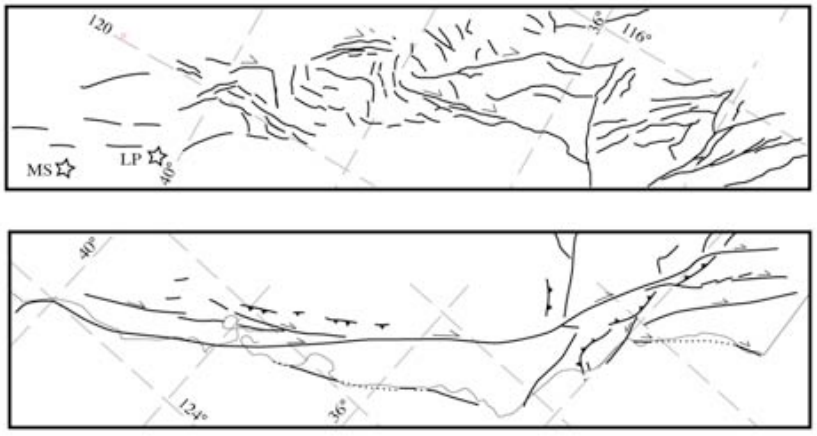

Figure 1-4. Pattern of faulting in Walker Lane (upper) versus San Andreas (lower). Maps rotated for convenience of comparison (which is to say - north is not up on either of the Figures). (adapted from Wesnousky, 2005)

The Local Scale: What you can see from here.

A little look around you and the little **Figures 1-5 & 1-6** below can help visualize things. We are at box 1 on the **Figure 1-5**. This northeast-trending east-facing escarpment that strikes off to the northeast from where we are standing is the Petrified Springs fault scarp. It is considered by some to be a right-lateral fault, and we'll look at that idea a bit more closely down the road. Behind it to the west is the Gabbs Valley Range, oriented with it's long axis to the northwest and parallel to the Petrified Springs fault. The two together impart a northwest 'structural grain' (who thought up that term?) which is typical of Walker Lane physiography: northwest striking right-lateral strike-slip faults and mountain ranges elongated to the northwest (Of course, like everything, it is a bit more complicated than that, but that's good enough for now). Now turn yourself north and eastward and you'll see a number of ranges whose long axes are oriented to the north-northwest. Each is bounded by an active normal fault and each is part of the Basin and Range. Due east and across Gabbs Valley is the Paradise Range. Panning your view to the north you'll then see a thin ridge extending southward into Gabbs Valley - that's the Monte Cristo Range. Then just a bit more to the north and farther in the distance you should be able to see Fairview Peak sticking up above the Monte Cristos. So we are standing right at the boundary of the northwest structural grain of the Walker Lane and the north-northeast structural grain of the Basin and Range. No better place to see it (**Figure 1-6).**

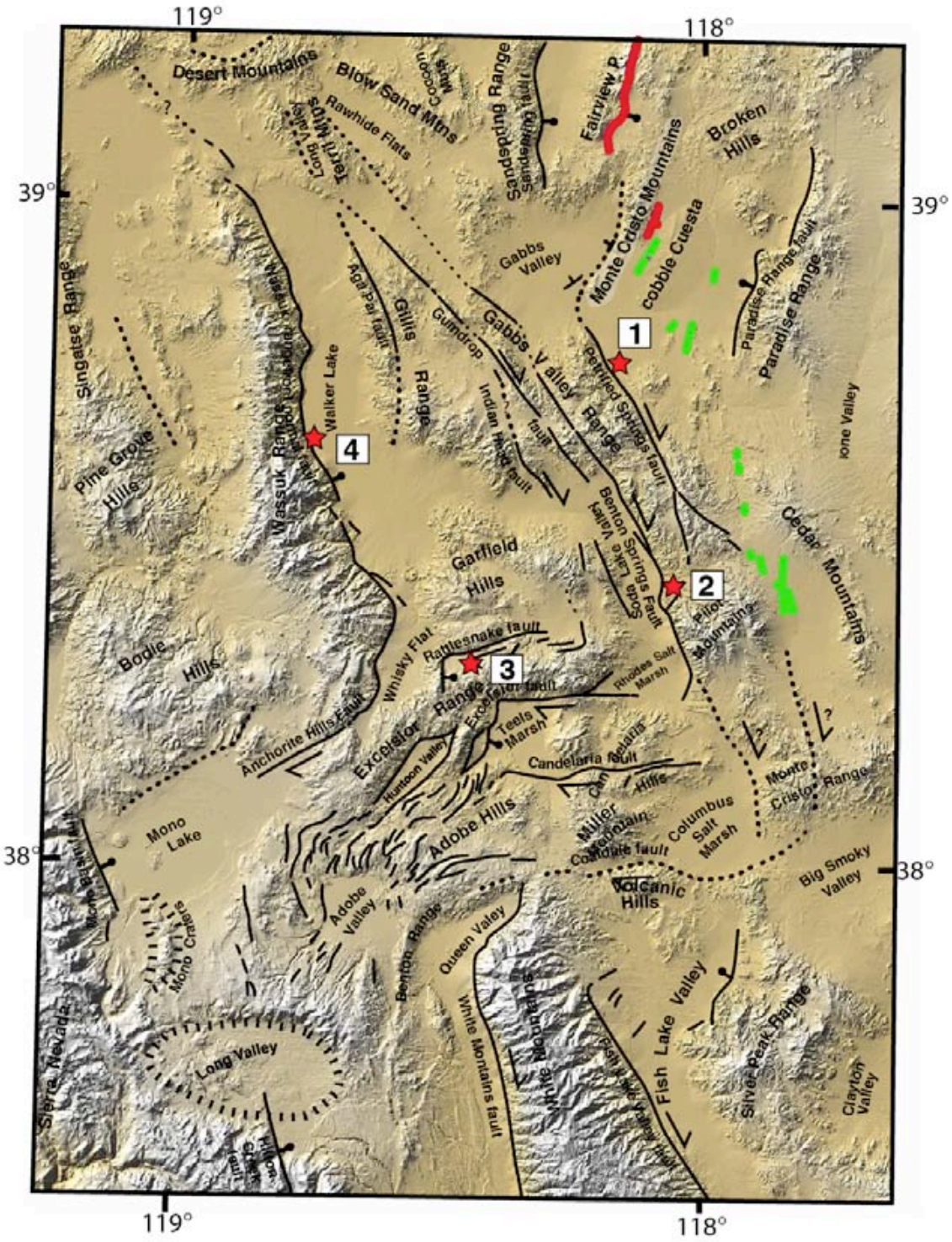

Figure 1-5. Geography & Physiograpy and location of stops 1, 2, 3, & Day 2's stop 4. Surface ruptures of the 1934 Cedar Mtn and 1954 Fairview Peak are in green and red, respectively. See X in Figure 1-3 for regional location

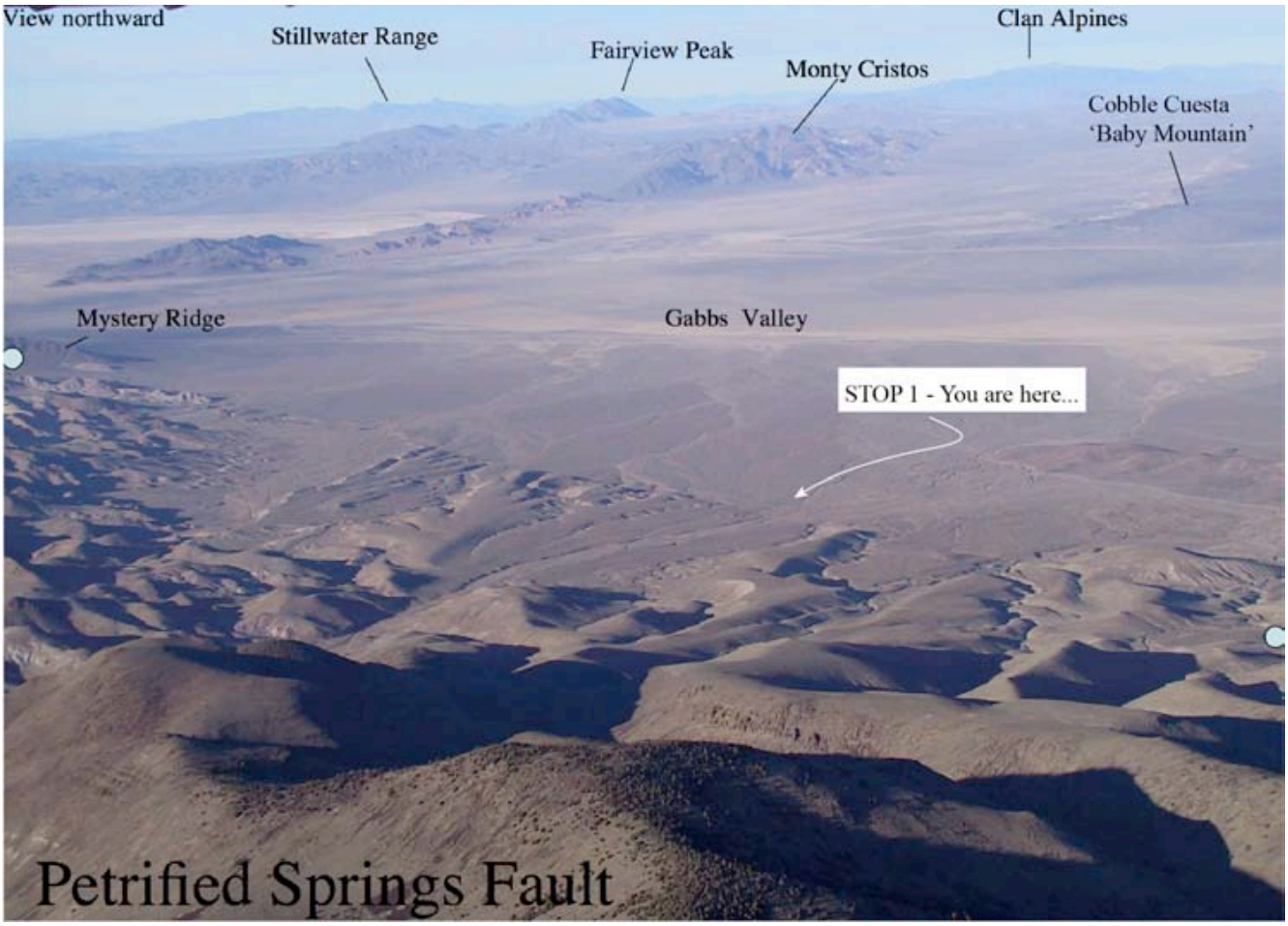

*Figure 1-6. View north over Petrified Springs fault (lineament between two blue dots) and Stop 1. The Petrified Springs fault marks the eastern boundary of the northwest striking Walker Lane and the boundary between the northeasterly alinement of the mountains of the Basin and Range. Fairview Peak, the Monte Cristos and Cobble Cuesta should be visible from the ground at Stop 1. The east flanks of the Stillwaters and Fairview Peak incurred surface rupture along rangebounding normal faults during the 1954 earthquakes (see **Fig 1-5**). The 1932 Cedar Mtn earthquakes extended northwestward into Gabbs Valley and produced discontinuous surface rupture scarps along the east flank of the Monte Cristos and Cobble Cuesta. The 1954 Fairview earthquake also produced ruptures along the east flank of the Monte Cristos, overlapping with those of the 1932 earthquake. Some of the 1954 Monte Cristo scarps showed apparent left-lateral motion.*

Earthquakes and where we sit.

During the last 150 years or so there have been a number of earthquakes in Nevada and southeastern California that have been sufficiently large to break the ground surface, commonly producing scarps of several meters or more over rupture lengths reaching to 40-50 km (Figures 1-7 and 1-8). The sequence of earthquakes encompasses a thin northerly oriented zone of greater than ~750 km length, extending from near Winnemucca, NV in the north to the Mojave Desert in the south. Prior to the 1990's the events included from north to south the M7.7 Pleasant Valley, the 1954 M 6.9 Dixie Valley, M 7.7 Fairview Peak and M6.6&6.8 Fallon Stillwater earthquakes, the M7.2 1932 Cedar Mountain earthquake, and the M7.8 1872 Owens Valley earthquakes. All these situated east of the Sierra Nevada were and still are referred to by most as earthquakes of the Central Nevada Seismic Belt, a term first coined by Bob Wallace back in 1977 (Wallace, R.E., Time-history analysis

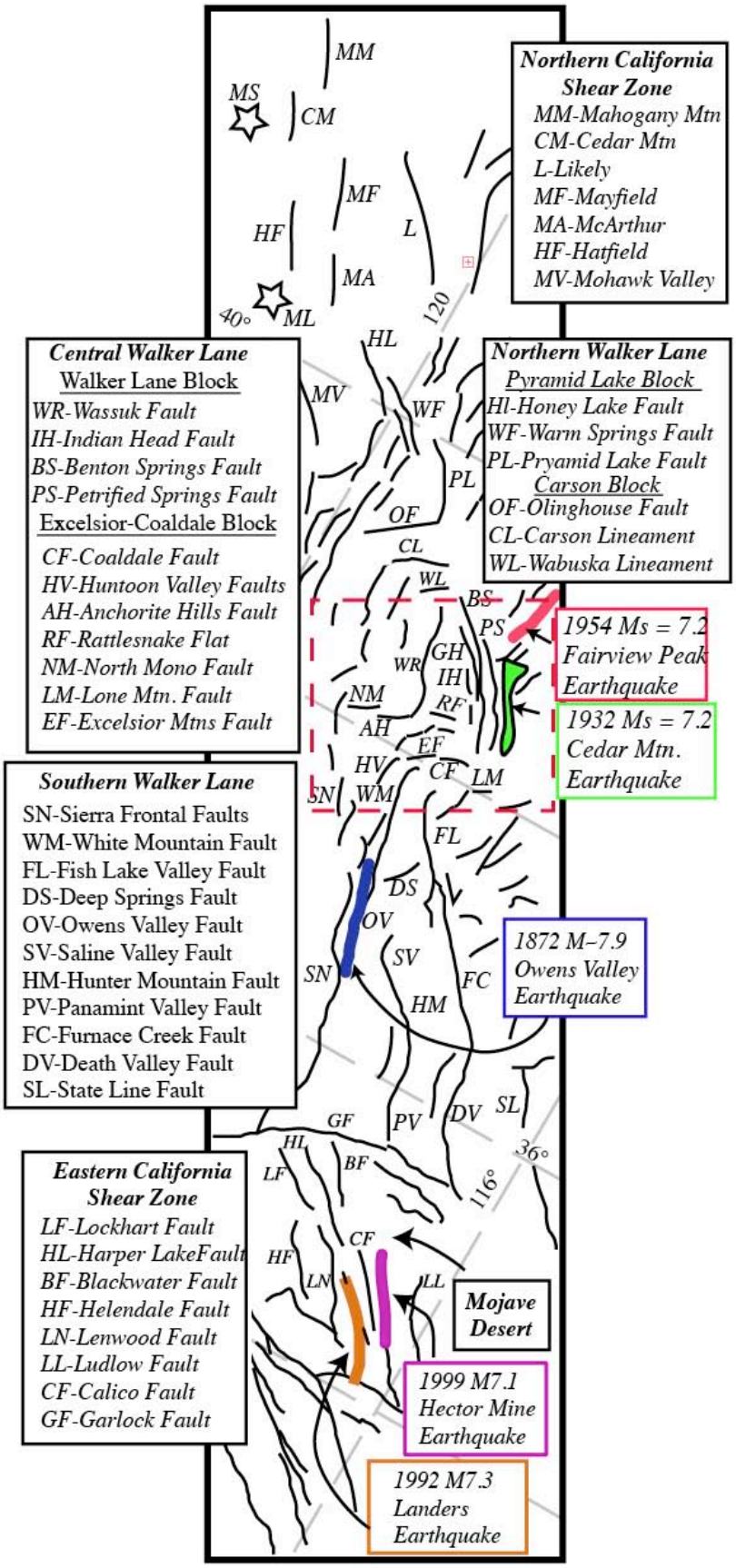

Figure 1-7. (above) Historical Earthquakes of Central Nevada Seismic Belt.

Figure 1-8 (left) Active faults and extent of historical surface rupture earthquakes in Walker Lane and Eastern California Shear Zone. Dashed box outlines Figure 1-6.

of fault scarps and fault traces - a longer view of seismicity, Proceedings, Sixth World Conference on Earthquake Engineering, 766-769, 1977). In the 90's we had the Landers and Hector Mountain earthquakes which apparently extended the Belt another couple hundred km or so to the south. Now that California is so much more involved we might steel ourselves for a name change. But Central Nevada Seismic Belt it is for now.

We are located within view of the ground that ruptured during each 1932 Cedar Mtn. Earthquake and the 1954 Fairview Peak earthquake. The earthquake ruptures were the focus of detailed studies by Caskey et al (1996) and Bell et al (1999), and it is from there that this little synopsis arises. The surface rupture during the 1954 Fairview Peak earthquake produced well-defined scarps along the southeast flank of Fairview Peak which is observable in the distance to the north and

also discontinuous smaller scarps along the southeastern flank of the Monte Cristos (**Figures 1-5, 6,& 9**). The earthquake was a pretty much even mix of normal down-to-the-east and right-lateral slip. The Cedar Mtn earthquake was of similar magnitude but of right-lateral strike-slip mechanism (and herein lies the little complexity alluded to previously of actually trying to define the exact location of the east boundary of the Walker Lane). Though of similar magnitude, the surface ruptures of the 1932 Cedar Mtn earthquake did not produce surface ruptures along a singular well-defined trace as is usually expected in earthquakes of such size. Rather, the earthquake produced a zone of discontinuous and relatively smaller striking fault scarps. The north trending zone of ruptures extended to and across part of Gabbs Valley. At the the latitude of about Cobble Cuesta and the Monte Cristo Mtns the orientation and zone of scarps turned northeastward. The northeasterly striking traces have been interpreted to indicate that right-lateral slip is being transferred over to the more northerly or northeasterly striking normal faults of the Basin and Range (Bell et al, 1999). This same process over the long-term is likely responsible for the creation and growth of the Basin and Ranges along the edge of the Walker Lane and results in a lessening of the slip rate across the Walker Lane as one goes northward (see refs in Wesnousky, 2005). The thought arises from examination of **Figures 1-5 & 6** when one recognizes that the the well-expressed Petrified Springs fault ends abruptly at Mystery Ridge. The right-slip accruing along the Petrified Springs fault must be accounted for somewhere. A reasonable thought is that at least some portion of the slip transfers to northeast striking normal faults which are responsible for development of the Monte Cristo Range and Fairview Peak. Cobble Cuesta, much smaller, as evidenced by the 1932 Cedar Mtn ruptures is due to the same process. In this regard, I'd suggest you are all bearing witness to the Birth of a Mountain when you look at Cobble Cuesta. It might more appropriately be referred to as 'Baby Mountain' **(Figure 1-9)**. Israel Russell long ago said the beauty of the desert is lost in the mid-day sun and the same is true for Cobble Cuesta. If you arrive in the evening, make sure to take a look over this way.

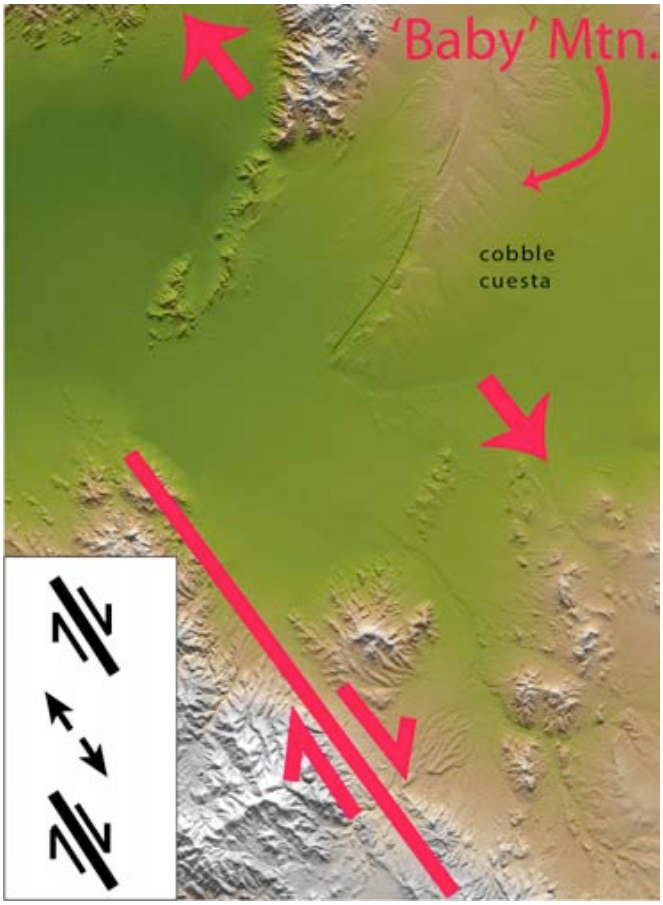

*Figure 1-9. The northwest striking right-lateral Petrified Springs fault ends abruptly at Mystery Ridge and is likely 'transferred' over to northeast striking extensional (normal fault) structures, much like extension occurs within and extensional step along a strike-slip fault (inset). The process likely in large part contributes to the development of the normal fault bounded ranges such as Fairview Peak and Monte Cristo Mtns (**Fig 1-6**). Similarly, the process appears responsible for the birth of Cobble Cuesta and in this regard is perhaps appropriately viewed as a 'Baby Mountain'.*

The Overall Geodetic Picture - courtesy of Bill Hammond and Corne Kreemer, NBMG

The deformation field across the western U.S. defined by the monitoring and analysis of Global Positioning System GPS monument sites is shown in **Figure 1-10.** The reference frame is chosen such that some point in the interior of the continent to the east is considered 'fixed'. The increasing length of the vectors westward across the region defines the ongoing accumulation of crustal strain. The largest arrows at the left of the figure indicate a total of 5 cm/yr of shear strain accumulation across the entire area. The difference in vector magnitudes about the region where we sit indicates about ~1 cm/yr of right-lateral shear accumulation is localized along the Walker Lane. During the course of this trip, discussion will meander to just where and how that shear strain appears to be accommodated on structures that we can see (or not).

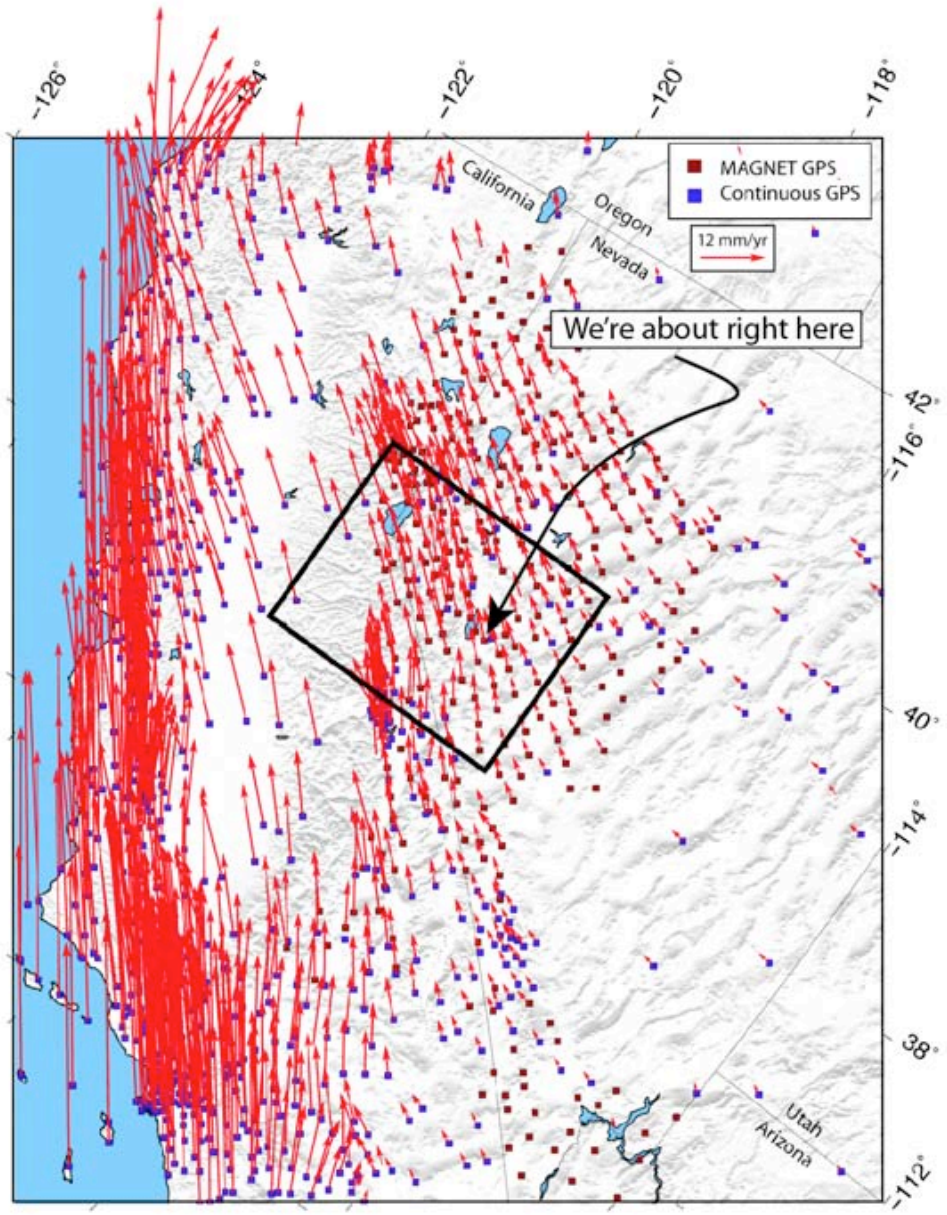

Figure 1-10. Data are obtained from the Mobile Array of GPS for Nevada Transtension (MAGNET) semi-continuous network and from the EarthScope Plate Boundary Observatory (PBO) and other continuous GPS stations. Processing, analysis and reference frame details are provided in Hammond et al., (2010). A minimum time series length of 2.0 years was used because shorter duration time series are less inaccurate. Within the Walker Lane in the vicinity of our

Petrified Springs Fault - You are there. The questions, things to see, and a li'l background.

Our purpose here is to allow all to wander about one of the better expressed strike-slip faults of the Central Walker Lane, talk a bit about what geology can say about how fast it is moving, and compare it to what geodecists say about things out here. The fault is the easternmost of the northeast-trending strike-slip faults in the Central Walker Lane. Prior Quaternary and bedrock geology maps of the Petrified Springs fault include Ekren and Byers [1985a] and Dohrenwend [1982a] (Figure 2-1). The fault has been moving for quite some time, sufficiently long so that the Tuffs of Mt. Ferguson show apparent right-lateral offset of ~12 km across the fault , and Ekren and Byers [1984] suggest 16 km of right-lateral offset is probable based on a more regional analysis of the distribution of Miocene tuffs. The timing of initiation is apparently not so well constrained at post 25 m.y.

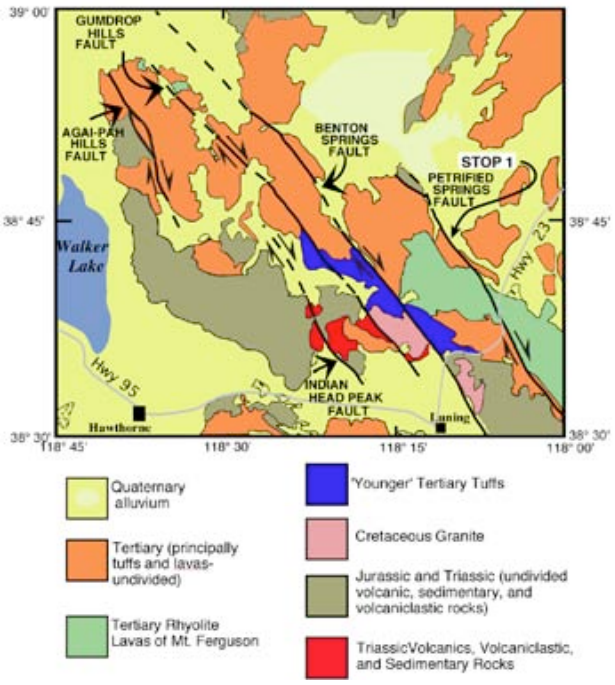

Figure 1-11. Map of active faults and dextrally offset Tertiary and older rocks in vicinity of Stop 1 simplified from work of Ekren and Byers (1984)

The Petrified Springs fault strikes southward about 30 km from a northern limit at Mystery Ridge to Calvada Flat (Figure 1-12 & 13). Linear valleys and ridges, deflected and laterally offset streams, sidehill benches, scarp face reversals, closed depressions, compressional ridges, and vegetation lineaments occur along the linear trace

A larger scale photo and sketch map of a portion of the fault along the west edge of Gabbs Valley illustrates some of these features (Figure 1-14). On the sketch map, the trace adjacent to Gabbs Valley is linear, the scarp generally faces northeast, and a vertical component of motion has uplifted a set of alluvial fan and pediment surfaces. The surfaces show increasing amounts of uplift as a function of relative age. A linear closed depression occurs along the southeastern end of the map area. A small left-step in trace is associated with a compressional ridge or 'push-up' in the northern section of the same map area. A beheaded stream incised into a Qi surface appears to record ~99 meters of right-lateral offset (Figure 1-14).

The alluvial surface that records the 99 m offset is composed of broad interfluves covered by a relatively continuous pavement of darkly varnished subangular to subrounded volcanic clasts. A soil chronosequence for a similar set of abandoned alluvial terraces has been previously developed about 20 miles to the south in Bettles Wells Canyon [Bell, 1995; Bell et al., 1999]. There, where we will visit later, numerous tephra layers of known age associated with a flight of progressively uplifted fan surfaces allowed [Bell, 1995; Bell et al., 1999] to correlate soil characteristics to fan

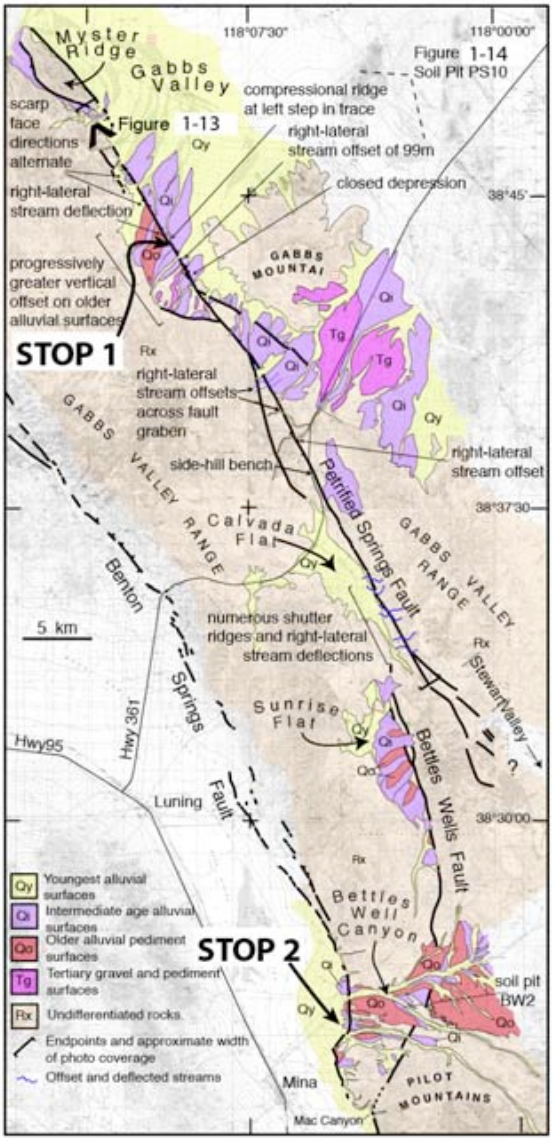

Figure 1-12. Petrified Springs Fault trace. The fault trace (bold lines) is annotated to mark features indicative of lateral offset and ongoing fault activity. Location of map in Figure 1-14 and soil pit PS10 are also labeled. Perspective of photo in Figure 1-13 shown by bold open ended V shape. Units Qy, Qi, and Qo are Quaternary surfaces of relatively increasing age. Units Tg and Rx encompass Tertiary gravels and undifferentiated bedrock, respectively. Detail of Benton Springs Fault shown in Figure 1-19. adapted from Wesnousky 2005

Figuure 1-13. View southeast along strike of Petrified Springs Fault trace (between white arrows). Vantage point of photo is shown in Figure 1-12. Brackets show approximate extent of photo and strip map in Figure 1-14. photo: wesnousky

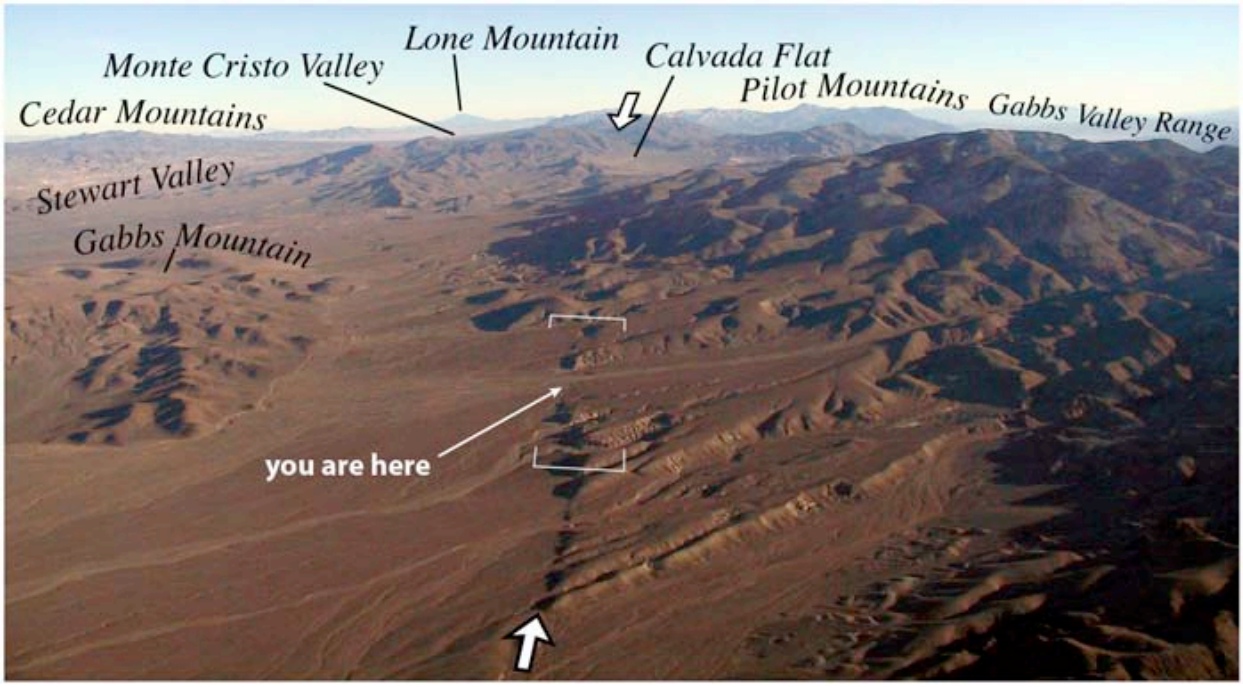

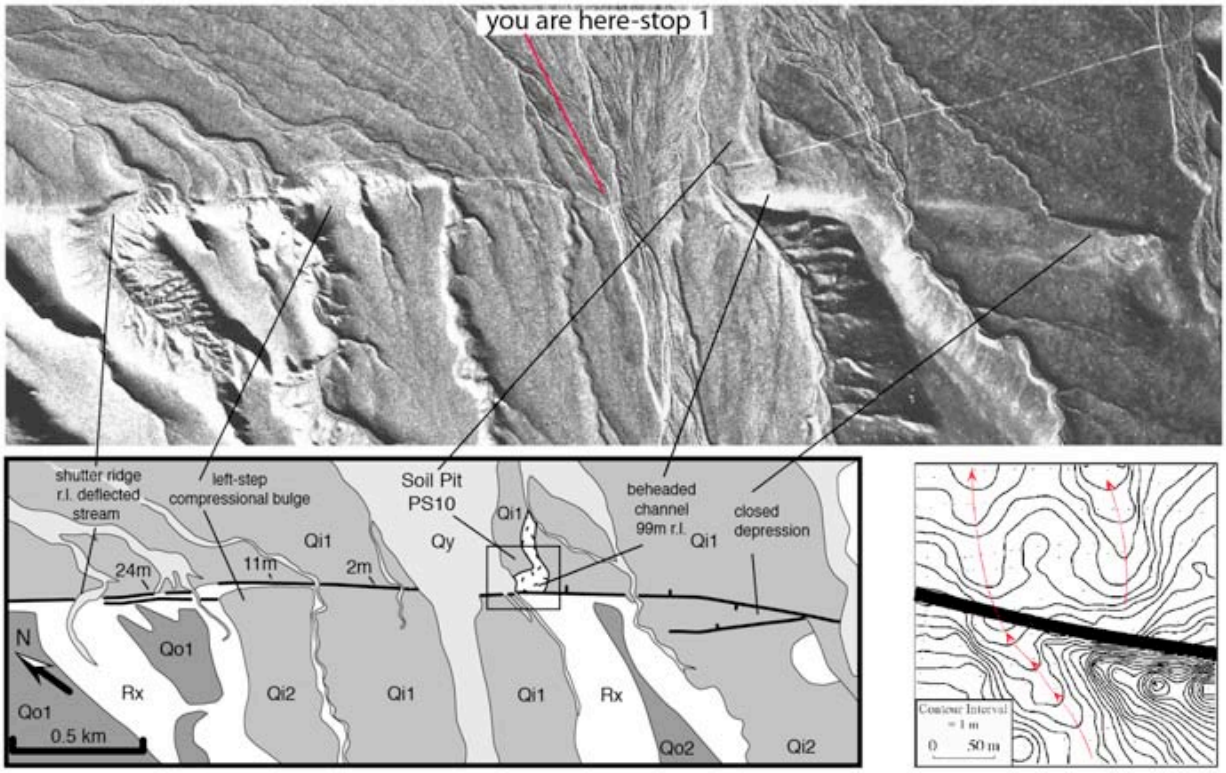

Figure 1-14 (above). Photo and sketch map show Quaternary surfaces, scarp heights, and features indicative of active faulting along a section of the Petrified Springs Fault trace adjacent to Gabbs Valley. Contour map at 1-m interval (lower right) (adapted from Wesnousky (2005)

Figure 1-15. Soil characteristics of soil pit PS10

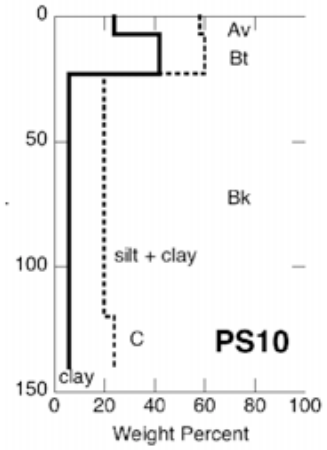

Av: Brown (10YR4/3d) loam, moderate medium to coarse subangular blocky and fine platy structure, slightly hard(d), sticky(w), slight effervescence, abrupt wavy boundary

Bt: Yellowish brown (10YR5/4d) clay, weak to moderate fine to medium subangular blocky structure, soft(d), slightly sticky(w), no effervescence, clear wavy boundary.

Bk: Light gray (10YR7/2(d)) loamy sand, moderate medium and coarse subangular blocky structure loose (matrix) and hard (peds)(d), nonsticky(w), violent effervescence (stage II+ carbonate development) diffuse boundary.

Ck: Light brownish gray (10YR6/2d) loamy sand, weak to structureless loose(d), non-sticky(w) violent effervescence.

Typical Characteristics of Bettles Well Qf2a and Qf2b soils from Bell (1995):

Qf2b: 7 cm Av, 7-10 cm Bt (7.5 YR), 60-100 cm Bk or Bqkm (state III-IV) horizons overly Wilson Crk Tephra; 36ka.

Qf2a: 7 cm Av, 25 cm Bt (7.5 YR), 50-60 cm Bk (stage II-III) contains Mono Craters Negit Causeway tephra; 60-100ka.

surfaces of known age. A soil pit excavated into the Qi1 surface (PS10 in Figure 1-14 & 15) shows characteristics similar to those reported for the Qf2a and Of2b surfaces of Bell (1995) in Bettles Wells Canyon which he interprets to be <60-90 ka, and <36 ka, respectively. The characteristics of the soil pit PS10 here listed in Figure 1-15. Assuming the Qf2a and PS10 surfaces are indeed similar in age and the entirety of the 99 m offset is tectonic in origin, the observations point to a right-lateral slip rate of >=1.1 to 1.65 mm/yr, a reasonable value given the robust geomorphic expression of the fault though not without a good deal of uncertainty. The pit remains open and available for all to take a look.

Shutter ridges and right-lateral stream deflections are numerous along the section of fault between Gabbs Valley and Calvada Flat where the trace is mostly confined to bedrock. (**Figure 1-13**). The fault trace bifurcates at the southern end of Calvada Flat. Ekren and Byers [1984] project the northern strand a distance of ~10 km and into Stewart Valley, somewhat on strike with a discontinuous zone of right-lateral surface fractures produced by the 1932 Cedar Mountain earthquake (also see **Fig. 1-5**). The southwestern strand is the Bettles Wells Fault. It strikes more southerly and continues another 15-20 km along the east flank of Sunrise Flat toward the Pilot Mountains at which point it appears to merge with the Benton Springs fault. The linearity of the trace, sidehill benches, and the alignment of bedrock knobs just outboard of the main rangefront are compatible with youthful displacement and a significant component of lateral slip along Sunrise Flat. Right-lateral displacements of older bedrock units are mapped along the section of fault between the alluvial deposits of Sunrise Flat and Bettles Wells Canyon [Oldow and Meinwald, 1992].

Stop 2. The Benton Springs Fault-a little background

Here we stop to examine the characteristics of another one of the Central Walker Lane right-lateral strike-slip faults: The Benton Springs Fault (Figures 2-1 & 2). The fault is well expressed in Quaternary alluvium at sites along the ~50 km from Rhyolite Pass in the north to Rhodes Salt Marsh in the south. Ekren and Beyers [1986b] infer the fault continues northward another 45 km beyond the Gabbs Valley Range to where it bounds the eastern flank of the Terrell Mountains. Right-lateral offset was recognized by Ferguson and Muller [1949]. Sections of the fault have since been mapped by Ekren and Byers [1985a; 1985b; 1986a; 1986b], Dohrenwend [1982a; 1982b], Speed [1981], and Stewart et al. [1982]. Ekren and Byers [1984] document a 6.4-9.6 km right offset of a steep contact of a Cretaceous granitic pluton (Figure 109) and an 8 km right offset of younger Tertiary tuffs. Lateral slip on the fault is entirely Tertiary and younger [Ekren and Byers, 1984; Ferguson and Muller, 1949].

The fault is confined to the Gabbs Valley Range between Rhyolite Pass and Soda Springs Valley (Figure 2-1. Displacement has led to development of a narrow fault-aligned valley. Within the valley, linear ridges, fault-aligned drainages, offsets of erosional ridgelines and active channel margins show recent right-lateral strike-slip (Figure 2-3). The fault runs along the west flank of the Gabbs Valley Range at the north end of Soda Springs Valley where it

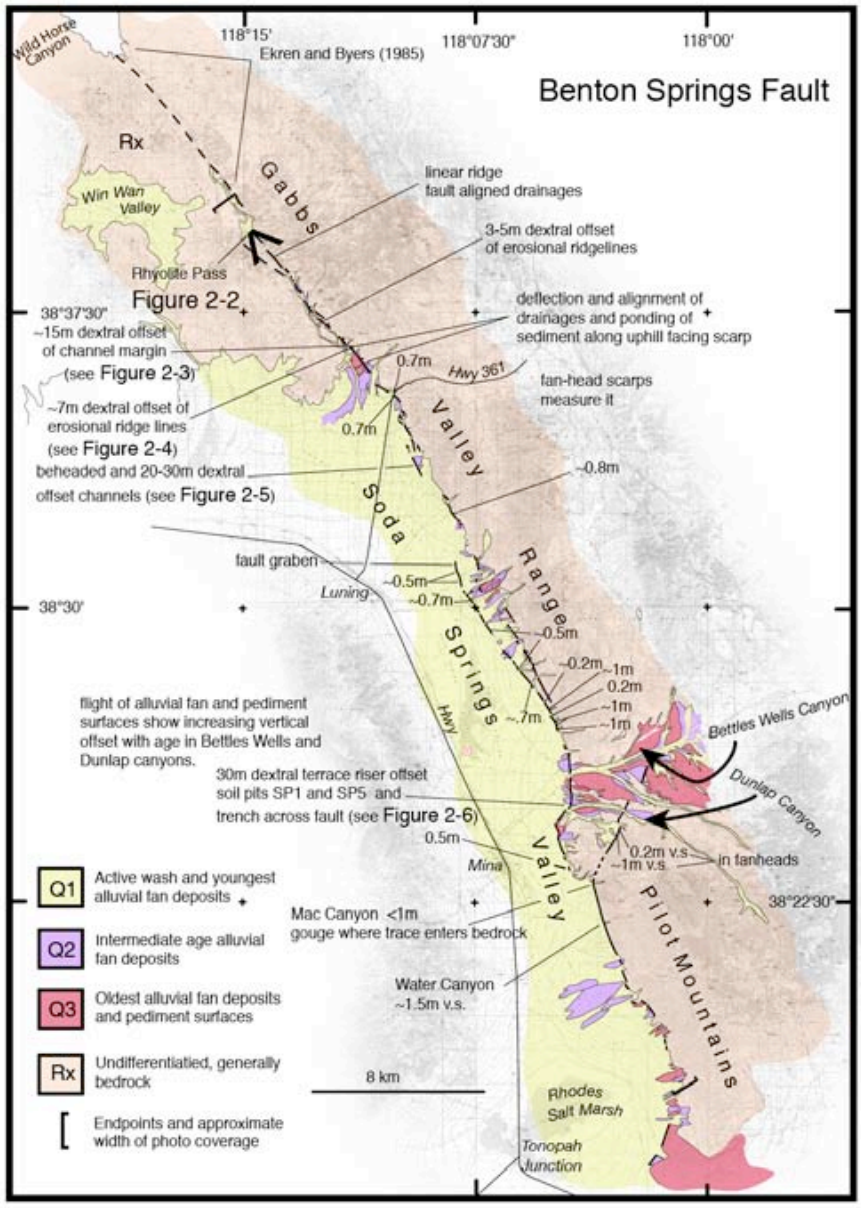

Figure 2-1. Map of Benton Springs fault trace. Numerical annotations are scarp height unless specifically indicated to be vertical separation (v.s.) or dextral. Perspective of photo in Figure 2-2 shown by open ended V shape. Locations of maps in Figures 2-3, 4 & 5 are marked. Units Qy, Qi, and Qo are Quaternary surfaces of relatively increasing age. The older alluvial surfaces (Qo) at the southern end of the Pilot Mountains overly Pliocene lake beds [Reheis et al., 2002]. adapted from Wesnousky (2005).

Figure 2-2. View south along Benton Springs Fault from Rhyolite Pass. The fault trace (between arrows) strikes southward and expressed by lineation of uphill facing scarps along a longitudinal valley in foreground, gradually bends right to flank the west flank of the Gabbs Valley Range, then takes an abrupt right bend at Bettles Wells Canyon before continuing along the west flank of the Pilot Mountains. Perspective of photo shown on map in Figure 2-1. Photo: Wesnousky

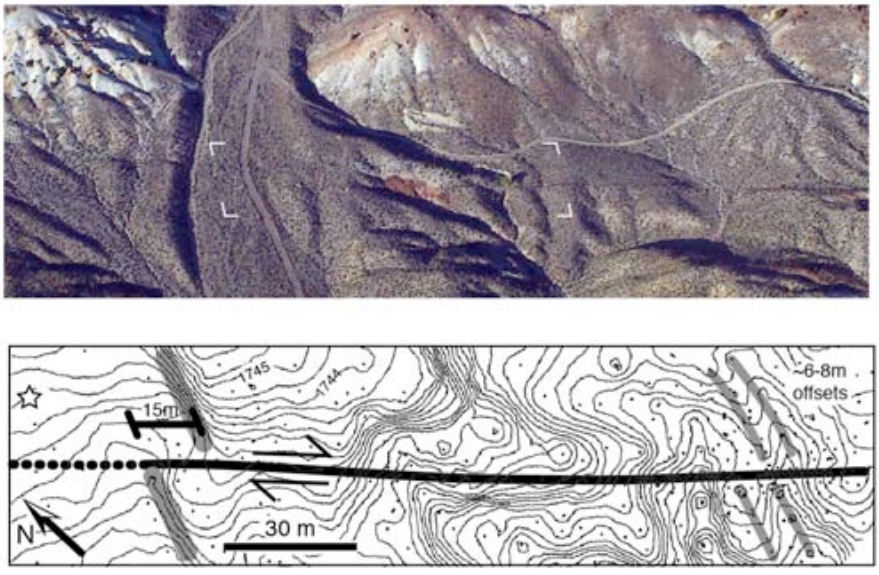

Figure 2-3. Photo and 0.5 m contour interval map show (shaded) right-lateral offsets of channels, channel margins and ridgelines along the northern section of the Benton Springs fault. Extent of contour map shown by white brackets in photo. Coordinates (UTM NAD27 CONUS) of point marked by star are E396102 N4274096. Figure location also shown in Figure 2-1. taken from Wesnousky (2005).

truncates an intermediate-age fan or pediment surface of granitic composition, about 3.5 km south of State Highway 361. Beheaded channels and shutter ridges record up to 30m of right-lateral displacement **(Figure 2-4)**. Displacement occurs on two subparallel strands south of Luning **(Figure 2-3)**. The western of the two strands has produced small grabens and generally west-facing scarps in young alluvium.

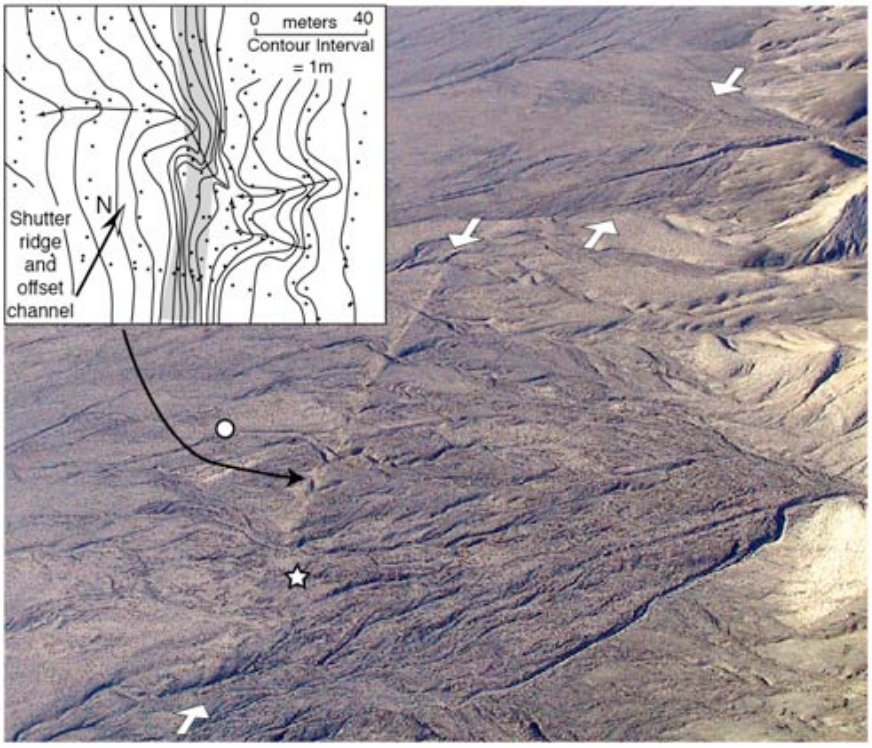

Figure 2-4. Photo and contour map show linearity of trace (between arrows), shutter ridges, and offset channels along section of Benton Springs Fault in northern Soda Springs Valley. View is to northwest. Contour map documents shutter ridge and ~30 m right-lateral offset of drainage channel in alluvium. Trend of scarp is shaded. White dot on photo sits at end of prominent beheaded and right-laterally offset channel. Coordinates (UTM NAD 27 CONUS) of point marked by star are ~N4268150 E399325. Location also annotated in Figure 2-1. Photo: Wesnousky

STOP 2 - The Place

The fault trace bends sharply to the right between Bettles Wells and Dunlap Canyons (Figure 2-1 & 2). Here the right-step apparently results in an increased normal component of displacement that has resulted in the abandonment of alluvial fan and pediment surfaces that record increasing displacement as a function of age (Figure 2-5). Also at Dunlap Canyon a terrace riser cut into the surfaces appears to record ~35 m of right-lateral displacement (Figure 2-5). Soil texture profiles SP1 and SP5 on the surface recording the offset are distinguished by virtually identical soil profiles Figure 2-6). The foot and hanging wall surfaces are identified as the Qf2a and Qf2b surfaces by Bell, 1995; Bell et al., 1999 (Figure 2-7), which are respectively reported to contain tephras of 60-100 ka and 36 ka and typically characterized by argillic Bt horizons. The interpretation would suggest that the surfaces interpreted to be offset are not in fact correlative. Yet, the soil pits SP1 and SP5 on the foot and hanging wall surfaces are virtually identical and are expressed by soil development significantly less than that reported for Qf2a and Qf2b surfaces (Figure 2-6). Given that there are numerous examples of right-slip along the fault such as exhibited in Figs 2-3 & 4, and that this particular 35 m offset is tectonic in origin, and that the surfaces are indeed correlative, dividing the ~35 m offset by a <36 ka age of the offset surface places a minimum bound on the right-lateral fault slip rate of ~1 mm/yr. That the soils of the offset surface appears considerably younger than those reported for the 36 ka Qf2b surface might further suggest that the lateral slip rate may be significantly higher than 1 mm/yr.

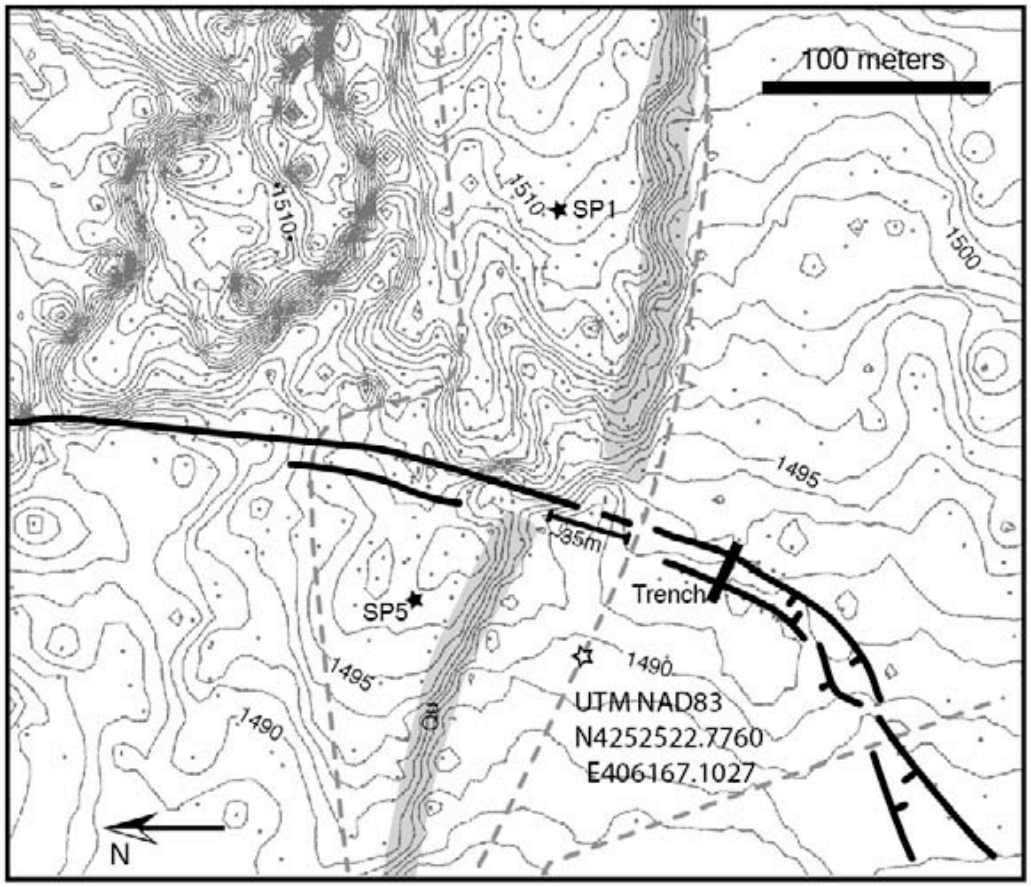

Figure 2-5 -STOP 2. *Photo and map of dextrally-offset terrace riser along the Benton Springs Fault (bold lines) at Dunlap Canyon. Approximate extent of contour map marked by white corner brackets in photo. Shaded zones in contour map highlight channel margin. Locations of soil texture profiles SP1 and SP5 denoted by white stars on photo and black stars on map. Locations also shown on Figure 2-1. Sketch of trench site is presented in Figure 2-6. Photo: Wesnousky*

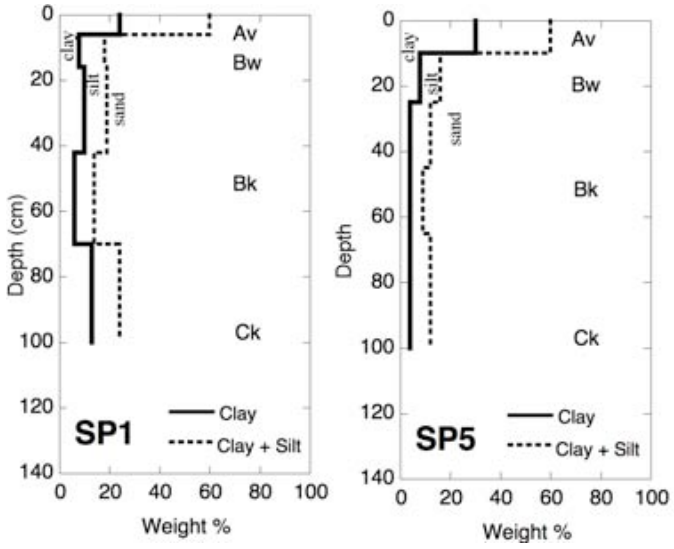

Figure 2-6. *Soil Textural profiles of pits SP1 and SP5 are virtually identical. Locations are shown on Figure 2-5.* ***SP1****: **Av** (0-6cm), Loam, (10YR7/3d-10YR5/4(w), moderate fine subangular blocky structure/vesicular, slightly hard (d), slightly sticky(w), abrupt smooth, strong effervescence; **Bw** (6-16 cm), Loamy Sand, 10YR6/3d, 10YR5/6(w), wea very fine subangular blocky and single grain, loose(d), nonsticky(w), clear wavy, strong effervescence; **Bk** (16-70 cm), Loamy Sandy, weak very fine subangular blcoky and single grain, loose(d), nonsticky(w), Stage II carbonate,violent effervescence, clear smooth boundary (carbonate generally concentrated in ~cm wide stringers - most stage I; **Ck** (70-100), sandy loam. **Profile SP5**; (0-10cm), Clay Loam, 7/3d-10YR5/6(w) , moderate medium & coarse subangular blocky structure/vesicular, hard (d),sticky&plastic (w), abrupt smooth, strong effervescence; **Bw** (10-25 cm), Loamy Sand, 10YR6/6d, 10YR4/4(w), weak very fine granular & single grain, loose(d), nonsticky(w), diffuse irregular?, slight & strong effervescence in carbonate stringers; **Bk** (25-65 cm), Sand, loose (d) & slightly hard subangular blocky, loose(d), nonsticky (w), Stage II carbonate, strong & violent effervescence, gradual to diffuse irregular (carbonate generally concentrated in ~cm wide stringers - most of horizon Stage I; **Ck** (65-100) sand*

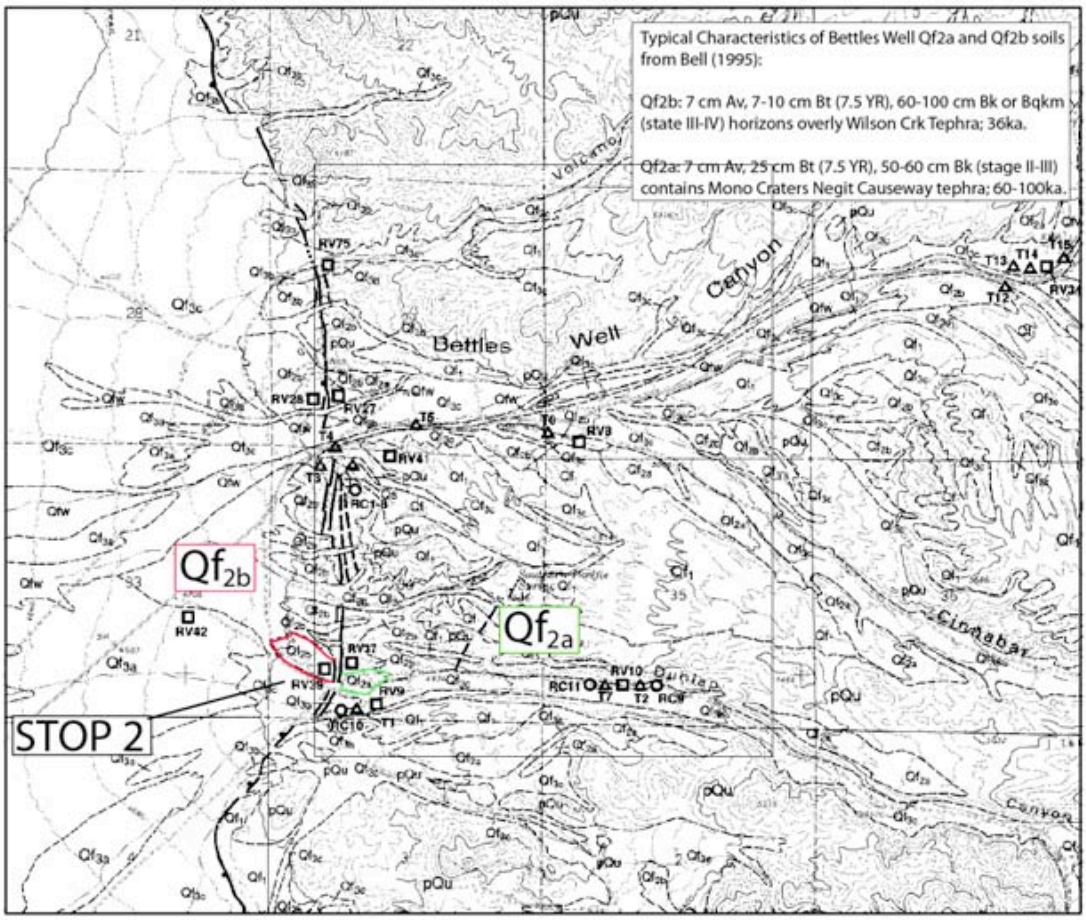

Figure 2-7*. Portion of geologic map of Mina Quad mapped by Bell (1995) showing correlations and interpretation of surface ages near Dunlap Canyon. The surfaces outlined in red and green are defined as Qf2b and Qf2a, respectively. The age of the surfaces and soil characteristics cited by Bell (1995) are given in the Figure. Soil pits SP1 and SP2 of this study are on these surfaces and display quite different characteristics.*

A trench excavated across a fault graben at Dunlap Canyon exposed alluvial gravels displaced by the fault (Figures 2-5). The exposure consisted largely of subangular poorly sorted coarse sand and pebble alluvial-fan gravel. The layer fabric is sketched to scale and fault displacements are shown in Figure 2-6. Distinct gravel beds may be followed continuously across small down-to-the-east displacements from the west end of the trench to a fault contact and zone of shear at about meter 6 to 7. The fabric and facies of gravel east of meter 6 do not match that observed to the west. The mismatch reflects significant strike-slip motion. Displacement along shear zones at meters 4 and 6 has produced a west-facing scarp. A gravel layer records apparent down-to-the-west normal displacement of ~1 m across the fault at meter 4 (horizontal arrows in Figure 2-6). Upsection, facies mismatches across the same strand suggest the presence of a strike-slip component as well. The age of a small piece of charcoal (Sample BT1-1RC) retrieved from a faulted massive fine sand layer on the south face shows the last displacement post-dates 2940±35 14C ybp (Table 1). A wedge of colluvium has developed above the shear zone at meter 6 to 7 since the last displacement. The colluvial wedge is thicker on the north face. There, small lenses of tephra form a discontinuous layer within the colluvium. Discrete pieces of charcoal reaching several millimeters in dimension and larger pods of burnt soil are also disseminated within and at the base of the colluvial wedge. The depth of preservation of both the tephra and charcoal within the wedge, the presence of burnt soil, and the lack of similar material in exposed footwall deposits suggest the charcoal was created, the tephra deposited, and both collected from the surface and preserved in the colluvial wedge at or near the time of the earthquake, rather than being reworked from preexisting footwall deposits. The age of a charcoal (sample BT1-5ARC) taken from the base of the colluvial wedge is 780±35 14C ybp. The ash (sample SGW-BT1-ASH1, Table 2 of Wesnousky, 2005) chemically correlates to numerous Late Holocene ashes emitted from Mono Craters with a best, though statistically insignificant, fit for ash emitted ~800-1200 14C ybp. The earthquake displacement and eruption may well have been coeval.

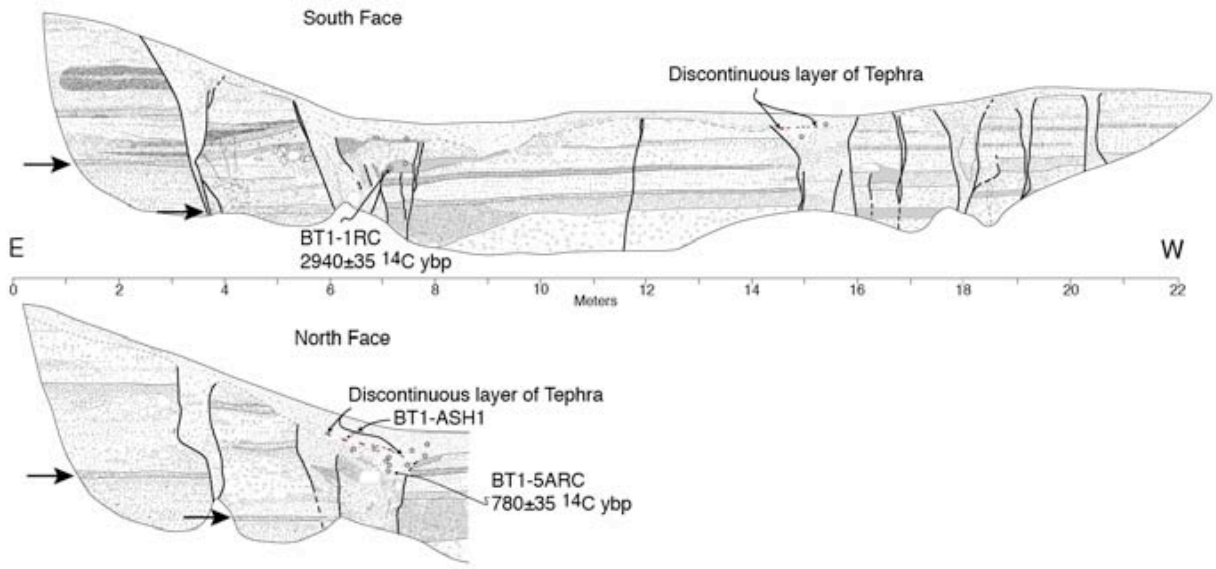

Figure 2-8*. Sketch of trench exposure shows alluvial packages displaced by graben-forming fault strands (bold lines) of Benton Springs Fault at Dunlap Canyon. The presence of Mono tephra and dating of charcoal (stars) in colluvium shed off the scarp produced by the last displacement indicate a surface rupture earthquake during the last ~1000 years. Horizontal arrows show down-to-west displacement of distinct layer. See text for discussion.*

The rangefront morphology and character of faulting along the Pilot Mountains (below) differ from that observed along the Gabbs Valley Range to the north (Figure 2-2). The Pilot Mountains display an abrupt and steep escarpment, triangular facets, and a fault trace that primarily separates bedrock from alluvium. In contrast, faulting along the Gabbs Valley Range is commonly outboard of the range, the rangefront less steep, and triangular facets smaller. Elevations in the Pilot Mountains are also consistently higher, reaching >9000 feet (2800 m), in comparison to elevations of the Gabbs Valley Range which are generally less than 8000 feet (2500 m) (Figure 2-2). Scarps that cut young alluvium at the base of the Pilot Mountains are present north of about Water Canyon (Figure 2-1). At Mac Canyon, an alluvial scarp strikes into bedrock and a zone of fault gouge >10m in thickness is present (Figure 2-1). The bedrock maps of Oldow and Meinwald [1992] and Oldow and Dockery [1993] show a linkage to the Bettles Wells Fault (Figure 1-13). Scarps in young alluvium and the alignment of escarpments in older pediment surfaces to the northeast of Mac Canyon suggest that transfer of slip to the Bettles Wells and faults to the east may continue today (Figures 1-13 and 2-1), though the exact mechanics of the transfer are not clear. The transfer of slip is probably responsible for the difference in character of faulting and rangefront morphology observed between the two ranges. As well, the slightly more southerly strike of the Pilot Mountains section of the fault may result in a relatively increased normal component of displacement.

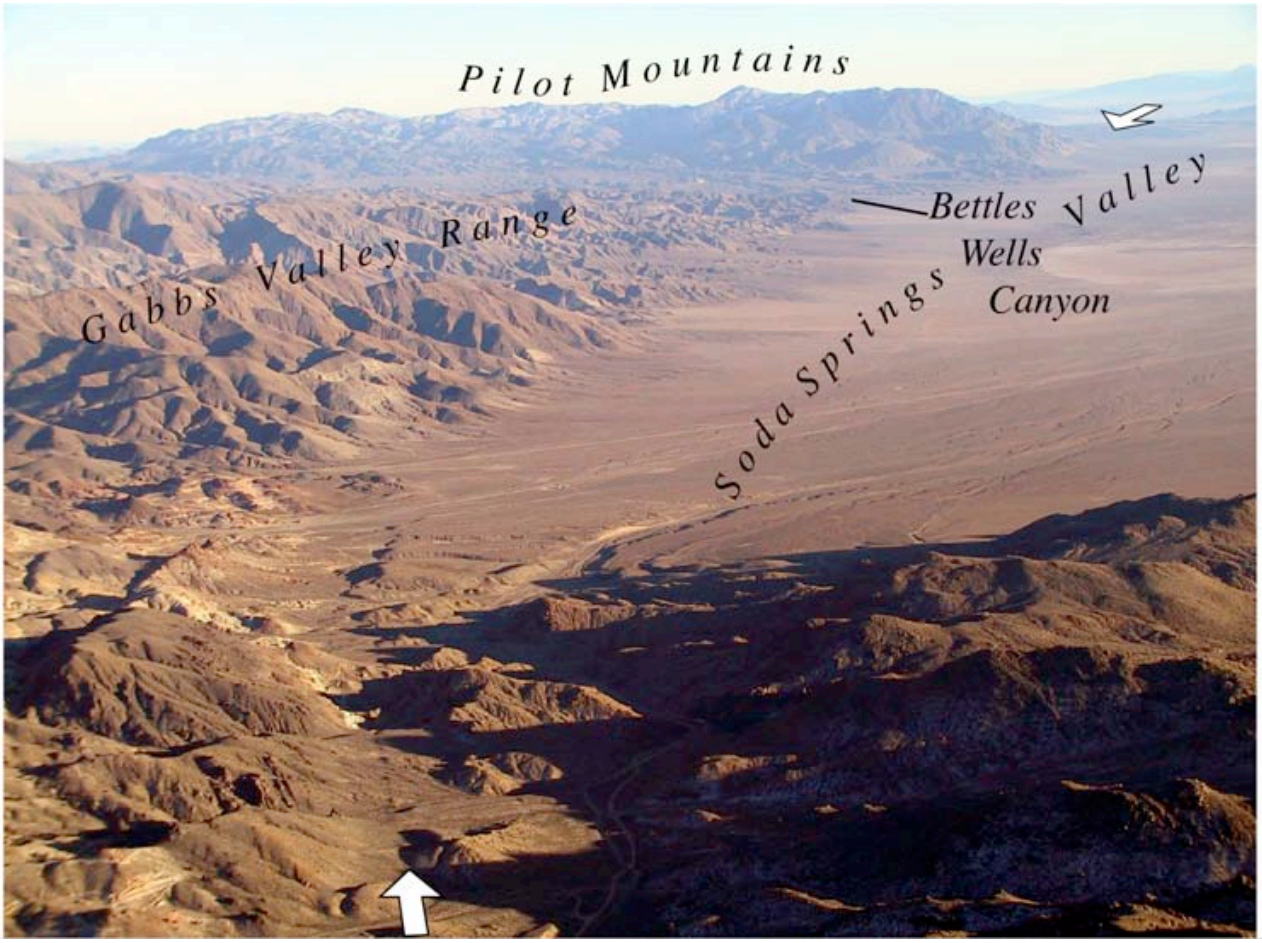

a little extra space - so why not for your convenience a little repeat of Fig 2-2 here....

Stop 3. The RattleSnake Flat Fault

The Rattlesnake Fault (**Figure 1-5 & 3-1**) strikes ~N75°E and is about 20 km in length. Quaternary displacement on the fault was first reported by Bucknam [1974]. He suggested a left-lateral strike-slip origin for the fault based on the orientation, linearity, and geomorphic expression of the fault. He was right. Apparent left-lateral offsets of Tertiary basalts across the fault are evident in later regional geologic maps [Carlson et al., 1978; Garside, 1982; Stewart, 1978; Stewart et al., 1984]. The trace cuts from Rattlesnake Flat in the west through a drainage divide to Garfield Flat in the east **(Figure 1-5 & 3-1)**. The fault trace is quite linear, often contained within bedrock, and forms linear enclosed depressions, uphill and alternately-facing scarps, sidehill benches and linear fault-bounded ridges (Figure 3-2a), indicative of lateral slip. The westernmost strand of the fault bends to the south along a bedrock-alluvial contact and produces an oversteepening of the base of the rangefront, more suggestive of normal faulting (**Figure 3-2b**). About 2 miles east of the drainage divide, between Rattlesnake and Garfield Flats, a left-stepping en echelon arrangement of several pressure ridges, the deflection of several drainages, and a beheaded stream channel are preserved in young alluvium and demonstrate youthful left-lateral offset (**Figure 3-3 - STOP 3**). The active fault trace continues eastward into Garfield Flat where it produces uphill-facing scarps in young alluvium (unit Qy) and either ends or is obscured by active fan deposits to the south of the Garfield Flat playa, where it may also step further southward to continue along the north flank of the Excelsior mountains [**Figure 1-5**, Garside, 1982]. The depression that marks Rattlesnake Flat reflects extension associated with the left bend and termination of the fault. The location of Garfield Flat is probably, at least in part, due to a similar accommodation of extension at the northeast terminus of the fault.

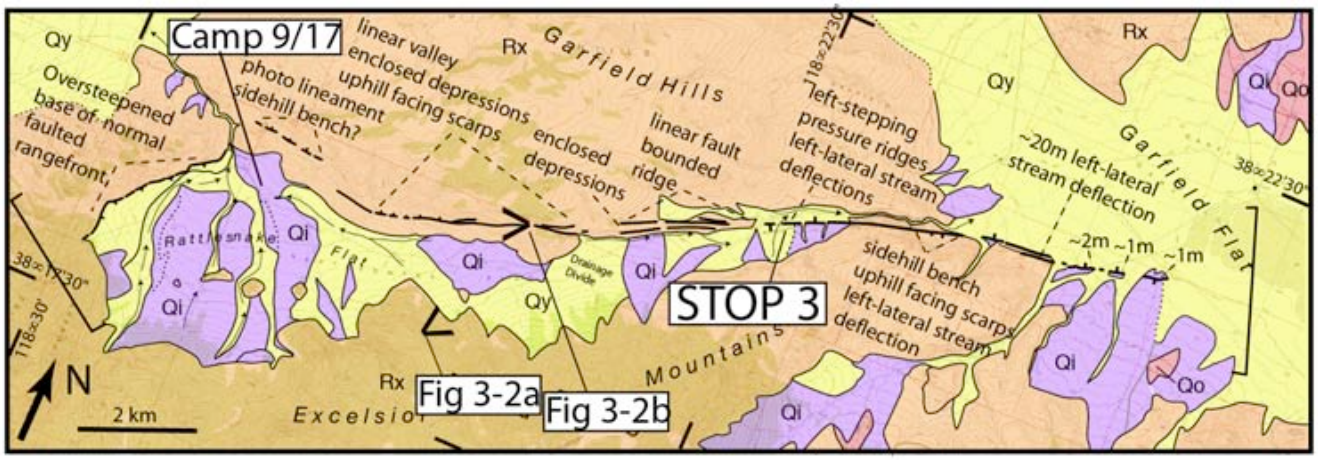

Figure 3-1. *Rattlesnake fault trace and distribution of Quaternary deposits. Scarp heights and features indicative of sense of offset and ongoing fault activity are annotated. Units Qy, Qi, and Qo are Quaternary deposits of relatively increasing age. Unit Rx is undifferentiated bedrock. Faults (bold lines) are dashed and dotted where approximately located or inferred, respectively. Direction of view for photos in Figure 3-2 indicated by open end of solid bold rotated V shapes. Topographic map is provided in Figure 3-3 of site marked by star which is STOP 3.*

The Rattlesnake fault is but one of a suite of east-west trending strike-slip faults that strike transverse to the general trend of the Walker Lane through here (see Teels Marsh, Candelaria, and Coaldale faults zones in **Figure 1-5).** Each the Rattlesnake, Teels Marsch and Coaldale faults zones are associated with paired basins on opposite sides of the fault. The pairing of basins at ends of the east striking faults may be the result of (a) simple lift-slip ransform of motion between normal fault basin or (b) clockwise rotation of crustal blocks with northeast trending zone of right shear. Elements of both processes appear responsible for the major basin in this portion of the Central Walker Lane (**Figure 3-4).**

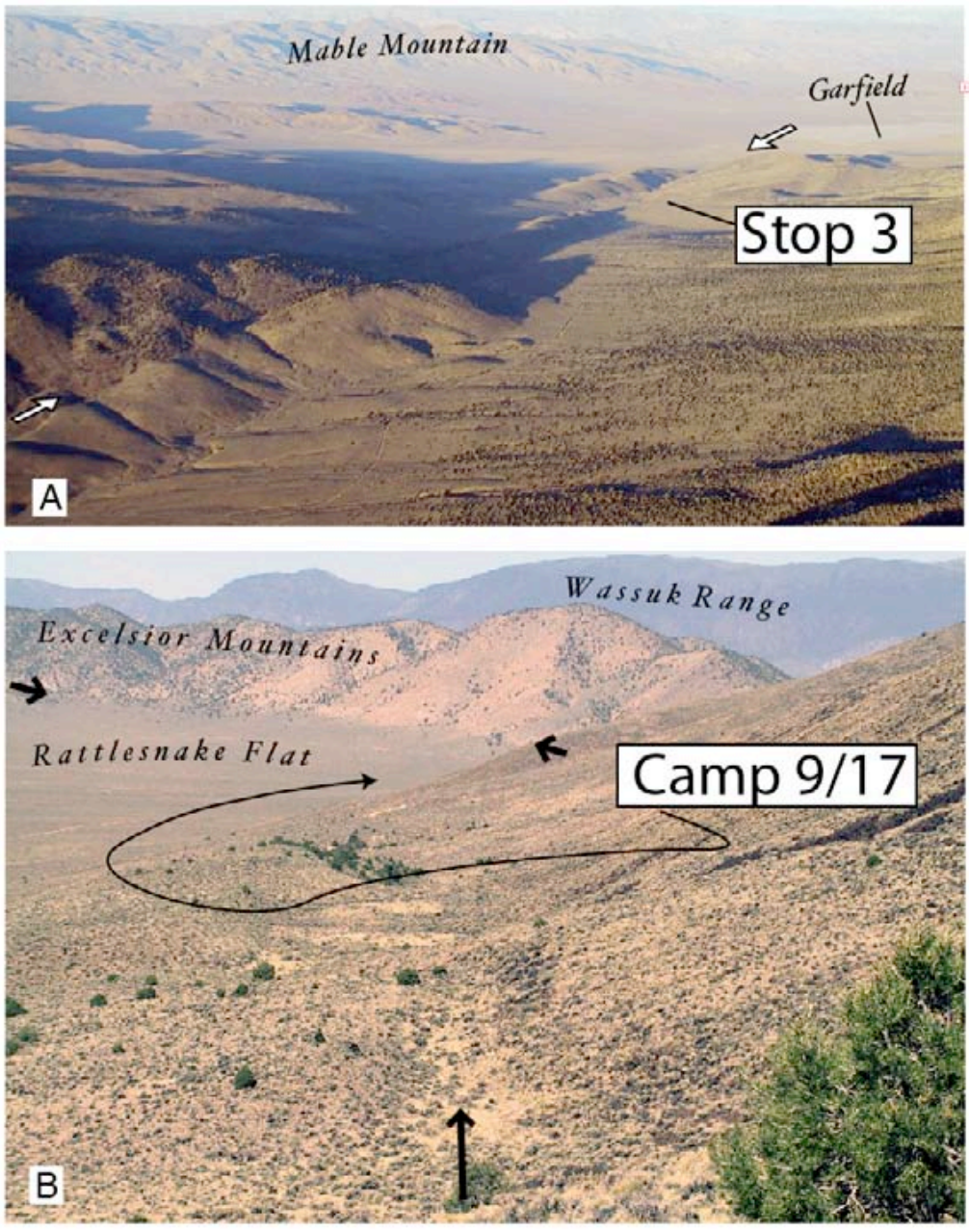

Figure 3-2. *Rattlesnake Fault. (a) View northwestward shows linear valleys and ridges, side-hill benches, closed depressions, and uphill-facing scarps, which define the strike of Rattlesnake Fault (along strike between arrows). View is to the northeast. (b) View westward along strike shows trace is characterized by sidehill bench and enclosed depression in foreground characteristic of strike-slip displacement. Trace bends sharply to south in distance and exhibits oversteepening of the rangefront and triangular facets indicating primarily normal fault displacement.* ***Perspective of photos shown on map in Figure 3-1****. Photos: Wesnousky*

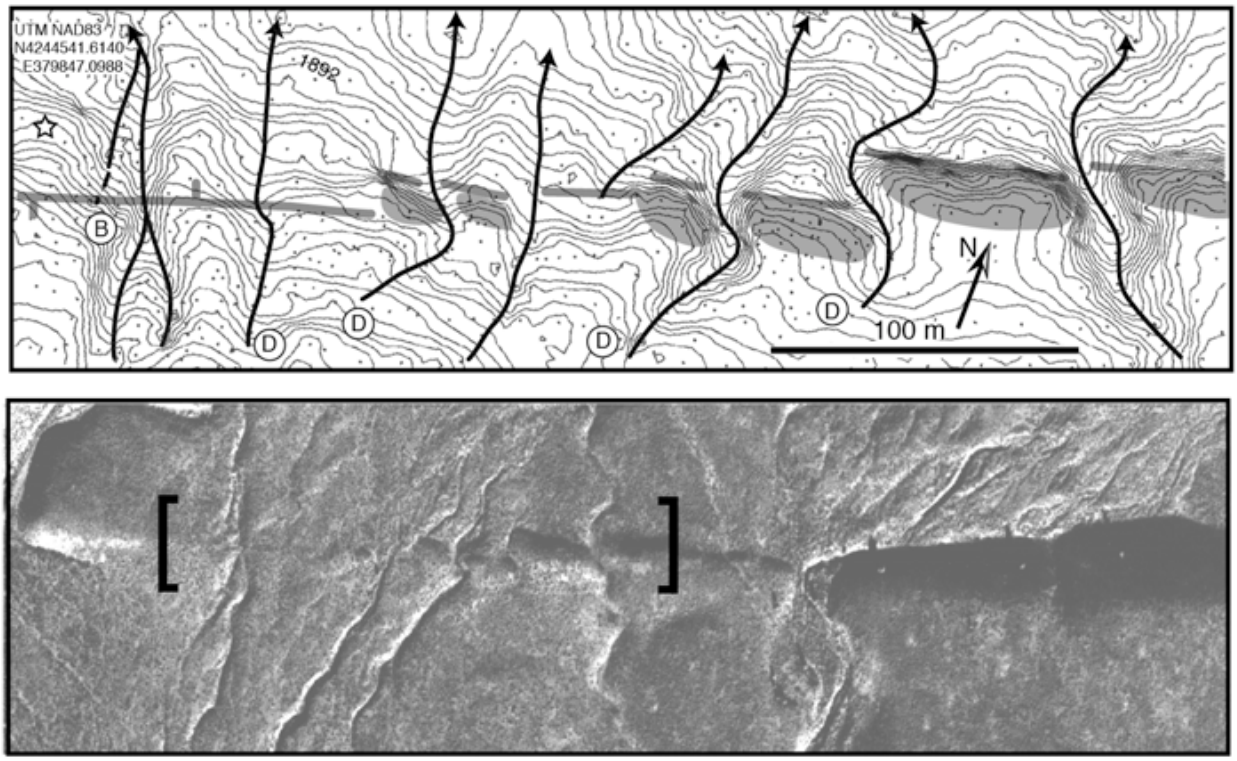

Figure 3-3 - STOP 3. *Topographic map (upper) and airphoto (lower) showing left-stepping en echelon pressure ridges, ephemeral stream channels (D) deflected left-laterally, and a beheaded channel (B) offset left-laterally about 12 m. Location of topographic map delineated by brackets in airphoto. Contour interval is 0.35 m. Control points for contour map are dots. Location is annotated on Figure 3-1 and aided by UTM coordinate of point (star).*

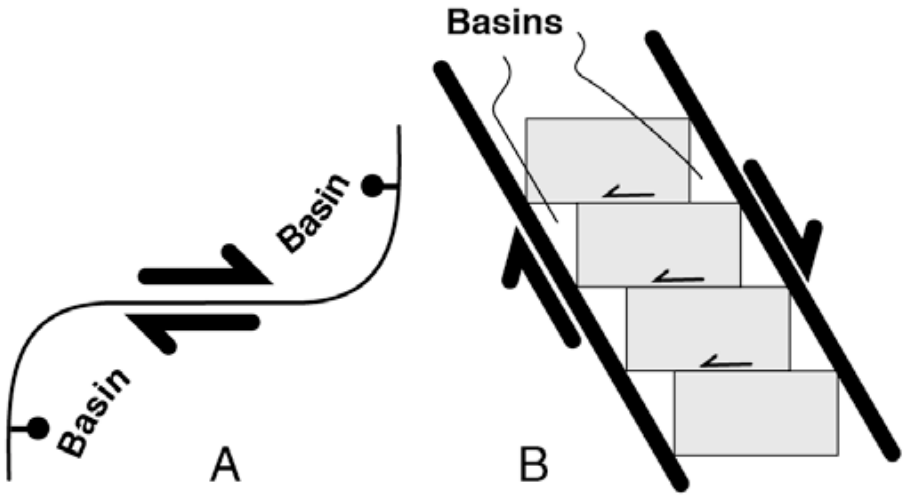

Figure 3-4. Strike-slip offset and crustal rotations appear to be the primary processes responsible for formation of basins in this portion of the Basin and Range, rather than normal faulting. See paragraph above for discussion.

STOP 3 - cont. -Sarah Nagorsen, Central Washington University..

THE ADOBE HILLS CALIFORNIA

Tectonic Setting

The Adobe Hills region is located within the western Mina deflection – a zone of northeast-striking, sinistral faults that transfer dextral fault slip from the northern eastern California shear zone into the Walker Lane Belt (Figure 1).

Northeast-striking sinistral faults in the Adobe Hills laterally displace older normal faults, Pliocene basalt flows, and underlying Miocene latite ignimbrite flows. The orientation and sinistral sense of motion across faults in the Adobe Hills supports the idea that the Mina deflections transmits fault slip via fault block rotation (Figure 2).

Offset Pliocene basalts across the Adobe Hills yield a minimum sinistral slip rate of about 0.4 - 0.5 mm/yr.

Evidence for Pleistocene fault slip in the Adobe Hills

The Adobe Hills region also lines the eastern edge of Mono Basin that once contained Pleistocene glacial Lake Russell. Paleoshorelines of Lake Russell indicate past highstands at least 160 meters higher than the present level of Mono Lake (Figure 3). Terraces and a bedrock channel in the western Adobe Hills document overflow of Lake Russell into Lake Adobe via the Adobe Hills Spillway. Pleistocene faulting in the Adobe Hills likely lowered elevations to provide a southeastern outlet for Lake Russell (Reheis et al., 2002).

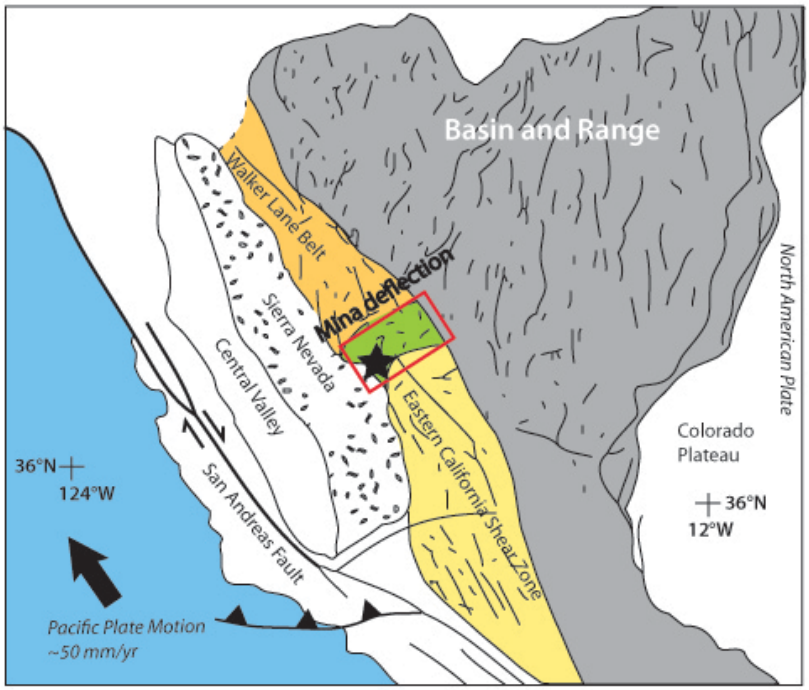

Modified from Lee et al., 2009

Figure 1 . Simplified regional fault map of the northern eastern California shear zone, Mina deflection, and Walker Lane Belt. Black star shows approximate location of the Adobe Hills region in the western Mina deflection.

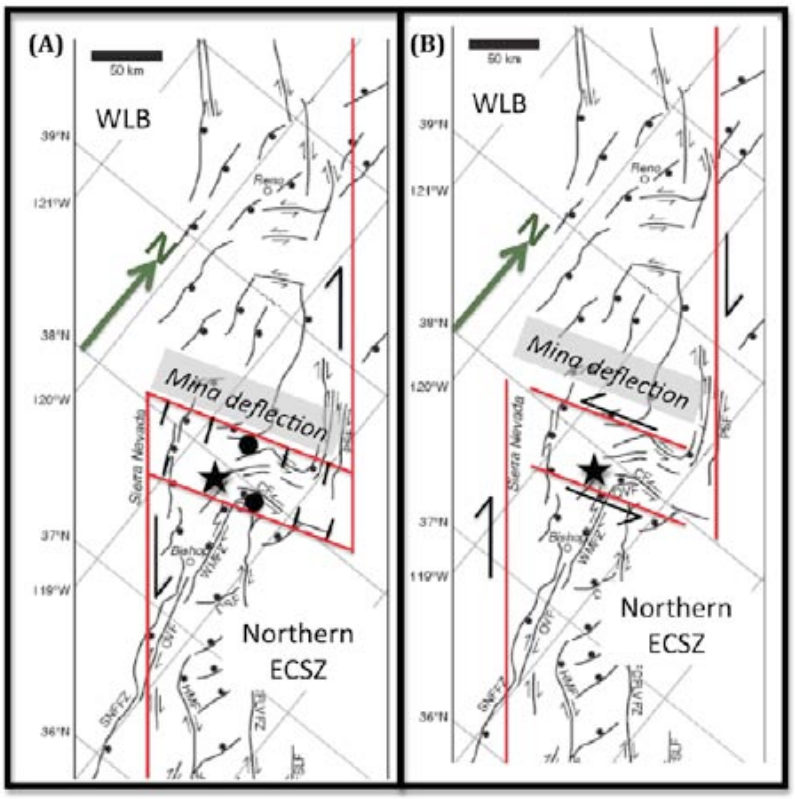

Figure 2 – Kinematic models proposed to explain fault slip transfer through the Mina deflection from the northern eastern California shear zone (ECSZ) to the Walker Lane Belt (WLB). Black star shows approximate location of the Adobe Hills region. (A) An extensional fault transfer model by Oldow et al. (1989; 1992) describes the Mina deflection as a large-scale pull-apart structure. (B) Block rotation model by Wesnousky (2005) predicts that rigid fault blocks and sinistral faults rotate clockwise during fault slip.

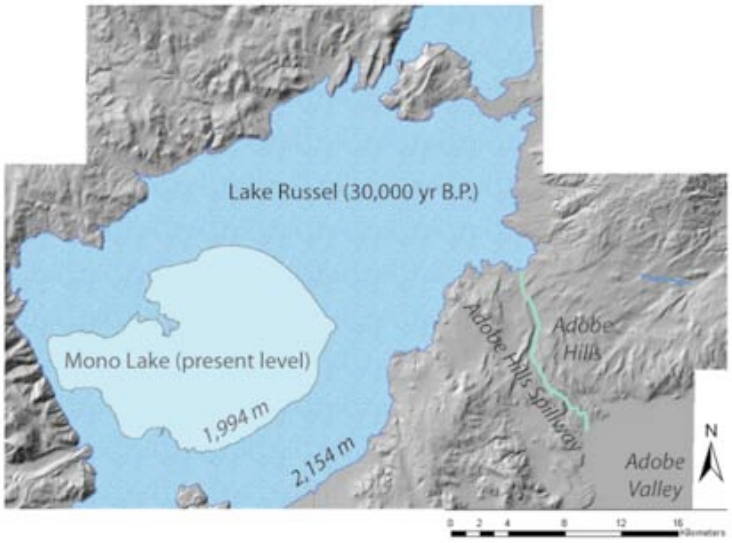

Figure 3 below left– DEM showing present water level of Mono Lake (1,994 meters), Pleistocene highstand of glacial Lake Russell (filled to its most continuous paleoshoreline), and the Adobe Hills Spillway.

REFERENCES

Lee, J., Garwood, J., Stockli, D., and Gosse, J., 2009, Quaternary faulting in Queen Valley, California-Nevada: Implications for kinematics of fault slip transfer in the Eastern California Shear Zone-Walker Lane Belt, Geological Society of America Bulletin, v. 121, p. 599 – 614, doi:10.1130/B26352.1.

Oldow, J.S., 1992, Late Cenozoic displacement partitioning in the northwestern Great Basin, in Lane, C., and Steven, D., eds, Geological Society of Nevada Walker Lane Symposium: Structure, Tectonics and Mineralization of the Walker Lane: Reno, Geological Society of Nevada, p. 17 – 52.

Oldow, J.S., Bally, A.W., Lallemant, H.G.A., and Leeman, W.P., 1989, Phanerozoic evolution of the North American Cordillera; United States and Canada, in Bally, A.W., and Palmer, A.R., eds., An Overview: Boulder, Colorado, Geological Society of America, Geology of North America, v. A, p. 139 – 232.

Reheis, M.C., Stine, S., and Sarna-Wojcicki, A.M., 2002, Drainage reversals in Mono Basin during the late Pliocene and Pleistocene: Geological Society of America Bulletin, v. 114, p. 991 – 1006.

Wesnousky, S. G., 2005, Active faulting in the Walker Lane: Tectonics, v. 24, TC3009, p. 1 – 35.

STOP 3 - cont. -Dylan Rood - UCSB & LLNL

Rates and timing of vertical-axis block rotations across the central Sierra Nevada-Walker Lane transition in the Bodie Hills, California/Nevada

Dylan H. Rood [a,b,*], Douglas W. Burbank [a], Scott W. Herman [a], Scott Bogue [c]

[a] *Department of Earth Science, University of California, Santa Barbara, CA 93106, USA*

[b] *Center for Accelerator Mass Spectrometry, Lawrence Livermore National Laboratory, Livermore, CA 94550, USA*

[c] *Department of Geology, Occidental College, Los Angeles, CA 90041, USA*

* Tel: 925-422-7378

Email address: rood5@llnl.gov (D.H. Rood)

We address the timing and spatial patterns of vertical axis block rotations across the central Sierra Nevada-Walker Lane transition by constructing a regionally extensive paleomagnetic dataset using 424 new samples from 47 sites from volcanic rocks of Early-Middle Miocene to Pliocene age. Our results underpin new insights about the evolution of block rotations within the Mina Deflection and Excelsior-Coledale domain, where dextral faults of the Eastern California Shear Zone step right into the central Walker Lane belt. Samples from the Upper Miocene (~9 Ma) Eureka Valley Tuff suggest clockwise vertical axis block rotations of 19-85° in the Bodie Hills between NE-striking left-lateral faults in the Bridgeport and Mono Basins (Fig. 1). Results in the Bodie Hills suggest clockwise rotations ($R \pm \Delta R$, 95% confidence limits) of 74 ± 8°, 42 ± 11°, and 14 ± 9° since Early to Middle Miocene (12-20 Ma), Late Miocene (8-9 Ma), and Pliocene (~3 Ma) time, respectively (Fig. 2), and permits a relatively steady rotation rate of 5 ± 2° Ma-1 (2σ) since the Middle Miocene with no detectable northward translation [Rood et al., in review]. Our data also suggest that rotation rates have probably not varied by more than a factor of two between or within each time interval. Furthermore, slip rates decrease by a factor of 3-5 northward between the northern Mono Basin to the Bridgeport Basin into the folded region of the Bodie Hills. The northward spatial pattern along strike of decreasing rates of fault slip on the Sierra Nevada frontal fault zone and increasing folding and block rotation in the Bodie Hills suggests that the region may be a transfer zone that accommodates N-S shortening and transrotation north and east of the Mina Deflection.

Our paleomagnetic data suggest rotations in the Bodie Hills began during or before the Middle Miocene, and are similar in age and long-term rate to block rotations in the Transverse Ranges associated with the early transtensional history of the San Andreas fault. We speculate that the timing of block rotations in the Bodie Hills indicates early dextral strain accommodation within the central Walker Lane resulting from the coupling of the Pacific-North America plates since the Middle Miocene. We also speculate that block rotations in the Bodie Hills may have occurred between reactivated faults in the Excelsior-Coledale domain and Mina Deflection whose orientations were controlled by crustal structure inherited from the Paleozoic (Sri = 0.7060 line, Fig. 1).

Geologic data in the Bodie Hills indicate that significant deformation can be accommodated by vertical-axis block rotations and folding in dextral shear zones such as the Sierra Nevada-Walker Lane transition. The identification of such deformation mechanisms is required for constructing valid deformation models, e.g., block models used to interpret modern geodetic data. Our results underscore the potential importance of such deformation styles in other areas of continental deformation; specifically, in areas of transtension or transpression where block rotations and folding are likely to occur in regions of dextral shear with unfavorably oriented sinistral faults, right-stepping dextral faults, and/or left-stepping normal faults. Moreover, structural complexity identified in the study area possibly suggests the importance of inherited crustal anisotropy to neotectonic

patterns (Sri = 0.7060 line, Fig. 1). The timing of rotation provides striking evidence for transmission of far-field stresses and transform plate boundary deformation deep into the North American plate beginning in the Middle Miocene.

The spatial variations in deformation patterns observed in this study provide insight into the modes of crustal deformation in transtensional zones. Regional patterns of fault slip rates and rotations show evidence for spatial compensation, whereby slip is transferred from one fault system to another or is accompanied by rotation or folding. North of Mono Basin, the 3-fold decrease in the slip rate on the Sierra Nevada frontal fault system northward suggests some component of deformation is being transferred to block rotations and folding between the Sierra Nevada and Walker Lane belt. Along-strike patterns in faulting, folding, and rotation also indicate several distinctive modes of deformation can function within a compact area. Within a 100-km distance

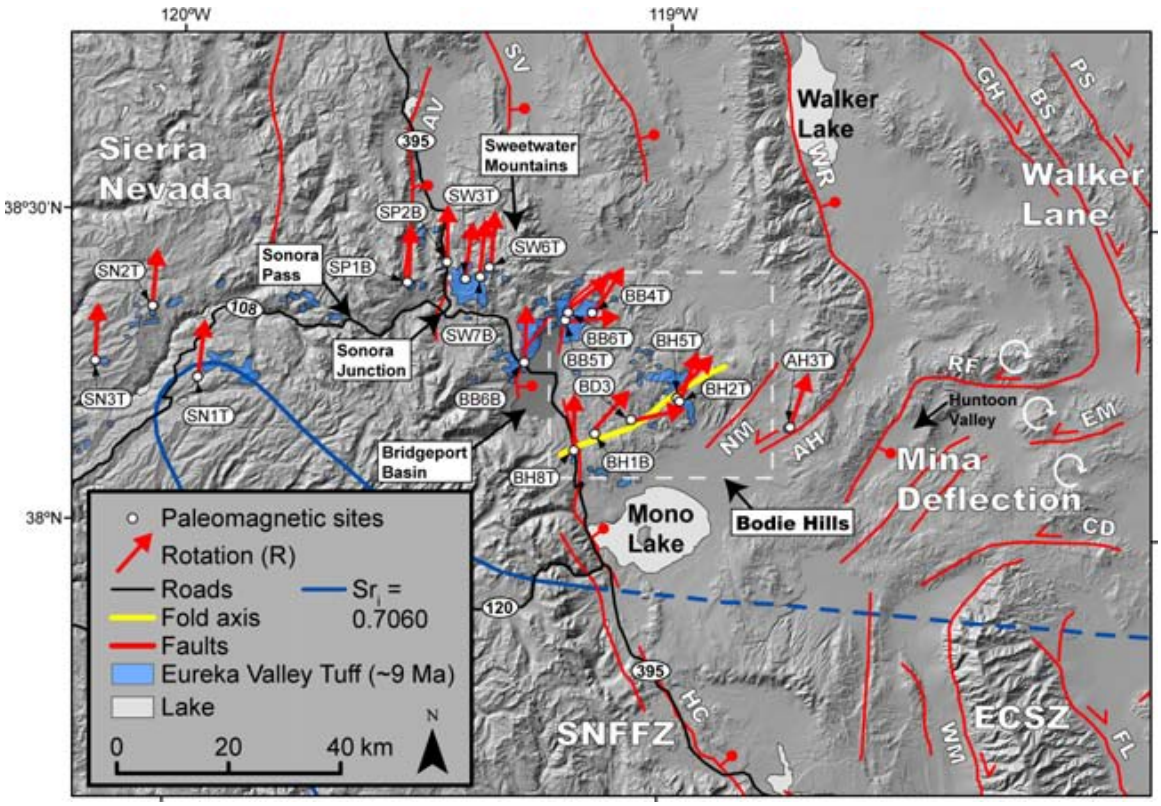

Figure 1. Map showing structure of the Sierra Nevada-Walker Lane transition in the study area, including faults, fold, and block rotations around the Mina Deflection. Also shows distribution of the Upper Miocene Eureka Valley Tuff, paleomagnetic sites, and clockwise rotations measured from paleomagnetic data. Sri = 0.7060 line is the location of the latest Precambrian–earliest Paleozoic rifted continental margin inferred from isotopic studies [Kistler, 1991]. AH=Anchorite Hills fault, AV=Antelope Valley fault, BS=Benton Springs fault, CD=Coaldale fault, ECSZ=eastern California shear zone, EM=Excelsior Mountains fault, FL=Fish Lake Valley fault, GH=Gumdrop Hills fault, HC=Hilton Creek fault, PS=Petrified Springs fault, NM=north Mono fault, RS=Rattlesnake fault, SNFFZ=Sierra Nevada frontal fault zone, SV=Smith Valley, WM=White Mountain fault, WR=Wassuk Range fault. Source: Rood et al. [in review].

along strike, tectonic patterns across Sierra Nevada frontal fault system show regions of trantension, transpression, and pure extension partitioned with dextral slip.

Our detection of vertical-axis block rotations is notable, but even rarer is the opportunity to reconstruct the rotations through time. Our work, however, would benefit from a more detailed absolute chronology of rocks sampled for paleomagnetism. Our data could accommodate a change of the rotation rate by a factor of two. Developing high-resolution dates for volcanic strata would potentially allow for stricter limits to be placed on changes in rotation rates.

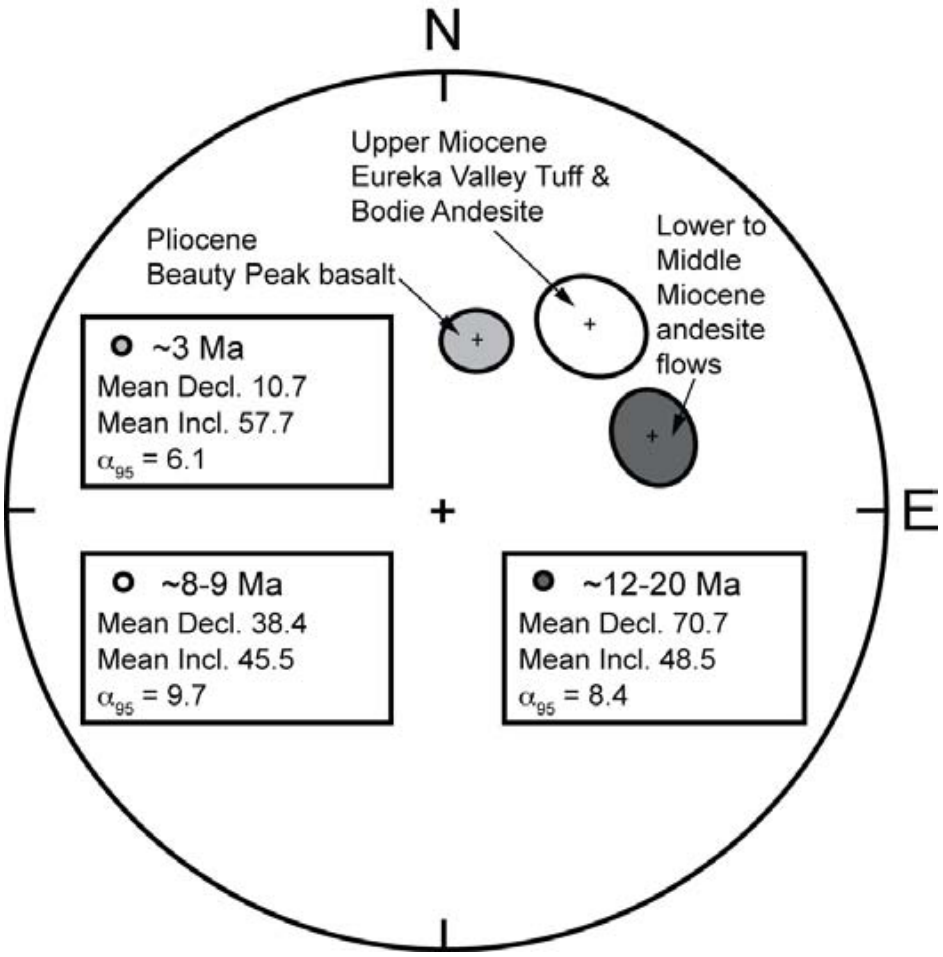

Figure 2. Formation-mean paleomagnetic directions and statistics for the Lower to Middle Miocene andesite flows, Late Miocene Eureka Valley Tuff and Bodie Andesite, and Pliocene Beauty Peak basalts in the Bodie Hills showing differential block rotation though time. A linear regression to the observed rotation magnitude versus age for the Bodie Hills data is consistent with a steady rate of clockwise block rotation of 5 ± 2°/My (2σ) since the Middle Miocene. Source: Rood et al. [in review].

References

Kistler, R. W. (1991), Chemical and isotopic characteristics of plutons in the Great Basin, In: *Geology and Ore Deposits of the Great Basin* (edited by Raines, G. L., et al.), Geological Society of Nevada, 107–110.

Rood, D. H., Burbank, D. W., Herman, S.W., Bogue, S. (in review), Rates and timing of vertical-axis block rotations across the central Sierra Nevada-Walker Lane transition in the Bodie Hills, California/Nevada, *Tectonics*

Day 2 - Sept 18 - Saturday - The Path...

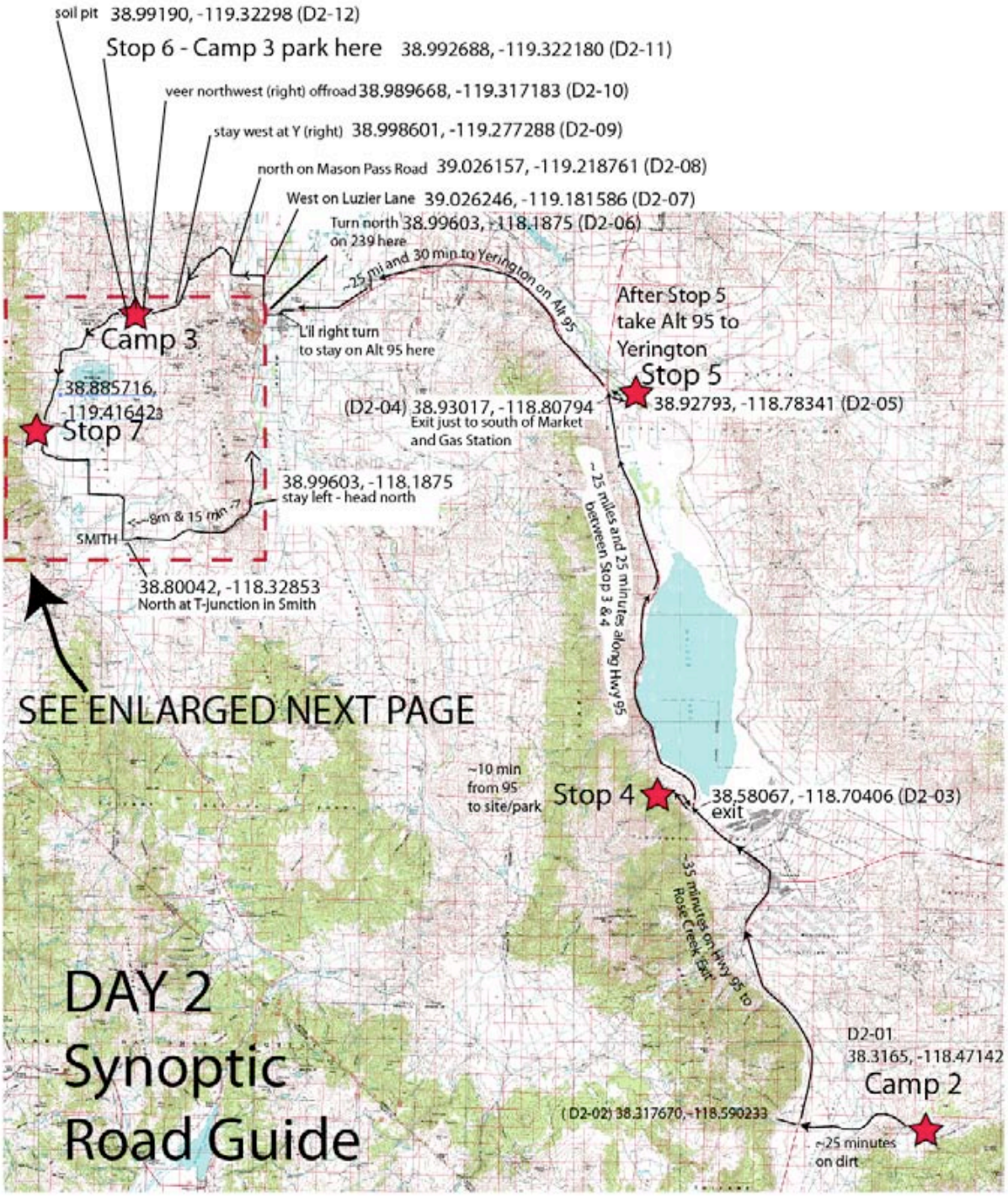

Figure 4-1a. *Day 2 Path Begins at Camp 2 and includes Stops 4, 5, and 6.*

Waypoints can be downloaded at FOP2010 website: http://neotectonics.seismo.unr.edu/0_FOP2010/FOP2010.html

Figure 4-1b next page

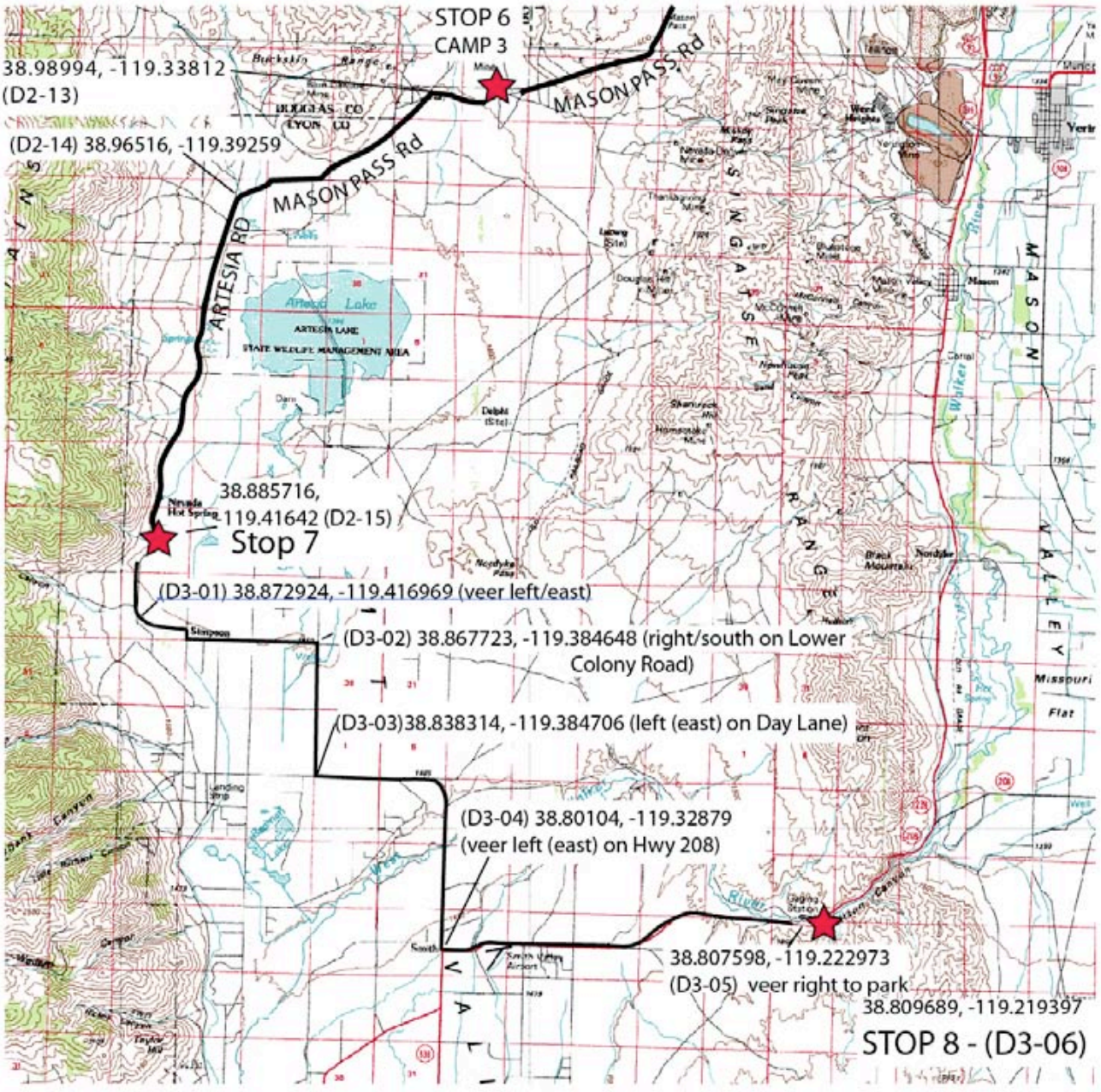

Figure 4-1. Enlargement of area in red box on prior page.

Waypoints can be downloaded at FOP2010 website: http://neotectonics.seismo.unr.edu/0_FOP2010/FOP2010.html

Stop 4 - Rose Creek, Wassuk Range

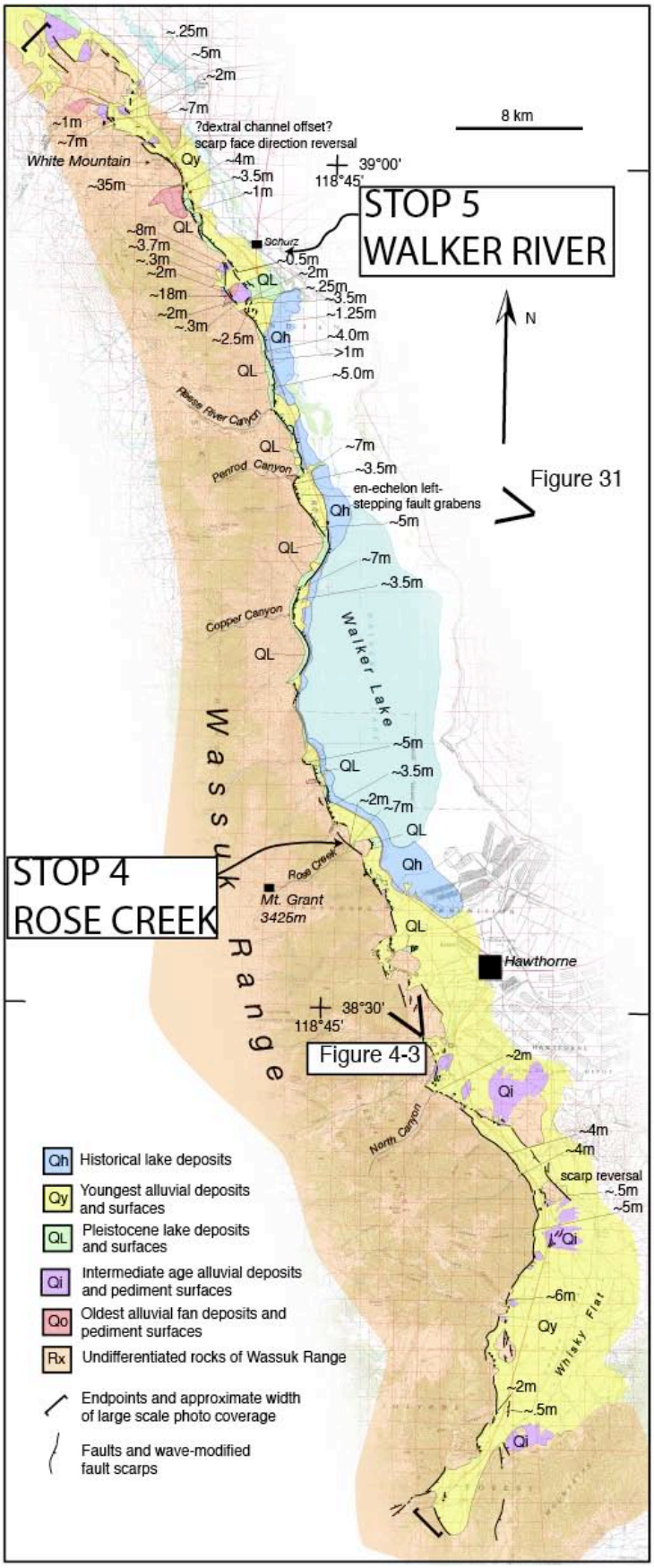

The Wassuk Range is an east-tilted fault block that strikes northwesterly about 50 miles, reaches elevations exceeding 3000 m, and is bounded on the east by a high-angle normal fault **(Figures 4-2 and 4-3**). Thermochronologic analysis suggests that much of an 8.5 km unroofing and uplift of the range occurred between ~15 Ma and ~12 Ma, followed by a later period of extension concentrated along the east flank of the range ~4 Ma [*Stockli et al.*, 2002]. The steep east flank of the range exhibits the abrupt sinuous trace and triangular facets characteristic of an active normal fault **(Figure 30**). The deepest part of the adjoining basin is filled by Walker Lake. Walker Lake has dropped ~40 m in level since the turn of the century due to human water diversions and reached elevations of ~1330 m during late Pleistocene about 13 ka [e.g., *Adams and Wesnousky*, 1999]. Holocene scarps commonly reach 4 m to 6 m height and are present at the mouths of active washes along the entirety of the rangefront. Longer-term Quaternary offset is preserved in 20 m to 40 m high scarps truncating older alluvial fan surfaces near White Mountain, southwest of Schurz, and Penrod Canyon.

Figure 4-2. Fault trace along Wassuk rangefront. Scarp heights labeled in meters. Units Qy, Qi, and Qo are Quaternary surfaces of relatively increasing age. Lacustrine deposits exposed primarily during historical lake recession denoted Qh. Surfaces largely unmodified since recession of late Pleistocene Lake Lahontan are QL. Unit Rx is undifferentiated rocks.. Perspectives of photo in Figure 4-3 is shown by open ended V shape. adapted from Wesnousky, 2005

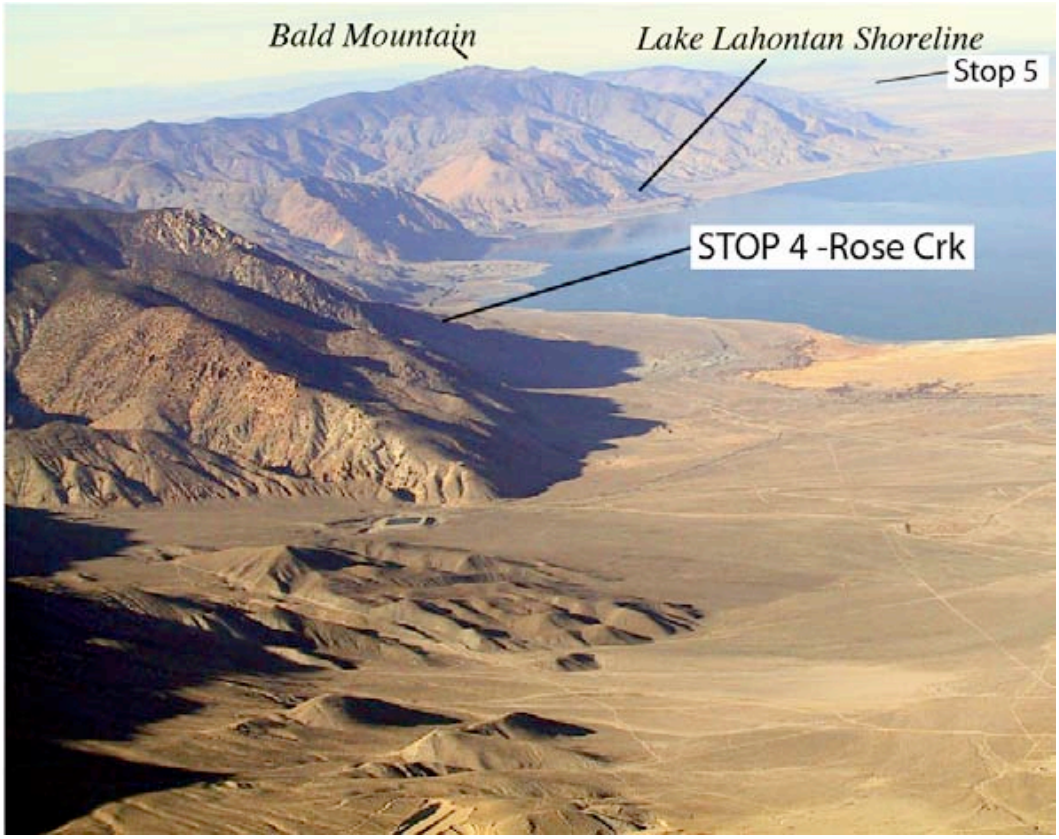

Figure 4-3. View north along Wassuk rangefront and Walker Lake from near North Canyon. Steep rangefront, triangular facets, and sinuous rangefront reflect active normal faulting. Perspective of photo shown in Figure 29. Wavecut benches and escarpments mark shoreline of pluvial Lake Lahontan along the base of the rangefront. Photo: Wesnousky

This particular stop will be hosted by

John Bell, NBMG
Jayne Borman, UNR
Nick Hinze, NBMB
Marith Reheis, USGS
Jeff Shoffner, Colorado School of Mines
Ben Surpless, Trinity College, TX.

Topics to be touched on include paleoseismology and a trench along the rangebounding normal fault , the history and rate of slip of the rangebounding fault, the role of neotectonics and geophysics in the search for geothermal, and discussion of ancient Lakes that once filled the basin. .

STOP 4 IS ON U.S. MILITARY PROPERTY. OUR ADMITTANCE AS WELL AS A GOOD DEAL OF THE RESEARCH TO BE PRESENTED IS THROUGH THE COURTESY AND FACILITATION OF JOHN PETERSON. IT IS THE WATERSHED FOR HAWTHORNE. RESTRICT YOURSELF TO THE PORTA-POTTIES PROVIDED AND UNDER NO CIRCUMSTANCES USE THE GREAT OUTDOORS. SAY HELLO AND THANKS TO JOHN, HE SHOULD BE HERE

STOP 4 - Jayne Borman, CNS - NBMG - DGS - UNR

Holocene earthquakes on the Wassuk Range fault zone: Paleoseismic observations from the Rose Creek Fan, Hawthorne, Nevada, USA.

Jayne Bormann, Alex Sarmiento and Steve Wesnousky
Center for Neotectonic Studies, University of Nevada, Reno

The broad fan emanating from Rose Creek is modified by both Lahontan and historical-highstand Lacustrine shorelines deposits at it's lower end and cut by fault scarp at it's head (Figure 4-4).

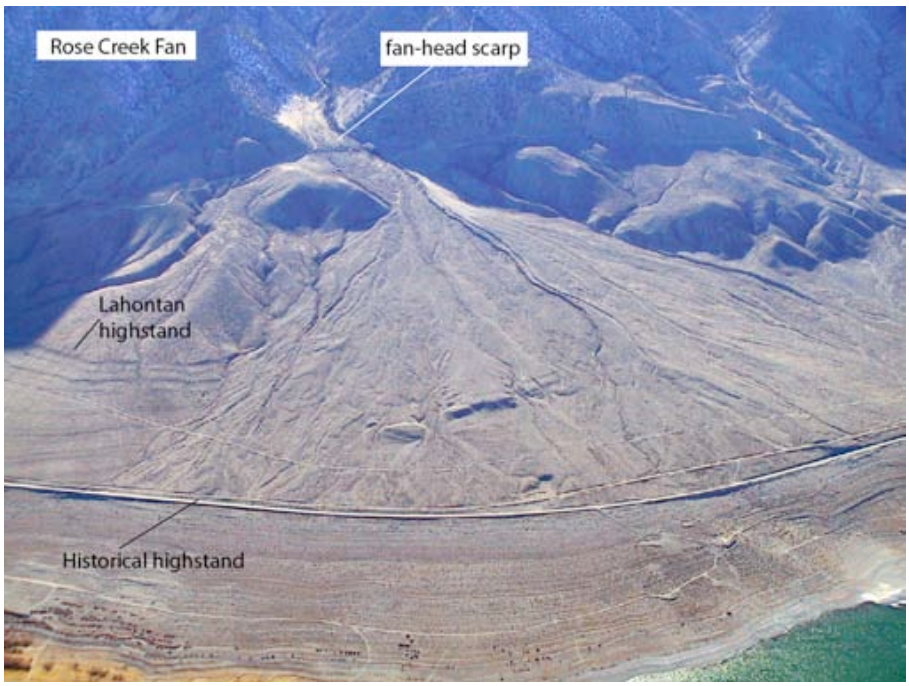

Figure 4a. Photo of Rose Creek Fan- viewed from the east.. Photo: Wesnousky

The scarp in the Rose Creek fanhead cuts across Rose Creek (Figure 4-4 & 5). The scarp height is ~7m south of the creek and abruptly decreases to ~2m south of the creek where it cuts a younger fan element. Demsey (1987) interpreted soils on the footwall to be Holocene and the multiple scarp sizes to indicate the occurrence of two surface rupture earthquakes at this locality during the Holocene. We excavated trenches across the scarp to confirm the idea and quantify the recency and recurrence of slip on the fault (Figure 4-5).

The Rose Creek South (RCS) trench was excavated across a ~7 m scarp cutting an intermediate age alluvial surface to the south east of Rose Creek (Figure 4-5). The ~30 m-long

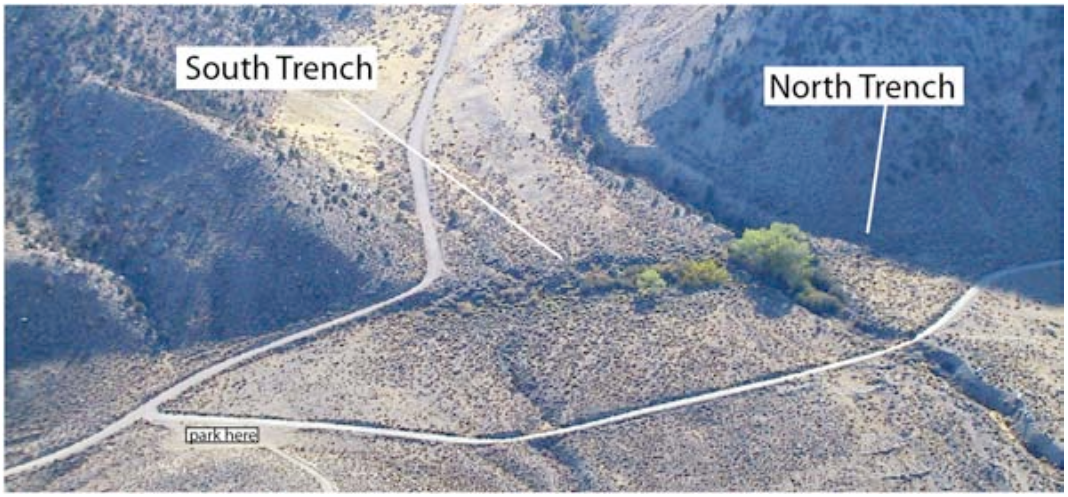

Figure 4-5. Character of Rose Creek fan-head scarp and location of trenches. photo: Wesnousky

exposure shows thick, massively bedded, eastward dipping debris flow deposits cut by the down-to-the-east WRFZ (Figure 4-6). The oldest unit exposed in the trench (unit 1) is a debris flow deposit capped by a 20-30 cm thick, organic-rich, peat-like layer. This unit is overlain by a thick package of light tan, massive, unsorted, matrix-supported debris flows (unit 2). Hiatuses in fan deposition are marked by slight reddening of the flow surfaces and are indicated in the trench log as thin dashed lines within the unit. Units 1 and 2 are cut by an eastward-dipping normal fault. Although the deposits are similar, an unambiguous match of internal layers present in unit 2 in the hanging and foot wall was not observed. Unit 3 is a tan, massive, wedge shaped gravel deposit that lacks internal stratigraphy and thins to the east, separating the exposures of unit 2. Units 2 and 3 are cut by fissures filled with reddish brown, loose, unsorted material with vertically aligned clasts (unit 4) in both the hanging and foot walls. Unit 4 is potentially offset by an upward continuation of the main fault strand, although this relationship is obscured by disturbed stratigraphy due to the presence of a large boulder in the trench wall. Unit 5 is an unfaulted, modern, slope-wash deposit that overlies units 2, 3, and 4 and is capped on the distal end of the hanging wall by a tephra bearing fluvial deposit (unit 6) and slopewash and aeolian sediments (unit 7).

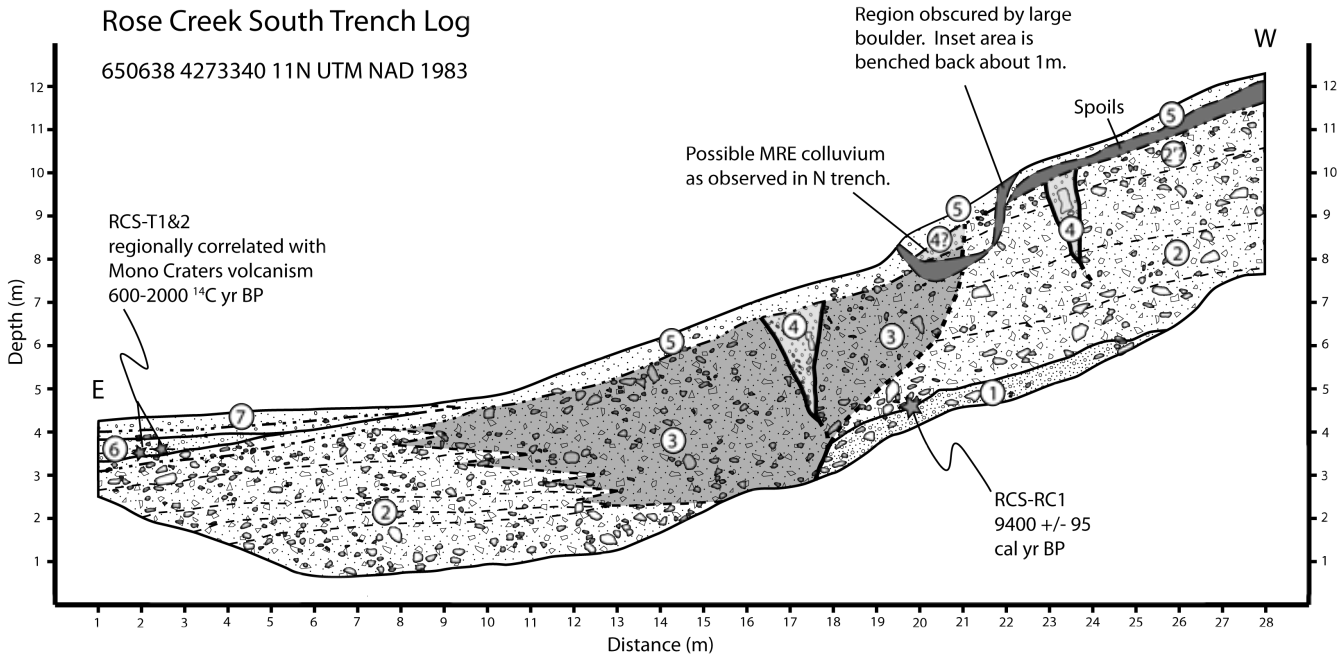

Figure 4-6. Sketch of the southern trench exposure across the Wassuk Range fault zone at the Rose Creek fan. Location is shown in Figure 4-5. Unit label numbers and shading correspond to description in text. The trench records the occurrence of at least two earthquakes between ~9400 cal years BP and 600-2000 ^{14}C years BP. The penultimate event is evidenced by the truncation of units 1 and 2 in the footwall and by the triangular shaped colluvial wedge (unit 3). A smaller most recent event is evidenced by the fissures (unit 4) that cut units 2 and 3.

The relationships in the RCS trench are interpreted to record at least two Holocene earthquake displacements. Fissures (unit 4) extending through units 2 and 3 to the base of the modern surface are interpreted to be evidence of the most recent event (MRE). Unit 3 is interpreted to be fault-derived colluvium from the scarp created during the penultimate event. The mismatch between layers of unit 2 in the hanging and foot walls allows for the possibility of one or more previous events. Radiocarbon analysis of charcoal taken from the peat-like layer at the top of unit 1

at meter 20 yields an age of ~9400±95 calendar years B.P. We interpret this date as a maximum bound on the age of the penultimate event. Additionally, the tephra found in undisturbed unit 6 is regionally correlated with the latest episode of Mono Craters volcanism and dates between ~600-2000 14C years B.P. (Wesnousky, 2005; J. Bell, Nevada Bureau of Mines and Geology, Reno, Nevada, personal communication, 2010), bracketing the age of faulting observed within the trench.

The Rose Creek North (RCN) trench was excavated across a ~2m scarp in a young alluvial fan surface to the northwest of Rose Creek (Figure 4-5). Figure 4-7 shows a sketch of the approximately 20 m long exposure. The trench exposed offset debris flow and alluvial gravel deposits in combination with a set of colluvial packages. The oldest unit exposed in the trench (unit 1) is composed of red brown alluvial gravel layers alternating with gray tan debris flow deposits. Although a similar fabric is present in unit 1 on both sides of trench, the correlation of layers within the unit is not possible. Unit 2 is composed of loosely compacted sand and gravel, with concentrations of clast supported cobbles and boulders. Unit 2 fills the fault-bounded fissure and forms a triangular shape that thins to the east over the hanging wall, separating the exposures of unit 1 in the trench. Unit 2 is overlain by a poorly consolidated, unsorted, gray tan debris flow (unit 3), which is displaced across unit 4. Unit 4 is composed of loose sand and gravels that fill a small fissure. The entire exposure is capped by a brown tan, matrix-supported, slope-wash deposit (unit 5) that contains a tephra bearing, waterlain subunit (unit 5a).

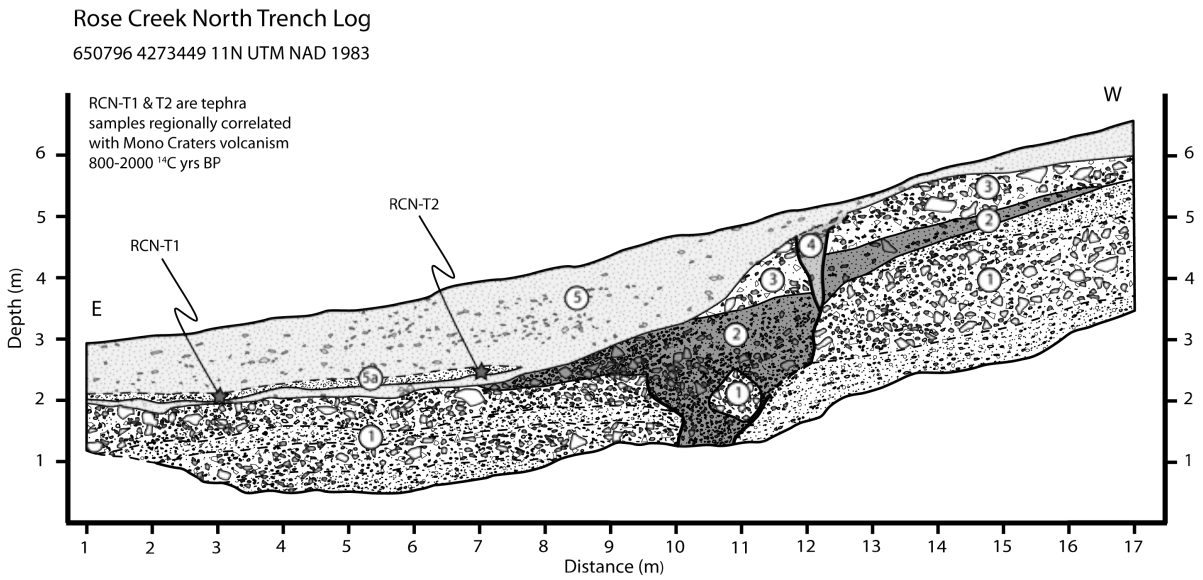

Fig4-7. Sketch of the northern trench exposure across the Wassuk Range fault zone at the Rose Creek fan.
Location is shown in Figure 4-5. Unit label numbers correspond to description in text. The trench records the occurrence of at least two earthquakes Holocene earthquakes predating 600-2000 ^{14}C years BP. The penultimate event is evidenced by the truncation of unit 1 in the footwall and by the large triangular shaped colluvial wedge and graben fill (unit 2). A smaller most recent event is evidenced by the offset of units 2 and 3 across the fault and by the resulting fissure fill (unit 4)

The stratigraphy in the RCN trench is interpreted to record at least two surface rupturing earthquakes. Unit 2 is a graben fill and fault-scarp derived colluvial unit that accumulated after unit 1 was offset during the penultimate event. The colluvium was overlain by unit 3, which was subsequently faulted during the most recent event (MRE). The presence of the Mono Craters tephra (unit 5a) in unfaulted hanging wall deposits indicates that both earthquakes recorded in the trench

occurred prior to ~600-2000 14C years B.P. The mismatch of unit 1 across the fault permits the possibility of at least one additional prior slip event. Vertical displacement for the MRE determined from offset of the base of unit 3 across the fault is at minimum ~0.7 m. A minimum of ~1.5 m of vertical displacement resulting from the penultimate event was determined by projecting the base of the colluvial wedge (unit 2) across the graben fill and measuring the thickness of the wedge..

Discussion and Conclusions. The stratigraphic, structural, and age relations described at the Rose Creek fault trenches and fan provide the framework for our interpretations bearing on the frequency, size, and timing of large earthquakes on the WRFZ. The RCS trench records at least two faulting events in a ~7 m scarp on an intermediate age fan surface between ~9400 cal years B.P. and the deposition of the Mono Craters tephra (Figures 3 and 5). The RCN trench also records at least two surface rupturing earthquakes, however the trench crosses a smaller ~2 m scarp in a younger fan surface (Figure 4-5). We interpret colluvial unit 2 in the RCN trench and unit 3 in the RCS trench to result from the same earthquake. Both units are of similar shape and form, with the exception that unit 2 in the RCN trench is not associated with a large scarp. The lack of a large scarp may be attributed to incision of the Qfi surface subsequent to the earthquake that produced the broad channel and younger surface in which the RCN trench sits and may have been associated with the deposition of unit 3 (Figure 4-7). We interpret the 0.7m offset of units 2 and 3 in the RCN trench to be correlative with the small fissures (unit 5) in the RCS trench (Figure 4-6), with both offsets resulting from the MRE. In light of the close proximity between the two trenches, we find it reasonable that sites share the same earthquake history: a large penultimate event followed by a smaller MRE. This conclusion opens the possibility that the simple scarps profiled by Wesnousky (2005) and Dempsey (1987) to the north and south of Rose Creek may also record multiple Holocene events.

In summary, our observations confirm multiple Holocene surface rupturing earthquakes along the WRFZ. The combined paleoearthquake record from both trenches records at minimum two earthquakes between ~9400 cal years B.P. and the deposition of the Mono Craters tephra, with a large penultimate event followed by a smaller MRE. This gives an average Holocene recurrence interval of ~3650-4450 years for surface rupturing earthquakes and establishes the WRFZ as a major structure accommodating extension in the Central Walker Lane.

Acknowledgements This work was supported by the National Science Foundation grant EAR-0635757 as part of the EarthScope project. We are grateful to the Hawthorne Army Depot and John Peterson for permitting us access to the Rose Creek site. Thank you to John Bell for helpful conversation regarding the age of faulting along the Wassuk Range and to Kyle House for his wealth of knowledge regarding the use of LiDAR data. Rich Koehler provided many thoughtful insights and suggestions that improved the clarity of this work.

References: Dempsey, K., 1987. Holocene faulting and tectonic geomorphology along the Wassuk Range, west-central Nevada. MS Thesis, Tucson, University of Arizona, 64 p.

STOP 4 - Nick Hinz - NBMG

Structural controls of three blind geothermal resources at the Hawthorne Ammunition Depot

Presented by Nick Hinz[1], John Bell[1], and Jeff Shoffner[1]
[1]Nevada Bureau of Mines and Geology, University of Nevada, Reno
[2]Colorado School of Mines

Text extracted from papers published in the 2010 Geothermal Resources Council Transactions (Hinz et al, 2010; Moeck et al., 2010; Shoffner et al., 2010)

Introduction and Geologic Setting

Previous studies have demonstrated that faults are the primary control on geothermal systems in the western Great Basin (e.g. Faulds et al., 2006). In cooperation with the U.S. Navy Geothermal Program Office, we have developed a structural model from which to identify and evaluate geothermal resources and select new drill target areas for future exploration at the Hawthorne Army Depot (HAD) in the southern part of Walker Lake basin, western Nevada.

The ~80 km-long Walker Lake basin marks a major physiographic break along the western boundary of the Walker Lane, coincident with a transition between a region dominated by NW-striking dextral strike-slip faults to the east and a region dominated by N- to NW-striking normal and dextral-oblique faults with locally high-magnitude extension extending westward to the Sierra Nevada (Oldow, 1992; Proffett, 1977; Stewart, 1988; Wesnousky, 2005). The Neogene structures of the Walker Lake basin are localized along a late Mesozoic crustal boundary, the Pine Nut fault system that separates rocks of the Sierran arc from most of the back-arc basin. Mesozoic basement rocks west of this boundary are composed of complexly deformed metamorphic rocks intruded by numerous granitic plutons. East of the boundary, Mesozoic basement rocks consist of metamorphic rocks that were deformed in the Luning-Fencemaker thrust belt and intruded by less abundant plutons (Oldow, 1983, 1984; Oldow et al., 1993).

The Wassuk Range records rapid extension between 15 and 12 Ma with a second stage of extension beginning at ~4-3 Ma. Dextral shear associated with the Walker Lane migrated through the region between ~12-6 Ma with the largest magnitude strike-slip faults developing to the east of Walker Lake basin. Kinematically linked with normal faults, the dextral faults locally reorganized concurrent with the renewed extension ~4-3 Ma (Oldow et al., 2008; Stockli et al., 2002; Surpless et al., 2002).

Structural Framework

The Walker Lake basin is a complex half-graben, bound on the west by the Wassuk Range front fault system and defined to the east by a broad, gently west-dipping ramp, cut locally by west-dipping antithetic faults. Within the map area, the Wassuk Range front fault bifurcates into two major strands from the Lucky Boy Mine area to the mouth of Cat Creek (faults A and B, Fig. 1). Based on field evidence, well data, and 3D seismic data, the major NW-striking strands of the range-front fault system dip ~30° to 55° NE, whereas the NE-striking part of fault A at the mouth of Cat Creek dips ~65° SE. The overlap area between faults A and B is cut by numerous N- to NE-striking, east- and west-dipping normal faults with ~45-65° dips. The Walker Lake basin half-graben contains up to 1.7 km of Neogene volcanic rocks and basin fill sediments and is cut by multiple N- to NW-striking E- and W-dipping normal faults, including the newly identified Hawthorne fault zone that extends NNW from the step-over region of the range- front to a N-striking, W-dipping antithetic

fault system coincident with the west side of the Gillis Range (Bell and Hinz, 2010; Shoffner et al., 2010). Displacement along these normal faults

Figure 1. Semi-transparent geologic map draped over shaded relief image. Gravity contours 0.5 mGal

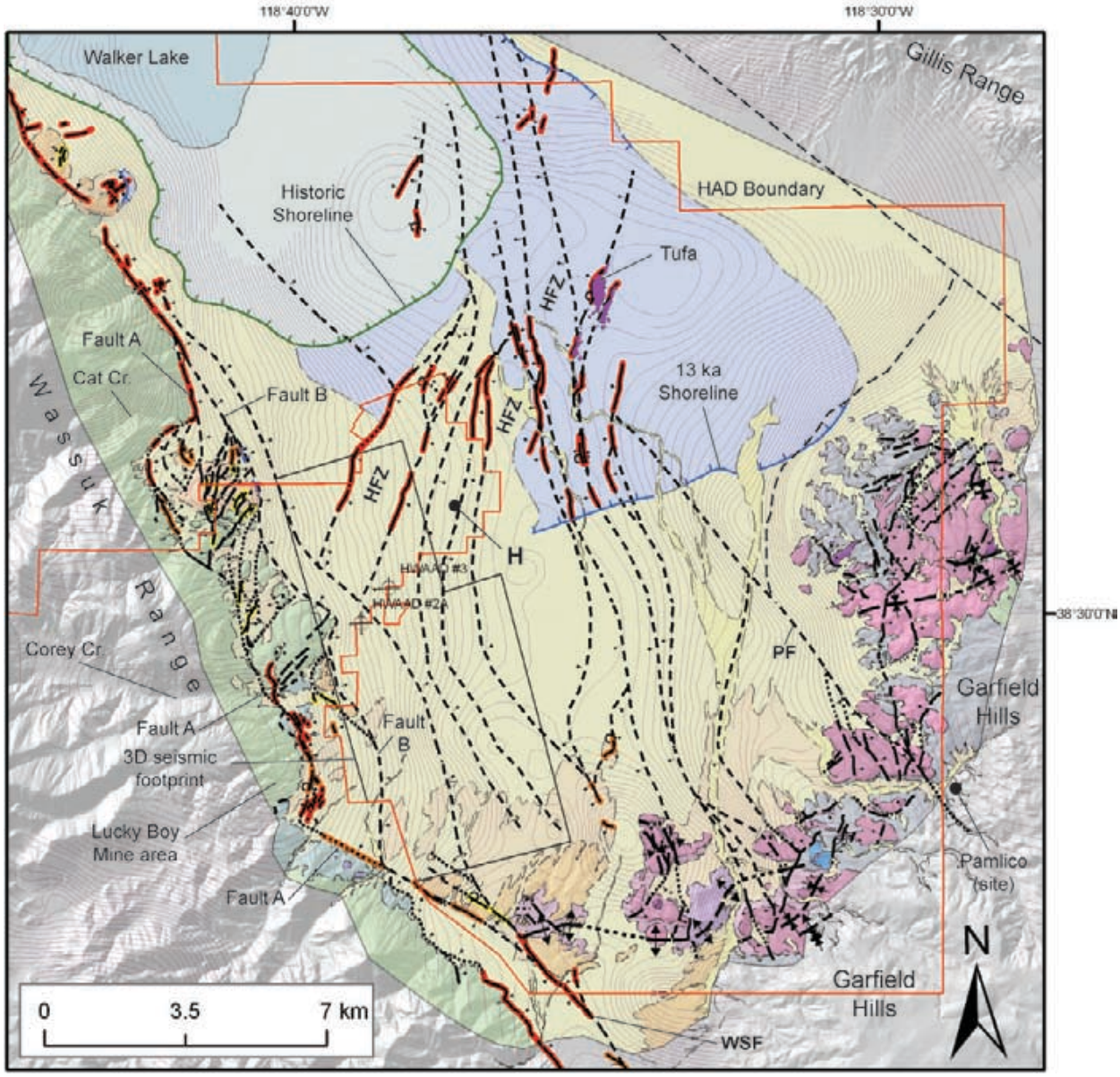

(Shoffner et al., 2010) are shown in light brown lines. Faults: highlighted red, Holocene; highlighted orange, Pleistocene; highlighted yellow, Quaternary undivided; dashed, inferred from subsurface and geophysical data. HAD boundary in red outline and 3D seismic data footprint in black outline. H, town of Hawthorne; HWAAD #2A and HWAAD #3, U.S. Navy GPO geothermal wells; HFZ, Hawthorne fault zone; PF, Pamlico fault; WSF, Willow Springs fault.

within the basin ranges up to 0.5 km. Tilt of Neogene strata filling the basin are not well constrained. Several west-tilted fault blocks identified in the 3D seismic data dip gently 15° west

with a decrease in dip up section. Dips range from 5 to 20° W in un-folded, late Miocene basaltic andesite that project into the basin along the west edge of the Garfield Hills.

The Garfield Hills are cut by a system of kinematically linked NW-striking dextral faults and NE-striking sinistral-oblique faults. The Pamlico strike-slip fault (informally named in this paper for the Pamlico site, Fig. 1) corresponds to a steep NW-striking, SW-decreasing gravity gradient that extends into the Walker Lake basin. Another steep gravity gradient that probably marks a NE-striking, NW-dipping fault bounds the NW end of the Garfield Hills. However, no exposures of this fault zone were identified at the surface. The Pamlico strike-slip fault may continue northwest into the basin with part of the strain stepping right around the northwest end of the Garfield Hills to another unnamed strike-slip fault and part of the strain continuing northwest linking with the Hawthorne fault zone near the south end of the tufa deposits. These geometries suggest that the embayment along the east side of Walker Lake basin north of the Garfield Hills has developed in a right step in a dextral fault system.

Gravity

The purpose of collecting gravity in the Southern Walker Lake Basin was to greater understand the structure at depth to minimize the need for exploratory drilling in on-going geothermal exploration. Unfortunately, gravity solutions are non-unique and resulting structural solutions are highly dependent on the assumed density contrast of the units modeled. Cross sections developed from detailed geologic fieldwork (Hinz et al., 2010) were the basic model for the gravity forward modeled profiles. Depth constraints were provided by two mid-depth drill holes (HWAD 2a: 1430 m and HWAD 3: 1220 m) that locally intersected basement depth at ~320 m and ~460 m, respectively. The density profile Figure 2 (Section D-D') shows the progressive down dropping of JKgr as well as the Ta unit on the west side of the valley, with the valley ramping up into the Garfield Hills. Thickness of the alluvium at the location of this cross section is approximately 1 km. This is not only consistent with geologic interpretations from Hinz et al. (2010), but fits the collected gravity data with low error. The contact between JKgr and Mzu is unknown and assumed in the section. Also, due to the geologic complexity of the Garfield Hills to the east, interpretations on the east side of the valley are oversimplified. Further work will hope to improve these results.

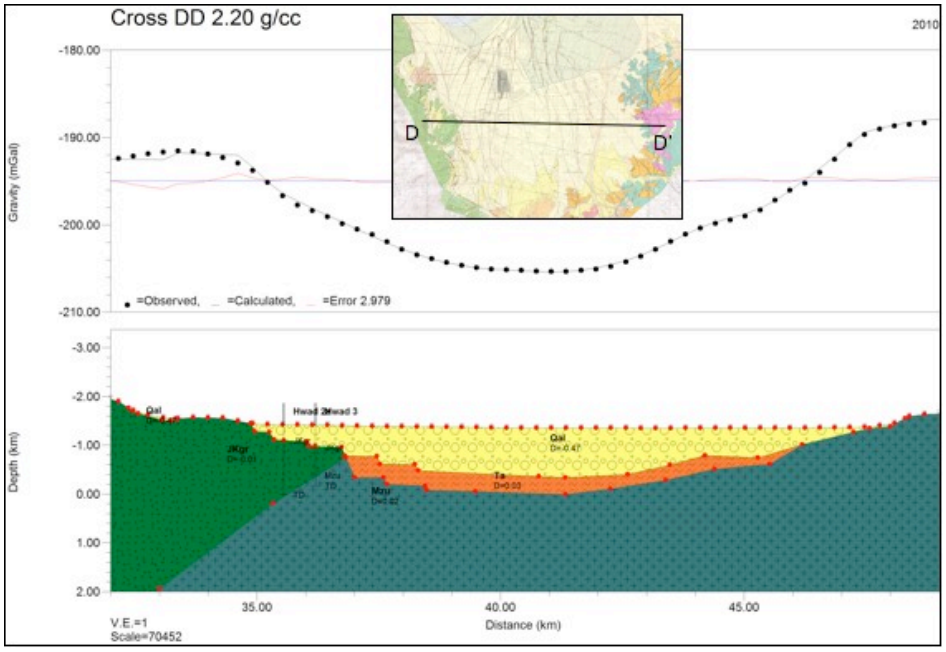

Figure 2. (Preceding page) 2D density section across Southern Walker Lake Basin showing four main units, Qal ($\rho = 2.20$), Ta ($\rho = 2.70$), JKgr ($\rho = 2.67$), and Mzu ($\rho = 2.69$), with the west showing a progressive down-dropping of the Wassuk Range and basement, and the east showing the ramping of the basement into the Garfield Hills.

Stress field determination

The stress field can be derived from fault slip data assuming a linear and direct relationship between strain and stress. Relating fault kinematics to stress states implies that all fault slip data were generated by the same deviatoric stress state. However, it is still under debate whether kinematic indicators from field based fault plane analysis can be used for stress field determination. One major challenge is the heterogeneity of data sets, caused by paleo stress fields or strain partitioning. In particular, strain partitioning along fault bends or relay ramps can evoke abnormal stress tensors in classical stress inversion from fault slip data (Angelier, 1994; Fodor, 2007). We present a methodology to calculate the stress tensor from field based data that incorporates possible local stress variations caused by strain partitioning and characteristic shear angles of different lithologies.

Our methodology involves the PTB method combined with a statistical analysis of shear stress vectors and stress ratios. The PTB method is a method that calculates the strain tensor from fault slip data. Assuming a linear relation of strain to stress, our methodology might deliver a reliable stress state when kinematically inconsistent structures are identified in the data set rather than in the field.

In particular, the PTB (P=Pressure T=Tension B=Intermediate) method is a kinematic analysis in brittle deformation that calculates the three theoretical principal strain axes for each individual fault-slip datum, i.e. a compressional axis P, a neutral axis B (which lies in the fault plane), and an extensional axis T (e.g. Sippel et al., 2009). Employing the Mohr-Coulomb failure criterion, the method incorporates a defined fracture angle between P and the slip surface. For this study, a fracture angle of 30° was applied. Assuming fault slip was induced by the same stress state, the orientation of each fault plane is dependent on the causative stress field. The application of PTB to the entire fault population of a particular location results in a comprehensive pattern of kinematic axes. Such a cumulative plot permits detection of kinematic consistencies as clusters of P, B, T axes in a heterogeneous data set.

The slip tendency method is also used in this study to calculate the state of stress of faults in the current stress field based on frictional constraints (Morris et al., 1996, Moeck et al., 2009). With this method, the ratio of shear to normal stress can be calculated for each fault or inferred faults. By calculating the normal stress, slip and dilation tendency can be determined. The slip tendency is expressed by $Ts = \tau/\sigma neff \geq \mu s$. With Ts=slip tendency, τ =shear stress, $\sigma neff$ =effective normal stress, μs = friction coefficient. The dilation tendency is expressed by $\tau d=(\sigma 1-\sigma n) / (\sigma 1-\sigma 3)$. If the slip tendency Ts equals or exceeds the frictional coefficient, the fault is likely to slip. Such a fault is referred to as critically stressed. Slip occurs when μs is between 0.6-0.8 (Byerlee, 1978). The dilation tendency is normalized to the normal stress σn and can have a maximum value of 1. Bi-modal dip refers to both possible dip directions, perpendicular to strike. **Results**

The resulting 3D structural geological model shows the fault and horizon geometries of a NNW-trending graben structure (Fig. 3). The release bend at the Wassuk Range front fault (red box in Fig. 3) is an area of structural complexity presumably caused by secondary faults in a transtensional

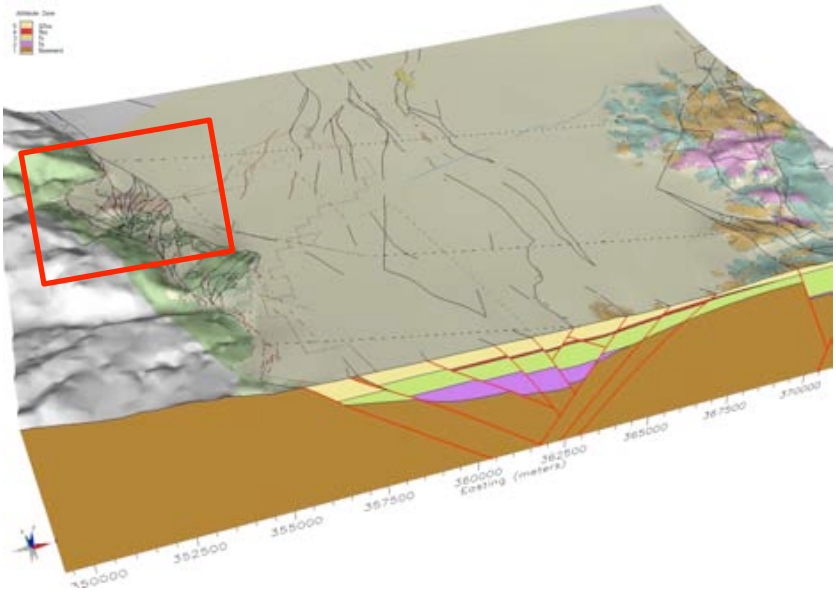

Figure 3. 3D geological model of the Hawthorne area. The red box surrounds the releasing bend at the Wassuk Range front fault. This area is shown in detail in figure 4.

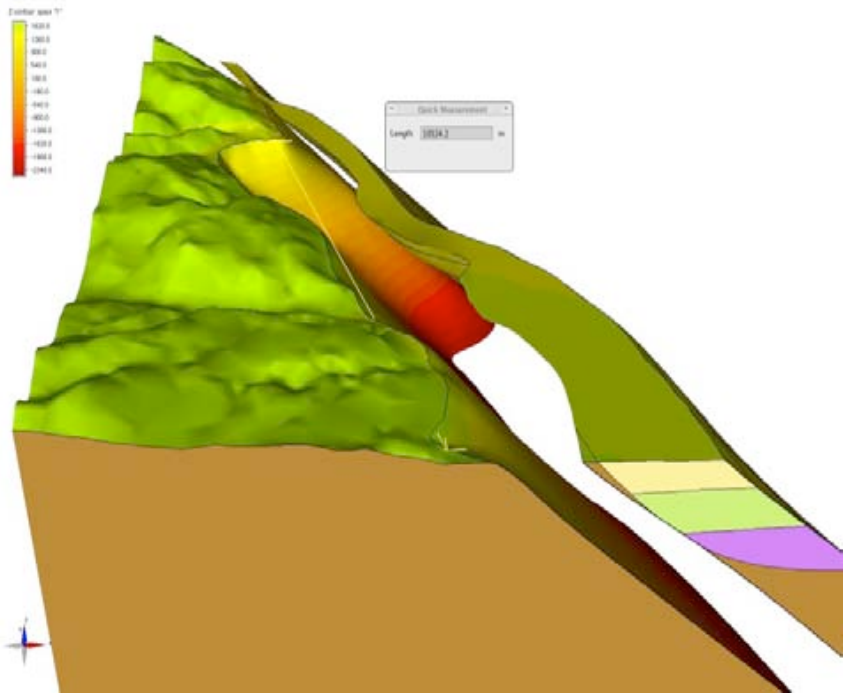

Figure 4. 3D perspective along the releasing bend at the Wassuk Range front fault. The release bend leads to a transtensional jog between two faults.

regime. The releasing bend has a dilational effect on the Wassuk Range front fault and on the geometry of the overall fault grain of this particular region (Fig. 4).

Most of the faults yielding slip data strike NE-SW and indicate normal dip slip to oblique slip motion (Fig. 5a). The stress field determination results in a normal faulting stress regime that indicates extension in NW-SE direction (127°, Fig. 5b). A fluctuation histogram shows the variation of calculated shear stress vector of the derived stress field to measured slip vectors (Fig. 6). This

variation shows basically the misfit of measured to calculated shear stress vectors and indicates different stress fields if two or more different peaks are present in the diagram (Meschede, 1994). The diagram in Figure 6b shows a half Gaussian distribution, indicating that half of the data set fits in the normal faulting stress regime and half of the data set has an error of more than 30%. The stress ratio, expressed by R = (s2-s1)/(s3-s1), indicates a transtensional stress regime with R=0.7 (Fig. 6a) (Delavaux & Sperner, 2003). Applying the derived stress field for the slip and dilation tendency analysis, it is evident that fault planes with a NE-SW orientation have the highest slip and dilation tendency (Fig. 7). It strongly depends, however, on the dip angle of faults as to whether they are likely to accommodate both dilation and shearing. Faults that dip 70°NW or SE (Fig. 7) have the highest tendency to slip and to dilate.

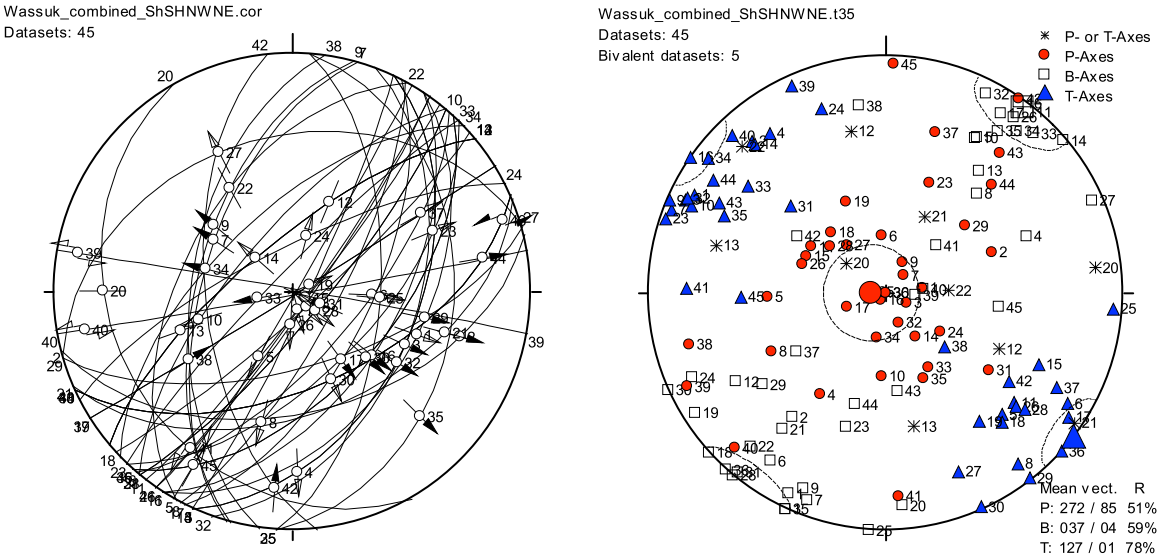

Figure 5. (A) Lower-hemisphere projection, Angelier-plot of the faults and slip vectors of faults, mapped by Hinz (Hinz et al., this volume). (B) PTB-plot of calculated strain axes, based on kinematic indicators of mapped faults.

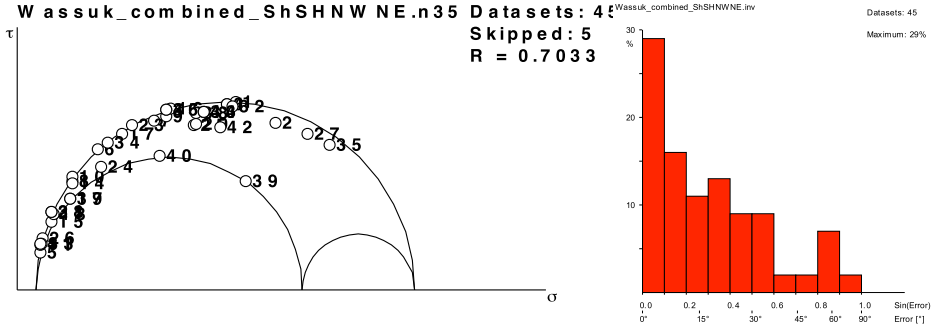

Figure 6. (A) Stress regime and stress ratio, expressed by the Mohr-Coulomb stress circle. (B) Fluctuation histogram of misfit angle between calculated and measured shear stress vector.

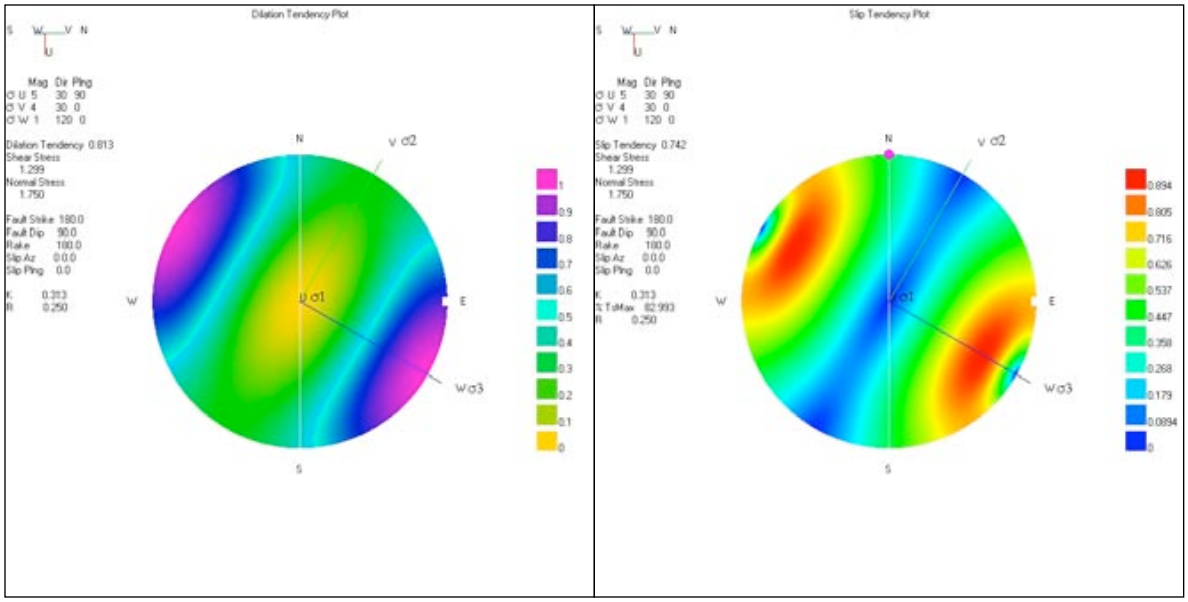

Figure 7. (A) Dilation tendency plot and (B) slip tendency plot, using the derived stress regime from this study. The star symbol indicates poles of planes, which are both highly dilational and prone to shearing, thus providing favorable structures for fluid flow.

Discussion and Conclusion

Based on the geologic, geophysical, temperature, and geochemical investigations, we suggest that three blind geothermal systems reside within the HAD, each controlled by distinct structures including a right step in the Wassuk Range front fault system and a complex pull-apart in the southeastern Walker Lake basin (Figs. 1, 8, 9). All three geothermal systems follow steeply dipping, NE-striking faults, consistent with slip and dilation tendency analysis indicating that NE-striking, 70° NW- and SE-dipping fault planes have the highest tendency to slip and dilate. Anomaly A parallels the Wassuk Range front adjacent to where the range-front fault zone bifurcates with a major right step in the most recently active part of the fault zone. We suggest that the higher fracture density associated with the abundant NE-striking faults between faults A and B and the right step in the normal-dextral Wassuk Range front fault have collectively induced dilation and facilitated deep circulation of fluids. Anomaly B resides at the northwest terminus of the Garfield Hills at the south end of an inferred pull-apart, whereby deep circulation is enhanced along a steeply N-dipping, ENE-striking normal fault transferring strain between the Pamlico fault and the unnamed NW-striking strike-slip fault along the southwest flank of the Gillis Range. Additional enhanced dilation at fault intersections between the Pamlico fault and ENE-striking sinistral-oblique faults accounts for broad anomaly wrapping around the northwest margin of the Garfield Hills. Anomaly C resides north of the city of Hawthorne, where tufa mounds form an NNE-trending lineament along part of the Hawthorne fault zone (Fig. 8F). The NW-striking Pamlico fault merges with Hawthorne fault zone near the south end of the tufa lineament, transferring strain into the NE-striking faults defining the northwest corner of a pull-apart. Deep circulation of fluids is facilitated along the steeply dipping NE-striking Hawthorne fault zone and at intersections with the Pamlico fault.

In summary, these findings are consistent with previous studies demonstrating that specific segments of fault zones are the primary control on geothermal systems in the western Great Basin (e.g. Faulds et al., 2006). The geothermal resources in the eastern part of HAD are

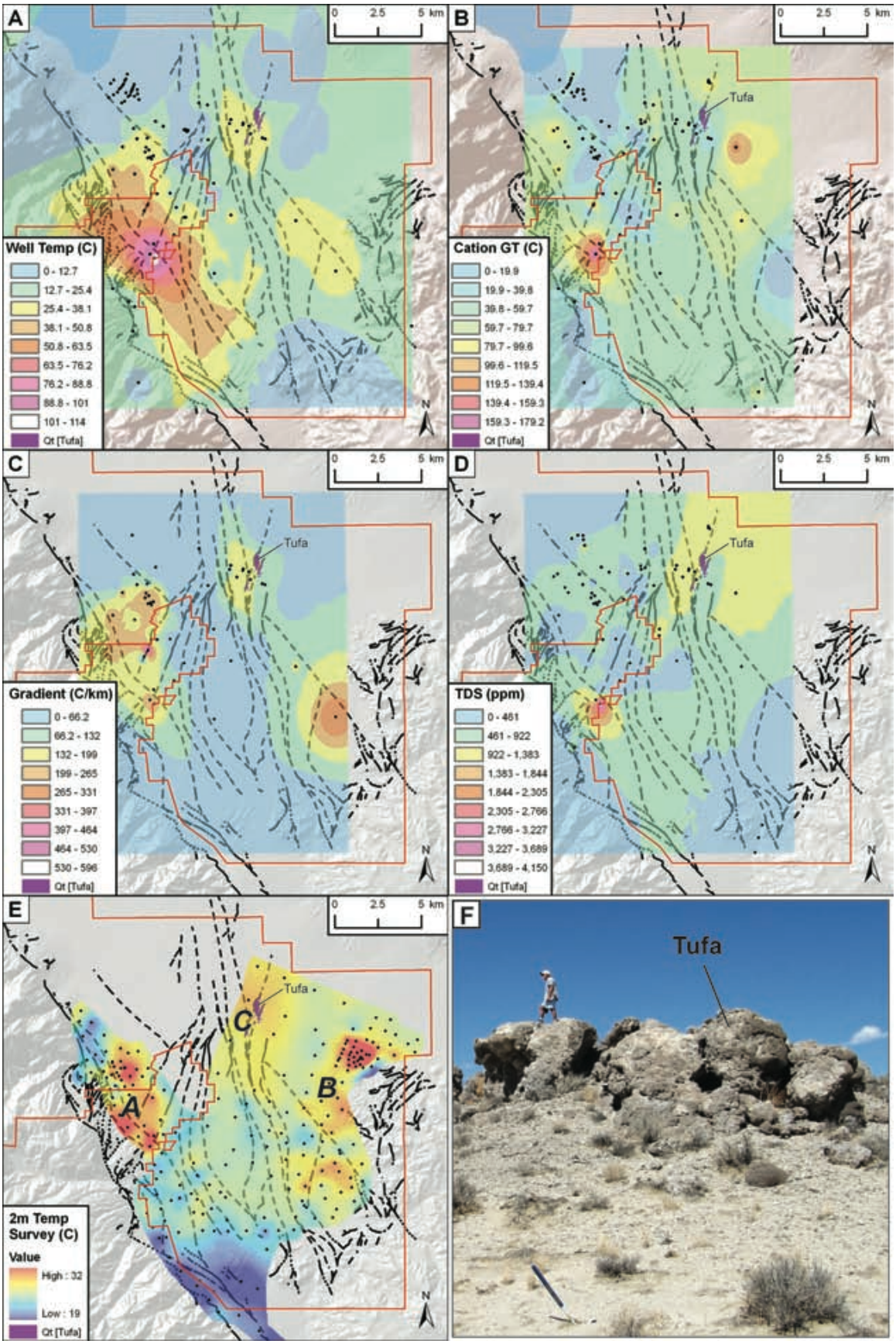

Figure 8. (Preceding page) Geothermal and geochemical anomalies for the HAD area shown with faults from Fig. 2. For A-D, black dots represent data points used to develop inverse distance weighted analyses, modified

from Penfield et al. (2010). For E, black dots represent data points used in kriging analysis (Kratt et al., 2010). A) Maximum well temperature at the bottom of each well. Depths vary from 10 to 1443 m, with 86% of wells ≤ 152 m and 96% are ≤ 310 m. B) Na-K-Ca geothermometry, C) Well temperature gradient, D) Total dissolved solids, E) 2-m temperature survey; A, B, C, correspond to anomalies described in text, F) Massive tufa heads associated with anomaly C.

structurally controlled by kinematically linked strike-slip and normal faults in the Walker Lane, whereas the geothermal resources along the Wassuk Range front in the western part of the HAD are controlled by oblique-slip (normal-dextral) range-front faulting (Fig. 9).

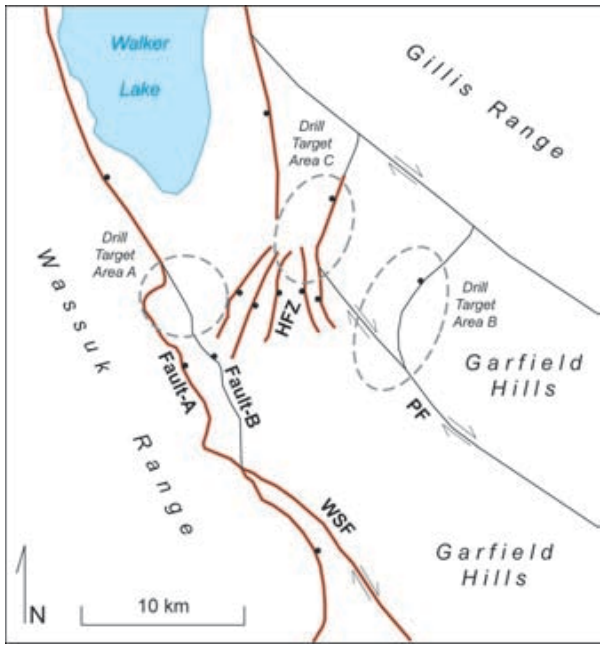

Figure 9. Simplified structure map of the HAD area showing primary faults and proposed drill target areas. Faults highlighted in red have been active in the Quaternary. HFZ, Hawthorne fault zone; PF, Pamlico fault; WSF, Willow Springs fault. Fault strands A and B of the Wassuk Range front fault system are also shown in Figure 2 and described in the text.

References Cited

Angelier, J., 1994. Fault slip analysis and paleostress field reconstruction, in Hancock, P.L., ed., Continental Deformation, Pergamon Press, Terrytown, New York, p. 53-100.

Byerlee, J.D., 1978. Friction of rocks. Pure Appl. Geophys. 116, 615-626.

Bell J.W., Hinz, N., 2010, Young Walker basin faults provide new insights into structural relations controlling geothermal potential at Hawthorne, Nevada: Geothermal Resources Council Transactions, v. 34, p. ?

Delavaux, D, Sperner, B. 2003. New aspects of tectonic stress inversion with reference to the TENSOR program. In: New insights into structural interpretation and modeling (D. A. Nieuwland, *ed.*). Geol. Soc. Spec. Pub., no. 212, 75-100.

Faulds, J.E., Coolbaugh, M.F., Vice, G.S., and Edwards, M.L., 2006, Characterizing structural controls of geothermal fields in the north-western Great Basin: A progress report: Geothermal Resources Council Transactions, v. 30, p. 69-75.

Fodor, L.I., 2007. Segment linkage and the state of stress in transtensional transfer zones: field examples from the Pannonian Basin. Geological Society, London, Spec. Pub, v. 290, 417-431.

Hinz, N.H., Faulds, J.E., Moeck, I., Bell, J.W., and Oldow, J.S., 2010, Structural controls of three blind geothermal resources at the Hawthorne Ammunition Depot, west-central Nevada: Geothermal Resources Council Transactions, v. 34, p. ?

Kratt, C., Sladek, C., and Coolbaugh, C., 2010, Boom and bust with the latest two-meter temperature surveys: Dead Horse Wells, Hawthorne Army Depot, Terraced Hills and other areas in Nevada: Geothermal Resources Council Transactions, v. 34, p. ?

Meschede, M., 1994. Methoden der Strukturgeologie; ein Leitfaden zur Aufnahme und Auswertung strukturgeologischer Daten im Gelaende und im Labor. Enke, Stuttgart, Federal Republic of Germany, pp. 175.

Moeck, I., Kwiatek, G., Zimmermann, G., 2009, Slip tendency, fault reactivation potential and induced seismicity in a deep geothermal reservoir. J. Struct. Geol., 31, 1174-1182.

Moeck, I., Hinz, N., Faulds, J., Bell, J., Kell-Hills, A., and Louie, J., 2010, 3D geological mapping as a new method in geothermal exploration: A case study from central Nevada: Geothermal Resources Council Transactions, v. 34, p. ?

Morris A., Ferrill D.A., Henderson DB., 1996. Slip tendency analysis and fault reactivation. Geology 24(3), 275-278.

Oldow, J.S., 1983, Tectonic implications of a late Mesozoic fold and thrust belt in northwestern Nevada: Geology, v. 11, p. 542546.

Oldow, J.S., 1984, Evolution of a late Mesozoic backarc fold and thrust belt, western Great Basin, USA: Tectonophysics, v. 102, p. 245-274.

Oldow, J.S., 1992, Late Cenozoic displacement partitioning in the northwestern Great Basin, *in* Craig, S.D., ed., Structure, tectonics, and mineralization of the Walker Lane: Reno, Nevada, Geological Society of Nevada Symposium Proceedings, p. 17-52.

Oldow, J.S., Satterfield, J.I., and Silberling, N.J., 1993, Jurassic to Cretaceous transpressional deformation in the Mesozoic marine province of the northwestern Great Basin, *in* Lahren, M., Trexler, Jr., J.H., and Spinosa, C., eds., Crustal evolution of the Great Basin and Sierra Nevada: Geological Society of America Field Guidebook, p. 129-166.

Oldow, J.S., Geissman, J.W., and Stockli, D.F., 2008, Evolution and strain reorganization within late Neogene structural stepovers linking the central Walker Lane and northern Eastern California Shear Zone, western Great Basin: International Geology Review, v. 50, p. 270-290.

Penfield, R., and 12 others, 2010, Geothermal site assessment using the National Geothermal Data System (NGDS) , with examples from the Hawthorne Army Depot area: Geothermal Resources Council Transactions, v. 34, p. ?

Proffett, J.M., Jr., 1977, Cenozoic geology of the Yerington district, Nevada, and implications for the nature and origin of basin and range faulting: Geological Society of America Bulletin, v. 88, p. 247-266.

Shoffner, J.D., Li, Y., Sabin, A., Lazaro, M., and Alm, S., 2010, Understanding fault characteristics for geothermal exploration using 3D gravity inversion in Walker Valley, Nevada: Geothermal Resources Council Transactions, v. 34, p. ?

Sippel, J.; Scheck-Wenderoth, M.; Reicherter, K.; Mazur, S. (2009): Paleostress states at the south-western margin of the Central European Basin System — Application of fault-slip analysis to unravel a polyphase deformation pattern, Tectonophysics, 470, 1-2, 129-146

Stewart, J.H., 1988, Tectonics of the Walker Lane belt, western Great Basin: Mesozoic and Cenozoic deformation in a zone of shear, *in* Ernst, W.G., ed., The Geotectonic development of California: Prentice Hall, Englewood Cliffs, New Jersey, p. 683-713.

Stockli, D.F., Surpless, B.E., Dumitru, T.A., and Farley, K.A., 2002, Thermochronological constraints on the timing and magnitude of Miocene and Pliocene extension in the central Wassuk Range, western Nevada: Tectonics, v. 21, 4, 10.1029/2001TC001295.

Surpless, B.E., Stockli, D.F., Dumitru, T.A., and Miller, E.L., 2002, Two-phase westward encroachment of Basin and Range extension into the northern Sierra Nevada: Tectonics, v. 21, 1002, doi:10.1029/2000TC001257.

Wesnousky, S.G., 2005, Active faulting in the Walker Lane: Tectonics, v. 24, TC3009, dio:10.$_{029}$/2004TC001645.

STOP 4 - Geoff Shoffner - Colorado School of Mines

The purpose of collecting gravity in the Southern Walker Lake Basin was to greater understand the structure at depth to minimize the need for exploratory drilling in on-going geothermal exploration. Unfortunately, gravity solutions are non-unique and resulting structural solutions are highly dependent on the assumed density contrast of the units modeled. Cross sections developed from detailed geologic fieldwork (Hinz et al., GRC 2010) were the basic model for the gravity forward modeled profiles. Depth constraints were provided by two mid-depth drill holes (HWAD 2a: 1430 m and HWAD 3: 1220 m) that locally intersected basement depth at ~320 m and ~460 m, respectively. The density profile figure (Section D-D') shows the progressive down dropping of JKgr as well as the Ta unit on the west side of the valley, with the valley ramping up into the Garfield Hills. Thickness of the alluvium at the location of this cross section is approximately 1 km. This is not only consistent with geologic interpretations from Hinz et al. (GRC 2010), but fits the collected gravity data with low error. The contact between JKgr and Mzu is unknown and assumed in the section. Also, due to the geologic complexity of the Garfield Hills to the east, interpretations on the east side of the valley are oversimplified. Further work will hope to improve these results.

Gravity measurements can help determine depth to bedrock throughout basins, which can be the reservoirs for geothermal fluids. We can also infer the dips on normal faulting at depth, thus refining and minimizing risk on future drilling targets. progressive down-dropping of the Wassuk Range and basement, and the east showing the ramping of the basement into the Garfield Hills.

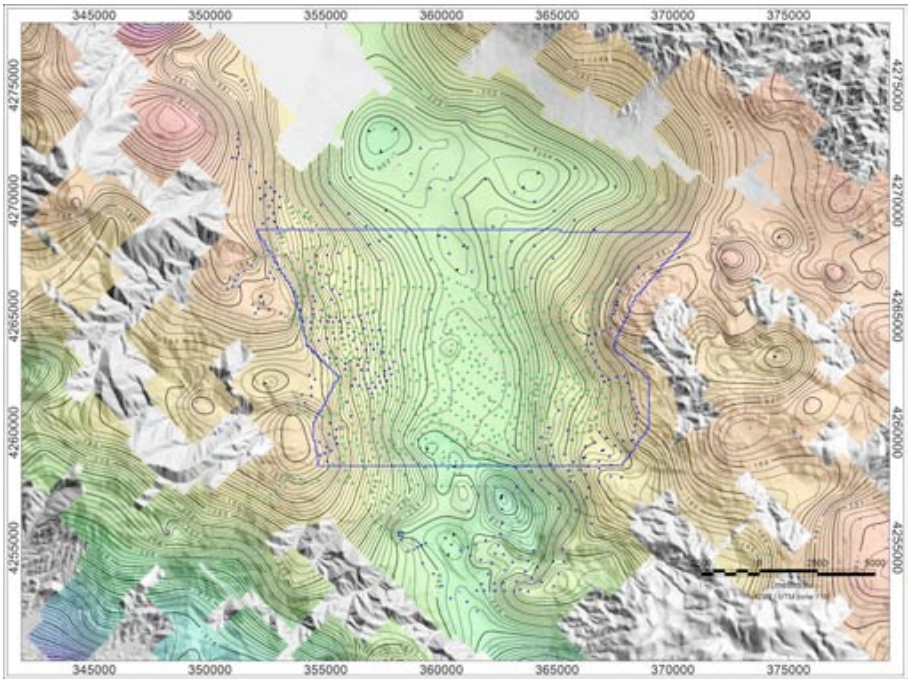

Figure 1: CBA 2.67 g/cc gravity map of the Southern Walker Lake Basin. Contour interval is 0.5 mGal. Area outlined in blue is the focus of the density sections.

STOP 4 - Marith Reheis, USGS

From Stop 4, we cannot go to the place of which Marith will speak, but a view westward across the Lake provides a view something like this. Thorne Bar is labeled. Below is a photo of the site from an airplane. The high albedo stuff which is visible from here is windblown sand. Upper photo courtesy of Riccado Civico.

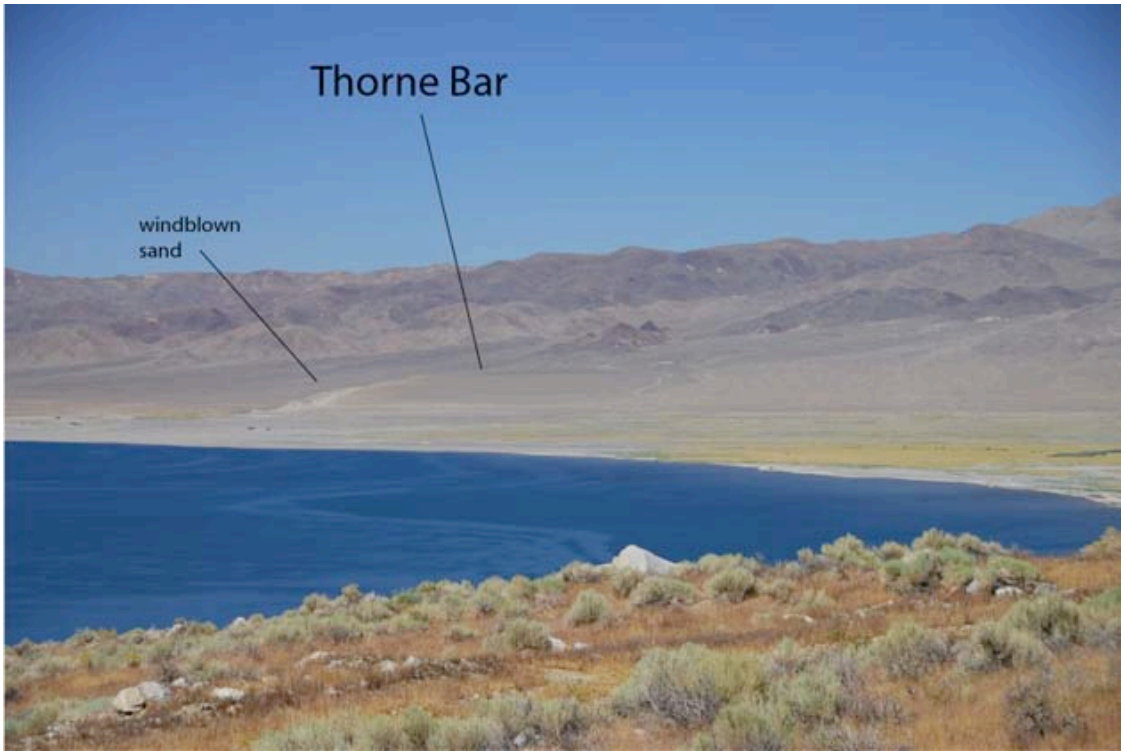

Thorne Bar: Ages of Nested Shorelines of Lake Lahontan

Marith Reheis and Fred Phillips

The following is abstracted from: Kurth, G., Phillips, F.M., Reheis, M.C., Redwine, J.L., and Paces, J.M., in press, Cosmogenic nuclide and uranium-series dating of old, high shorelines in the western Great Basin, U.S.A.: Geological Society of America Bulletin

The Thorne Bar shoreline complex lies at the mouth of a large canyon of the Gillis Range near Walker Lake, Nevada (fig. 1A). The Walker Lake subbasin was part of Lake Lahontan at its highest levels during the Sehoo highstand. The altitude of Adrian Pass, the present-day threshold to the main Lahontan basin, is now 1308 m. However, this threshold has likely been lowered by periodic erosion (King, 1993), and the Walker River has been episodically diverted north through Adrian Pass to become tributary to the Carson River (Benson and Thompson, 1987; Bradbury et al., 1989). Thorne Bar is a well-preserved, V-shaped, cuspate gravel barrier with shorelines at the Sehoo level (~1333 m, ~4380 ft) and several higher shorelines at four different altitudes up to 1402 m (~4600 ft; fig. 1 and table 1). The barrier morphologies are increasingly subdued and degraded with height (Reheis et al., 2002).

We employed cosmogenic ^{36}Cl to directly date the timing of deposition of the lacustrine beach barriers. Our sampling strategy aimed to minimize two issues encountered when dating constructional beach barriers: erosion and inheritance. These constructional features are ridges formed when waves erode rock and sediment and deposit sand and gravel at or just below lake level. Depending on fetch distance, wind, and pre-existing surface slope, they may be steep-sided with narrow crests or gently sloping with broad crests. Regardless, their positive topographic relief means that they are more rapidly eroded by rilling and gullying than more extensive planar features such as fluvial terraces and alluvial fans. To minimize the effects of erosion, we selected the most stable sites on the basis of geomorphic criteria (flat or gently sloping surfaces with intact desert pavement overlying a stone-free eolian cap or Av horizon).

Terrestrial cosmogenic nuclide (TCN) inheritance refers to an inventory of the cosmogenic nuclide that is inherited when a younger landform (such as a beach ridge) includes material eroded from an older landform (such as an alluvial fan) that has already undergone exposure to cosmic radiation. Cosmogenic nuclide inheritance was evaluated for each sampled beach barrier using depth profiles, similar to Anderson et al. (1996). In the Basin and Range, lakes commonly erode and redeposit material from pre-existing alluvial-fan deposits. Depending on fan age and the depth at which erosion removes sediment, inheritance may be variable between clasts, between stratigraphic layers, and between barriers constructed at different times.

The surfaces of the lacustrine features in this study have been modified since deposition by eolian inflation and by erosion. Eolian inflation occurs as dust accumulates just below the surface over time and can result in a surficial gravel pavement overlying a silt layer. With time, desert pavements remain at the land surface and are inflated vertically due to the underlying accumulation of windblown dust (Wells et al., 1995; McFadden et al., 1998). The TCN content of the eolian sediment is not a factor in data interpretation (because the fine-grained eolian fraction is physically removed by sieving), but the calculations must account for the shielding effect of dust-derived surface inflation. We estimated net surface aggradation (inflation) and erosion using soil properties and geological observations. The net gain of <2-mm particles, $CaCO_3$, and soluble salt by incorporation of eolian sediment beneath the desert pavement within the eolian cap (generally includes Av, Bw, and Bt horizons) was calculated and converted using bulk density data to a gravel-

free sediment thickness that was added to the top of a beach barrier. The eolian inflation rate, or negative erosion rate, in mm/kyr, was then calculated for shoreline sediments with independent age control (for example, ^{14}C and U-series ages) by dividing the inflation thickness by the age. These estimates indicate that surface erosion rates exceed eolian accretion rates in less than 100,000 yr after a barrier is formed.

Description of Thorne bar sample sites

The Thorne Bar shoreline complex (fig. 1) consists of nested cuspate beach barriers and pocket barriers composed primarily of pebble- and cobble-sized gravel of granitic and lesser metavolcanic lithologies. Tufa cement is locally present. The beach gravels were partly reworked during successive lake highstands. Five barriers in the Thorne Bar complex (figs. 1B, 1C; table 1) were sampled in trenches and dated using ^{36}Cl; two of these barriers were also dated using U-series on lake tufa.

The lowest site (TB02-00, 1325 m altitude; fig. 1B) lies on a large, V-shaped, cuspate barrier complex; this complex extends upslope to the northeast to an altitude of about 1333 m (the Sehoo highstand level of Lake Lahontan). The weak soil profile in the bar consisted of a sandy, 3-4-cm-thick Av horizon over a slightly oxidized, gravelly Bw horizon about 10 cm thick, developed on well-stratified lake sand and gravel with intact bedding.

The next higher feature studied (TB00-01) is a small, distinct pocket barrier at an altitude of 1332-1333 m that formed across the mouth of a small drainage cut into the north side of the main Thorne Bar barrier (fig. 1). The soil had a 7-cm-thick Av horizon, a gravel-free Bw horizon 13 cm thick, and soil structure and oxidation extending to 50 cm depth; it was better developed than that at TB02-00. In addition, clay skins coating clasts were observed at depths of 1-2 m on all trench walls, at and below a change in bedding dip. Clay skins at such depths in this climate are not expected; if pedogenic, they should be accompanied by blocky structure, oxidation, or abundant pedogenic carbonate. The altitude of the TB00-01 barrier is consistent with formation during the MIS-2 Sehoo highstand (Adams and Wesnousky, 1999).

Above the pocket barrier, there are two nested barrier ridges that form part of the Thorne Bar complex and mark highstands between about 1333 and 1370 m (figs. 1B, 1C). Both barriers are moderately preserved with rolling-to-flat surfaces on top and dissected sideslopes, suggesting moderate erosion. Both barriers contain gravel-free Av horizons underlying desert pavements, indicating eolian inflation. The barrier surface at the lower trench site (TB00-02; 1351 m) is better preserved than that at the upper one (TB00-03; 1357 m). The soil properties suggest that the two soils are similar and that both are older than soil TB00-01. The TB00-03 surface is more eroded than TB00-02, and TB00-02 more than TB00-01.

The highest barrier ridge (TB00-04; 1399 m) is much more eroded than the lower four. This barrier forms the northeast-southwest-trending topographic crest of the Thorne Bar complex. A silty layer 0.5 m below the surface of the sample pit contains abundant reworked shards of probable Bishop ash (~760 ka) as identified by glass chemistry (A. M. Sarna-Wojcicki, U. S. Geological Survey, written commun., 2001) and it has normal magnetic polarity (Reheis et al., 2003). These two characteristics indicate the barrier is younger than ~760 ka. The presence of this fine-grained layer and another at ~1.5 m depth suggests that the beach gravel here is interbedded with back-barrier lagoonal or playa sediment, an indication of the backwasting of the original barrier. The poorer degree of morphologic preservation, topographic position, and probable 760-ka tephra indicate that this is the oldest barrier sampled.

Dating Results

The ^{36}Cl profile age for TB02-00, 17±8 ka (table 1), is consistent with deposition during the MIS-2 Sehoo highstand, which is radiocarbon dated at ~15.9 cal ka (Adams and Wesnousky, 1998). As described above, the barrier complex at this site is below the Sehoo highstand altitude of 1343 m and was probably formed during the early stages of lake regression.

The ^{36}Cl profile age for the next higher barrier at site TB00-01, $72^{+24}/_{-20}$ ka, was unexpected, and suggests that the barrier was originally formed during MIS 4. This pocket barrier was identified by Adams and Wesnousky (1999) as a Sehoo highstand feature, based on correlation of soil development with other dated Sehoo shorelines; however, the ^{36}Cl modeling results are robust. Field observations show that the dated pocket barrier lies in a protected location between two higher ridges that are remnants of the 1353-m highstand (fig. 1B). We hypothesize that the pocket barrier was mainly formed during a previous MIS-4 highstand in the Walker Basin and was preserved during the MIS-2 lake cycle due to its relatively protected position, the rapid rise of the lake to its highstand, and the short time the lake occupied the highstand position. If so, such a transgression would have had to remove most of the pre-existing surface soil (the eolian cap) formed following MIS 4 without significant reworking of the subjacent coarse gravel.

In addition to the problem presented by the topographic position of this barrier, such an age assignment also raises questions with respect to soil development. Adams and Wesnousky (1999) considered the degree of soil development on this barrier to be typical of soils developed on Sehoo highstand features. Our soil profile data are in agreement with this assessment (table 1). However, we note that, in general, soils at Thorne Bar do not show a marked increase of soil development with time, perhaps due to low rates of dust infiltration and (or) greater rates of erosion. Adams and Wesnousky (1999) found much overlap in soils formed on Sehoo and pre-Sehoo deposits in the Lahontan basin. Reworking during the MIS-2 highstand of a pre-existing, post-MIS-4 soil could account for the similarities with Sehoo-age profiles, and flushing of the fines from such a soil might help to account for the anomalous clay skins on pebbles at greater than 1 m depth observed in TB00-01.

At site TB00-02 (1351 m), ~18 m higher than the presumed Sehoo highstand, the barrier rises from about 1335 to 1353 m. This site yielded a ^{36}Cl profile age of $127^{+73}/_{-19}$ ka (table 1). Although the preferred age falls within the interglacial period MIS 5e, the ^{36}Cl age range is overall consistent with construction of the 1353-m barrier during MIS 6 (190-130 ka). U-series analysis of a sample of massive, detritus-“free” tufa cementing clasts from a site on the north side of the Thorne Bar complex within the altitude range defined by the barrier associated with TB00-02 yielded an age of 128 ±6 ka. Large pluvial lakes during MIS 6 are documented elsewhere in the western Great Basin, including Owens Lake (Smith et al., 1997), Lake Bonneville (Oviatt et al., 1999), and Lake Manly (Machette et al., 2008).

The barrier sampled by profile TB00-03 (1357 m) ranges between 1355 and ~1370 m in altitude, higher than the MIS 6 barrier. This pit yielded a ^{36}Cl profile age of $227^{+97/-50}$ ka, most consistent with the 1370-m barrier being deposited during MIS 8 or early in MIS 7, but a wide range of ages correlative with either MIS 7 or 8 are permissible. U-series analysis on two samples of a tufa “head” within layered beach gravel associated with shoreline features in the range of the altitude of the TB00-03 barrier (fig. 1), yielded ages of 167 ±17 and 211 ±37. These ages may reflect a highstand older than MIS 6; the older age is similar to the modeled ^{36}Cl age. However, secondary loss of U may also account for the apparently older age and slightly higher initial ^{234}U/^{238}U AR observed in EL97-37-u3. Little is known about the extent of pluvial lakes elsewhere in the Great Basin during

this period. In pluvial Lake Owens, Smith et al. (1997) inferred at least a moderate highstand during this time and Bradbury (1997) observed an interval very strongly dominated by fresh-water diatoms at ~230 ka, whereas Oviatt et al. (1999) recognized no coeval highstands of Lake Bonneville.

The highest barrier in the Thorne Bar complex, sampled by TB00-04 (1399 m), ranges from 1370 to 1402 m in altitude. The profile yielded an age of $450^{+570/-310}$ ka (table 1). The profile data contain a significantly lower ^{36}Cl inventory than lower and younger barriers, likely owing to erosion and removal of the upper part of the original profile. If the TB00-04 surface is assumed to be stable and erosion rates low, ages only slightly older than 100 ka are calculated. Under high postulated erosion rates (~10 mm kyr^{-1}) ages of ~500 ka are calculated, but the total resulting erosion of ~5 m is large. The presence of abundant shards of probable Bishop ash (760 ka) in a fine-grained layer in the TB00-04 trench provides an additional age constraint. In addition, an important outcrop a few kilometers north of Thorne Bar contains a purer layer of probable Bishop ash unconformably overlain by beach gravel some 40 m thick that extends upward to an altitude of 1398 m (fig. 1A). This gravel is correlated to the 1399-m barrier at Thorne Bar (Reheis et al., 2002a), and is provisionally correlated with MIS 16, ~660-620 ka, a time of maximum global ice extent (Imbrie, 1984). A ^{36}Cl age range of 450-1020 ka modeled with high erosion rates of 10-12 mm/yr is consistent with this correlation.

Discussion and Lacustrine History

^{36}Cl profile ages and U-series ages for constructional lacustrine features at Thorne Bar, combined with one tephra identification, indicate highstands at ~10-25 ka (MIS 2), 50-95 ka (MIS 4), 100-200 ka (most likely late MIS 6), ~170-250 ka (MIS 7-8?), and as old as ~700 ka (table 1). Walker Lake had a direct connection to Lake Lahontan, and thus the results are particularly relevant in the context of the longer-term history of Lake Lahontan.

Our observations indicate a MIS 4-late MIS 5 lake that reached about the same altitude (1333 m) as the latest MIS-2 (Sehoo) shoreline. However, Adams and Wesnousky (1999) employed soil descriptions over a wide area to conclude that all of the ca. 1333-m highstand shorelines were of the same age, about 15.9 ka cal. Other pre-Sehoo shoreline sites elsewhere in the Lahontan basin consist mostly of lags of beach clasts on wave-cut benches at altitudes of ca. 1370 and 1400 m (Reheis et al., 2002a), identical to the altitudes of the upper two barrier ridges at Thorne Bar. The significant apparent conflict is with regard to the ~70-ka age for the 1333-m pocket barrier. We hypothesize that the most likely explanation for this discrepancy is a relatively recent establishment, or a re-establishment, of full hydraulic connection between the Walker Lake sub-basin and the rest of the Lahontan system, as recently suggested by Adams and Redwine (2007). The simplest explanation for the existence of a sequence of middle to early late Pleistocene shorelines between altitudes of 1350 and 1333 m in the Walker Lake sub-basin, but apparently nowhere else in the Lahontan basin, is that the Adrian Pass sill altitude has been progressively lowered since MIS 6, either by erosion or tectonics, as previously suggested by King (1993). If this explanation is correct, the ~70 ka shoreline at 1333 m could correspond to a lower lake level in the main Lahontan basin whose deposits are now buried. This explanation would imply that the altitude of Adrian Pass was reduced from ca. 1350 to 1333 m in altitude between MIS 6 and MIS 4, and from 1333 to 1308 m between MIS 4 and the present. Finally, the results of this study suggest there may be confusion between recognized MIS 2 and MIS 4 shorelines in the western Great Basin, in view of the range of soil properties found by Adams and Wesnousky (1999) to be characteristic of soils formed on Sehoo-age shoreline deposits.

References Cited

Adams, K.D., and Redwine, J.L., 2007, Pleistocene overflow, basin integration, and an explanation for the distribution of OIS 6 and OIS 2 highstands in the Great Basin: Geological Society of America Abstracts with Programs, v. 39, no. 6, p. 270.

Adams, K. D., and Wesnousky, S. G., 1998, Shoreline processes and the age of the Lake Lahontan Highstand in the Jessup embayment, Nevada: Geological Society of America Bulletin, v. 110, p. 1318-1332.

Adams, K. D., and Wesnousky, S. G., 1999, The Lake Lahontan highstand age, surficial characteristics, soil development, and regional shoreline correlation: Geomorphology, v. 30, p.357-392.

Anderson, R. S., Repka, J. L., and Dick, G. S., 1996, Explicit treatment of inheritance in dating depositional surfaces using in situ ^{10}Be and ^{26}Al: Geology, v. 24, p. 47-51.

Benson, L.V., and Thompson, R.S., 1987, Lake-level variation in the Lahontan Basin for the past 50,000 years: Quaternary Research, v. 28, p. 69-85.

Bradbury, J. P., 1997, A diatom-based paleohydrologic record of climate change for the past 800 k.y. from Owens Lake, California, *in* Smith, G. I., and Bischoff, J. L., eds., An 800,000-year paleoclimate record from Owens Lake, California: Boulder, Colo., Geological Society of America Special Paper 317, pp. 99-112.

Imbrie, J., 1984, and 8 others, 1984, the orbital theory of Pleistocene climate; Support from a revised chronology of the marine δ^{18}O record, *in* Berger, A.L. and others, eds., Milankovich and climate, Part I: Dordrecht, D. Reidel Publishing Co., p. 269-305.

King, G. Q., 1993, Late Quaternary history of the lower Walker River and its implications for the Lahontan paleolake system: Physical Geography, v. 14, p. 81-96.

Machette, M. N., Slate, J. L., and Phillips, F. M., 2008, Terrestrial cosmogenic-nuclide dating of alluvial fans in Death Valley National Park, California: U.S. Geological Survey Professional Paper 1755, 51 p.

McFadden, L.D., McDonald, E.V., Wells, S.G., Anderson, K., Quade, J., and Forman, S.L., 1998, The vesicular layer and carbonate collars of desert soils and pavements: formation, age and relation to climate change: Geomorphology, v. 24, p. 101-145.

Oviatt, C.G., Thompson, R.S., Kaufman, D.S., Bright, J., and Forester, R.M., 1999, Reinterpretation of the Burmester Core, Bonneville Basin, Utah: Quaternary Research, v. 52, p. 180-184.

Reheis, M.C., Sarna-Wojcicki, A.M., Reynolds, R.L., Repenning, C.A., and Mifflin, M.D., 2002, Pliocene to middle Pleistocene lakes in the western Great Basin: Ages and connections, *in* Hershler, R., Madsen, D.B., and Currey, D.R., eds., Great Basin Aquatic Systems History: Washington, D.C., Smithsonian Institution Press, p. 53-108.

Reheis, M., Redwine, J., Adams, K., Stine, S., Parker, K., Negrini, R., Burke, R., Kurth, G., McGeehin, J., Paces, J., Phillips, F., Sarna-Wojcicki, A., and Smoot, J., 2003, Pliocene to Holocene lakes in the western Great Basin: New perspectives on paleoclimate, landscape dynamics, tectonics, and paleodistribution of aquatic species, *in* Easterbrook, D.J., ed., Quaternary Geology of the United States (INQUA 2003 Field Guide Volume): Reno, Desert Research Institute, p. 155-194.

Smith, G.I., Bischoff, J.L., and Bradbury, J.P., 1997, Synthesis of the paleoclimatic record from Owens Lake core OL-92, *in* Smith, G.I., and Bischoff, J.L., eds., An 800,000-year paleoclimatic record from core OL-92, Owens Lake, southeast California: Geological Society of America Special Paper 317, p. 143-160.

Wells, S.G., McFadden, L.D., Poths, J., and Olinger, C.T., 1995, Cosmogenic ^{3}He surface-exposure dating of stone pavements: Implications for landscape evolution in deserts: Geology, v. 23, p. 613-616.

FIGURE 1 on next page. Maps and profile of Walker Lake subbasin of Lake Lahontan and Thorne Bar area. A, Sketch map of Walker Lake subbasin modified from Reheis et al. (2002a). TW is site of dated tufa samples EL97-4 and EL97-5 on footwall block of Wassuk fault. TB, area of Thorne Bar. Dashed box is outline of Figure 1B. Star, 4 km north of Thorne Bar, is 760-ka Bishop ash locality described in Reheis et al. (2002). B, Geomorphic map of Thorne Bar overlaid on aerial photograph, showing sample trench locations and altitudes. C, Schematic topographic profile along crest of Thorne bar showing altitudes of sample sites. Profile constructed using topographic maps and differentially corrected GPS positions; includes projected points.

Table 1. Trench altitude, soil data (N.D., no data), and cosmogenic ^{36}Cl age

Profile no.	Trench altitude (m)	Eolian additions (g/cm^2/column)	Profile devel. index (PDI)	Age (ka)	Plus (ka)	Minus (ka)	Inheritance age (ka)
TB02-00	~1325	N.D.	N.D.	17	8	8	93±14
TB00-01	1333	21.2	13.1	72	24	20	72±11
TB00-02	1351	36.0	17.6	127	73	19	30±7
TB00-03	1357	45.1	15.8	227	97	50	27±7
TB00-04	1399	31.5	23.3	450	570	310	15±4

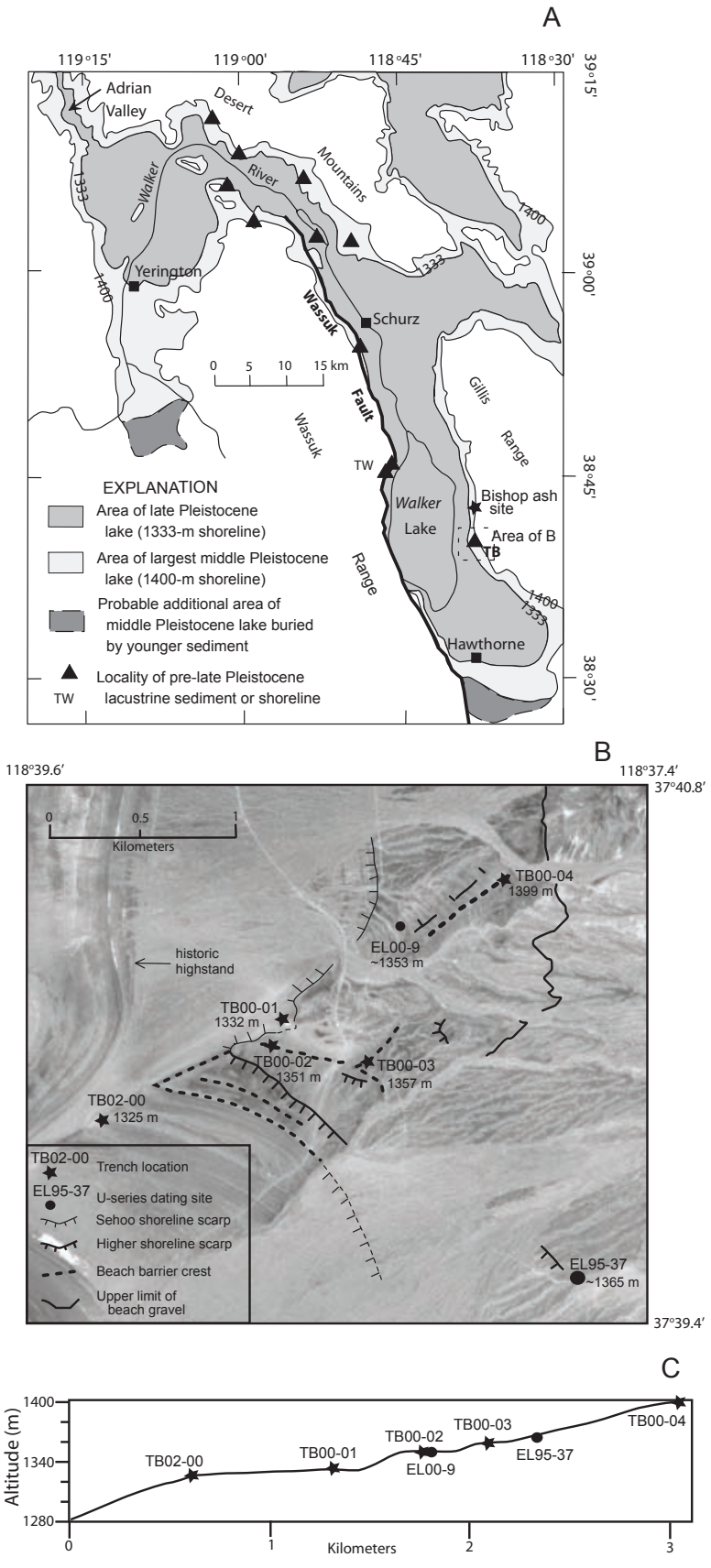

FIGURE 1 Maps and profile of Walker Lake subbasin of Lake Lahontan and Thorne Bar area. A, Sketch map of Walker Lake subbasin modified from Reheis et al. (2002a). TW is site of dated tufa samples EL97-4 and EL97-5 on footwall block of Wassuk fault. TB, area of Thorne Bar. Dashed box is outline of Figure 1B. Star, 4 km north of Thorne Bar, is 760-ka Bishop ash locality described in Reheis et al. (2002). B, Geomorphic map of Thorne Bar overlaid on aerial photograph, showing sample trench locations and altitudes. C, Schematic topographic profile along crest of Thorne bar showing altitudes of sample sites. Profile constructed using topographic maps and differentially corrected GPS positions; includes projected points.

STOP 4 - Ben Surpless, Trinity College, San Antonio, TX
Evolution of a segmented normal fault system: a reconnaissance study of the Reese River-Penrod Canyon fault system, northern Wassuk Range

Introduction

The Wassuk Range fault system, within the actively-deforming Walker Lane belt, is among the most active in the Basin and Range province (e.g., DePolo and Anderson, 2000). Late Quaternary slip across the east-dipping, high-angle range-bounding normal fault of the range has produced fault scarps that cut alluvium at many locations along the eastern range front. At the mouth of Penrod Canyon, in the central Wassuk Range, a large, abandoned alluvial fan displays a well-defined escarpment striking approximately N30°E at a right-step in the NNW-striking range-front fault system (Fig. 1). This escarpment displays eroded wave-cut benches created by late Pleistocene lake-level highstands, and well-preserved Holocene fault scarps subparallel and proximal to the base of the escarpment suggest that this segment of the range-bounding fault system remains active today (Wesnousky, 2005).

The position of this alluvial fan is intriguing, because the pre-Quaternary geology of the Penrod Canyon shows clear evidence for dextral deformation associated with the structural evolution of the central and northern Wassuk Range. In addition, the Wassuk Range itself appears to have evolved such that faults through the Penrod Canyon have segmented the Wassuk Range, with a significant dextral offset of the range crest across faults that define the canyon. Presented here are new reconnaissance data that constrain rates of Quaternary slip along the range-front fault system and suggest post-13 ka tilting of the abandoned Penrod Canyon alluvial fan. These data may have implications for both the long-term evolution of the central Wassuk Range fault system as well as the evolution of a major, segmented range-front normal fault at a segment boundary.

Pre-Quaternary structural evolution of the Penrod Canyon area

The Wassuk Range is composed primarily of Mesozoic granites and granodiorites with roof pendants of Mesozoic metasedimentary and metavolcanic rocks (Pre-Tertiary plutonic and metamorphic rocks on Fig. 1). Unconformably overlying these units are Oligocene silicic ash-flow tuffs, Middle Miocene andesites, and younger Tertiary sedimentary units interbedded with Late Miocene basalts and basaltic andesites (Tertiary volcanic and sedimentary rocks on Fig. 1; e.g., Bingler, 1978; McIntyre, 1990; Dilles, 1993; Dilles and Gans, 1995; Surpless, *in press*). Both the Tertiary unconformity and the deposition and deformation of dated Tertiary sedimentary units provide constraints on the structural evolution of both the central and northern Wassuk Range, which is summarized below.

~*15 - 13 Ma*

Immediately south of Penrod Canyon, large-magnitude extension (>150%) was accommodated by east-dipping, high-angle normal faults spaced at 1 – 2 km intervals. The timing of this event is based on both cross-cutting relationships and low-temperature thermochronologic data. These data also suggest that this period of elevated extensional strain ended by ~13 Ma (Stockli et al., 2002; Surpless et al., 2002). During this same period in the northern Wassuk Range, Dilles (1993) documented a series of strike-slip faults that moved synchronously with oblique-slip normal faults to accommodate an average of 50° stratal rotation of fault blocks, with a dominant extension directed

WNW-ESE to NW-SE. The strike – slip faults were largely accommodation structures between zones of oppositely dipping normal faults and exhibit little lateral displacement (Dilles, 1993), although the faults were parallel to the most prominent faults in the Walker Lane to the east (e.g., Benton Springs fault). In the northern Wassuk Range, this period of tectonicsm ended by 14 Ma (Dilles, 1993).

~*13 Ma – 7 Ma*

Following this pulse of large-magnitude extension, McIntyre (1990) documented several dextral and oblique slip faults in the Penrod Canyon area that were active during the deposition of Miocene Wassuk Group sediments. The high-angle Reese River fault (RRF in Fig. 1) accommodated up to 3350 meters of right lateral displacement and pre-dates the younger Penrod Canyon and Cottonwood Springs faults (PCF and CSF, respectively, in Fig. 1) (McIntyre, 1990). The Cottonwood Springs and Penrod Canyon faults moved synchronously and accommodated more than 4100 meters of oblique-slip displacement in a geometry that created a pull-apart basin for the deposition and deformation of the Miocene Wassuk Group (Figs. 1 and 2; McIntyre, 1990).

During this same time period, the Buck Brush Spring fault, to the south of the Penrod Canyon area, accommodated approximately 800 meters of dextral displacement (Fig. 1; Surpless, *in press*), subparallel to the Reese River fault and subparallel to the dominant strike-slip faults of the central Walker Lane, to the east. By 7 Ma, movement along these faults and other related faults in the Penrod Canyon fault system came to an end (McIntyre, 1990; Dilles, 1993).

7 Ma – Quaternary time

Low-temperature thermochronologic data suggest that rates of footwall uplift related to extension remained low in the central Wassuk Range until about 4 Ma (Stockli et al., 2002). At that time, thermochronologic data suggest a renewed pulse of extension that has continued to the present, potentially related to a fundamental change in plate boundary dynamics. Murphy and others (2009) also suggest a fundamental kinematic reorganization of the boundary at this time, based on their graphical inversion analysis of contemporary velocity and strain across the Walker Lane at this latitude. Stockli and others (2002) constrain a time-averaged rate of footwall uplift at 0.5 – 0.75 mm/yr for the central Wassuk Range since 4 Ma. Structural reconstructions and thermochronologic data imply that this uplift was accommodated primarily by the range-front fault system that remains active today.

Modern deformation of the central and northern Wassuk Range

Geodetic data suggest that the Walker Lane accommodates up to 25% of the relative dextral motion between the Pacific and North American plates (e.g., Minster and Jordan, 1987; Dixon et al., 1995; Bennett et al., 1999), and several workers have suggested that the Wassuk Range is the approximate present-day boundary between extension-dominated transtension to the west and dextral-dominated transtension to the east (e.g., Oldow, 2003; Wesnousky, 2005; Surpless, 2008; Murphy et al., 2009), implying that the rangefront system might be expected display some evidence for both dextral and extensional strain. However, the range front fault system exhibits little evidence for significant dextral strain, and the presence of 20 – 40 meter high scarps cutting older alluvial fan surfaces in the central and northern Wassuk Range suggests long term Quaternary dip-slip displacment (Wesnousky, 2005).

The relatively simple morphology of abundant Holocene scarps exposed in drainages along much of the range front implies a single-event origin (e.g., Wallace, 1977; Wesnousky, 2005). Demsey (1987) split the range-front fault system into segments based primarily on scarp morphology, with one of the most prominent divisions between segments occurring at Penrod

Canyon. Immediately to the north of Penrod Canyon, there is no evidence for Holocene faulting along the rangefront, suggesting that ongoing deformation to the north of Penrod Canyon may be accommodated by a fault or fault system within the range (Demsey, 1987).

Based on trenching, soil development, and fault scarp morphology, Demsey (1987) documented two significant earthquakes in the last 5000 years along the range front fault system, with 2 – 3 meters of offset per event, and obtained a vertical slip rate of 0.4 – 0.5 mm/yr based on her work. These two events affected different segments of the fault system: in the southern Wassuk Range, a single M 7.0 – 7.1 earthquake at approximately 4500 y.b.p. resulted in displacement along ~30 km of the rangefront, and along a segment further north, a single M 7.2 – 7.5 earthquake at approximately 2500 y.b.p. resulted in displacement along ~ 50 km of the rangefront, extending up to but not to the north of the abandoned Penrod Canyon alluvial fan (Demsey, 1987).

The Penrod Canyon alluvial fan and fault slip rates

Alluvial fans associated with major normal fault systems most commonly form with apices proximal to the fault responsible for their formation. The abandoned Penrod Canyon fan exhibits a fault scarp that cuts the upper alluvial surface 200 meters to the ESE of the approximate original fan apex, implying a possible migration in active faulting to the ESE since the time that fan formation began. As displacement associated with the newer fault increased, the fan was eventually abandoned, and the younger, active fans have apices to the NW and SE of the Quaternary fault scarp (Fig. 3). By constraining the age of the upper alluvial surface of the abandoned Penrod Canyon fan and measuring the fault offset, an approximate limit can be placed on the rate of vertical slip along that fault segment.

The abandoned upper alluvial surface displays 40 meters throw relative to the active alluvial surface on the hanging wall of the normal fault (Fig. 3a). This value is assumed to be the minimum throw across the fault since the alluvial surface was truncated, because past and present alluvial deposition on the hanging wall have buried the correlative upper alluvial surface exposed on the footwall. Cosmogenic nuclide ^{10}Be concentrations from two large boulders on the abandoned alluvial fan surface yield surface exposure ages of 91 +/- 12 ka and 106 +/- 15 ka (Fig. 3b). These ages give the maximum age for the latest deposition on the upper surface of the alluvial fan. Based on the measured minimum fault throw and the maximum exposure ages, the time-averaged slip rate along this fault segment is greater than 0.4 mm/year.

This value is the same, within error, as an estimate based on previous paleoseismic work for the last 5,000 years of fault motion (Demsey, 1987) and is slightly lower than the time-averaged slip rate since the Late Pliocene of 0.5 – 0.75 mm/year. These data imply a relatively constant rate of extensional deformation along the range-bounding fault system of the central Wassuk Range since the Late Pliocene.

Rangefront fault system development

Large normal fault systems generally develop over time by the interaction of overlapping en echelon faults rather than by propagation of a single fault surface (e.g., Anders and Schlische, 1994; Schlische and Anders, 1996; Ferrill et al., 1999). As a major fault system grows, these en echelon segments intersect each other either by formation of new faults between segments or by curved propagation of the en echelon fault tips (Peacock and Sanderson, 1994; Childs et al., 1995). Thus, the abandoned Penrod Canyon fan is located at an intriguing position along the Wassuk Range front fault system. The fan is located at the boundary between segments of the range-front fault system, at a right step where Holocene scarps are evident to the south and are not present to the north (Demsey, 1987). The Penrod Canyon fan also occurs along strike of the Miocene Reese River

dextral strike-slip fault and is adjacent to the dextral pull-apart basin formed prior to 7 Ma (Figs. 1 and 2).

Although these older faults have not been shown to be active, they provide pre-existing zones of weakness that could play a role in ongoing deformation. In fact, Demsey (1987) suggests that modern extensional strain may be accommodated by faults to the west of the range front north of Penrod Canyon, which implies that some displacement might be transferred by one or more faults in the Penrod Canyon. This transfer of slip from the range front to the interior of the range along a former dextral strike-slip fault system could signal a migration of dextral deformation from faults east of the Wassuk Range toward the west, or alternatively, the reactivated faults that are part of the system could simply act as slip transfer structures. A third alternative might involve the evolution of the en echelon system, with the southern segment, south of Penrod Canyon, becoming the dominant plane of deformation, with new deformation beginning within the former footwall of the northern Wassuk Range, along strike of the southern segment.

The morphology of the large. older scarp of the abandoned Penrod Canyon fan provides evidence for recent tilting that may be related to the existing fault geometry of the rangefront system. The most prominent wave-cut bench on the scarp corresponds to the 13 ka, 1330 meter Seehoo highstand of Lake Lahontan (e.g., Demsey, 1987; Adams et al., 1999) and can be used as a paleohorizontal strain marker, permitting an estimate of post-13 ka tilting. The NE exposure of the wave-cut bench is at 1319 meters, and the SW exposure, 250 meters away, is at 1326 meters (Fig. 3), suggesting ~1° tilt since 13 ka. Although this tilt can't be constrained in three dimensions, the direction of the tilt might suggest deformation similar to the dextral pull-apart type deformation documented earlier in the evolution of the Wassuk Range fault system, with the northern portion of the fan dropping relative to the range front fault to the north.

Future work

While initial research results are encouraging, extensive work remains to better constrain deformation at and adjacent to the right step in the rangefront fault system, adjacent to the abandoned Penrod Canyon alluvial fan. This work includes:

1) additional sampling for cosmonuclide exposure age analyses to better constrain the age of the upper alluvial surface;
2) field investigation of faulting at the right step in the rangefront system;
3) detailed documentation of the morphology of both the older Pleistocene and younger Holocene scarps;
4) shallow seismic investigation of exposed faults to better constrain fault orientation and subsurface structures; and
5) trenching across the exposed Holocene scarps, if deemed useful.

With a little luck, this research will shed light on the evolution of a segmented fault system at a segment boundary. In addition, this work might also reveal the interplay of dextral and extensional deformation at the boundary between zones of partitioned transtension.

References:

Adams, K.D., Wesnousky, S.G., and Bills, B.G., 1999, Isostatic rebound, active faulting, and potential geomorphic effects in the Lake Lahontan basin, Nevada and California: Geological Society of America Bulletin, v. 111, p. 1739 – 1756.

Anders, M.H., Schlische, R.W., 1994. Overlapping faults, intrabasin highs and the growth of normal faults. Journal of Geology, v. 102, p.165-180.

Bennett, R.A., Davis, J.L., Wernicke, B.P., 1999. Present-day pattern of Cordilleran deformation in the western United States. Geology 27 (4), 371 – 374.

Bingler, E.C., 1978. Geologic map of the Shurz quadrangle. Reno, NV, Nevada Bureau of Mines and Geology Map 60.

Childs, C., Watterson, J., Walsh, J.J., 1995. Fault overlap zones within developing normal fault systems. Journal of the Geological Society, vol. 152, p. 535-549.

Demsey, K., 1987, Holocene faulting and tectonic geomorphology along the Wassuk Range, west-central Nevada: [unpublished M.S. thesis] Tucson, University of Arizona, 62 p.

dePolo, C.M., and Anderson, J.G., 2000, Estimating the slip rates of normal faults in the Great Basin, U.S.A.: Basin Research, vol. 12, p. 227 – 240.

Dilles, J.H., 1993, Cenozoic and normal and strike-slip faults in the northern Wassuk Range, western Nevada: In Craig, S.D., (Ed.), Structure, tectonics, and mineralization of the Walker Lane, Walker Lane Symposium Proceedings, Reno, NV, Geological. Society of Nevada, p. 114-136.

Dilles, J.H., and Gans, P.B., 1995, The chronology of Cenozoic volcanism and deformation in the Yerington area, western Basin and Range and Walker Lane: Geological Society of America Bulletin, vol. 107, p. 474 – 486.

Dixon, T.H., Stefano, R., Lee, J., and Reheis, M.C., 1995, Constraints on present-day Basin and Range deformation from space geodesy: Tectonics, vol. 14, p. 755 – 772.

Ferrill, D.A., Stamatakos, J.A., and Sims, D., 1999, Normal fault corrugation: implications for growth and seismicity of active normal faults: Journal of Structural Geology, vol. 21, p. 1027 – 1038.

House, P.K., and Adams, K.D., 2009, Preliminary [DRAFT] geologic map of the southern part of the Lower Walker River area, Mineral County, Nevada: Nevada Bureau of Mines and Geology, 1:24,000 scale.

Lal, D.,1991, Cosmic ray labeling of erosion surfaces: in situ nuclide production rates and erosion models: Earth and Planetary Science Letters, v. 104, p. 424–439.

Ludington, S., McKee, E., Cox, D., Moring, B., and Leonard, K., 1996, Pre-Tertiary Geology of Nevada: USGS Open File Report 96 – 2, 1:1,000,000 scale.

McIntyre, J., 1990, Late Cenozoic structure of the Central Wassuk Range, Mineral County, Nevada: [unpublished MS thesis] Corvallis, Oregon State University.

Minster, J.B., and Jordan, T.H., 1987, Vector constraints on western U.S. deformation from space geodesy, neotectonics and plate motions: Journal of Geophysical Research, vol. 92, p. 4798 – 4804.

Murphy, J.J., Watkinson, J., and Oldow, J., 2009, Spatially partitioned transtension within the central Walker Lane, western Great Basin, USA: application of the polar Mohr construction for finite deformation: Geological Society of America Special Paper 447, p. 55 – 70.

Oldow, J.S., 2003, Active transtensional boundary zone between the western Great Basin and Sierra Nevada block, western U.S. Cordillera: Geology, vol. 3, p. 1033 – 1036.

Peacock, D.C.P., and Sanderson, D.J., 1994, Geometry and development of relay ramps in normal fault systems: American Association of Petroleum Geologists Bulletin, vol. 78, p. 147-165.

Schlische, R.W., Anders, M.H., 1996. Stratigraphic effects and tectonic implications of the growth of normal faults and extensional basins. Geological Society of America Special Paper 303, p. 183-203.

Stewart, J.H., and Carlson, J.E., 1978, Geologic Map of Nevada: Miscellaneous Field Investigations, MF-930, USGS.

Stockli, D.F., Surpless, B.E., Dumitru, T.A., 2002, Thermochronological constraints on the timing and magnitude of Miocene and Pliocene extension in the central Wassuk Range, western Nevada. Tectonics 21(4), doi: 10.1029/2001TC001295.

Stone, J.O., 2000, Air pressure and cosmogenic isotope production: Journal of Geological Research, v. 105,p. 23753–23759.

Surpless, B.E., Stockli, D.F., Dumitru, T.A., Miller, E.L., 2002. Two-phase westward encroachment of Basin and Range extension into the northern Sierra Nevada. Tectonics 21 (1), doi: 10.1029/2000TC001257.

Surpless, B.E., *in press*, Geologic map of the central Wassuk Range, western Nevada: Geological Society of America Maps.

Wallace, R. E., 1977, Profiles and ages of young fault scarps, north-central Nevada: Geological Society of America Bulletin, vol. 88, p. 1267 – 1281.

Wesnousky, S.G., 2005, Active faulting in the Walker Lane: Tectonics 24, doi: 10.1029/2004TC001645.

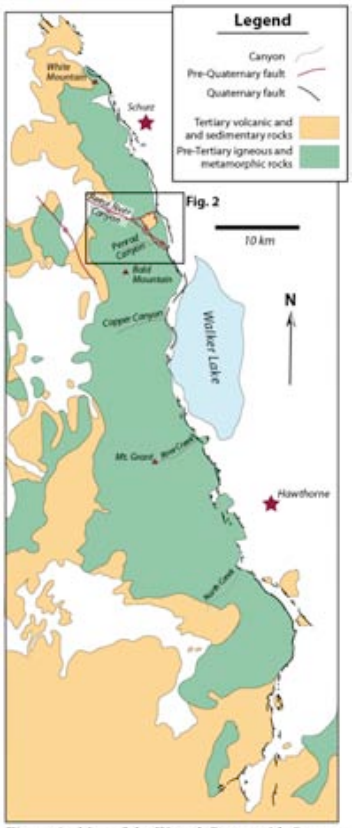

Figure 1. Map of the Wassuk Range with Quaternary range front faults and faults of the Penrod and Reese River canyons highlighted. Note the offset in the position of the Tertiary unconformity across the Reese River - Penrod fault system. Map significantly modified from: Stewart and Carlson, 1978; Ludington et al., 1996; Wesnousky, 2005; and Surpless, 2010.

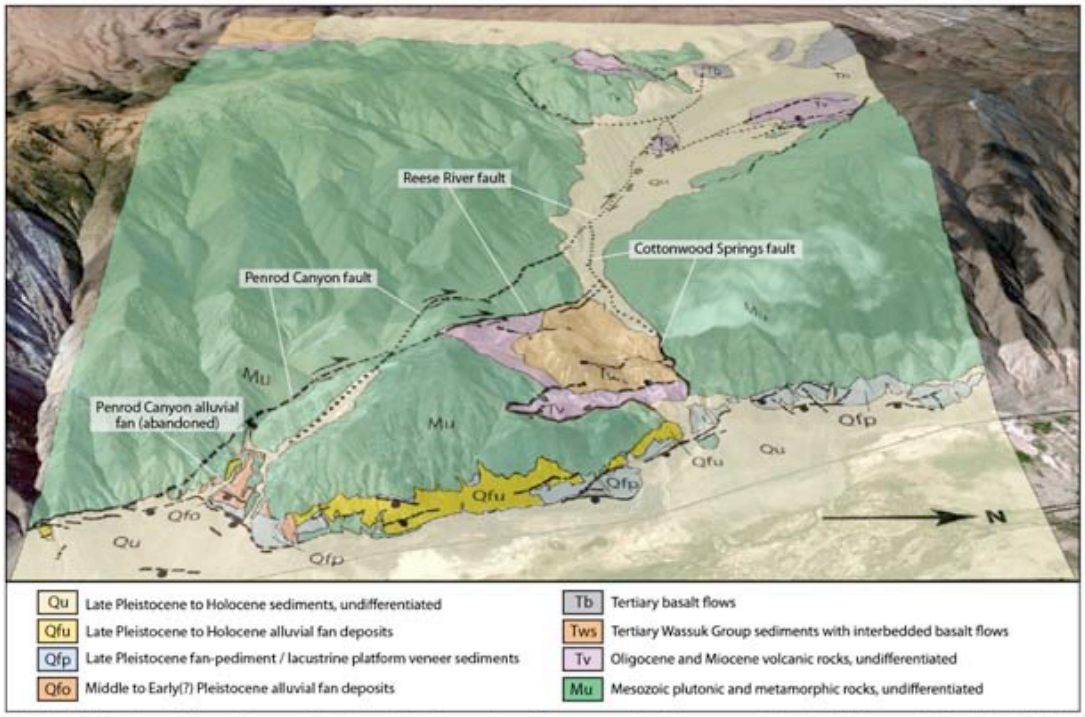

Figure 2. Oblique view of the geologic map of the Reese River Canyon - Penrod Canyon area draped over topography and aerial imagery in Google Earth, looking west. See Figure 1 for location. The Reese River fault accommodated up to 3350 meters of dextral movement prior to 7 Ma, and the Penrod Canyon - Reese River - Cottonwood Springs fault systems are hypothesized to have worked in concert with a dextral range-front fault system to the north of the Cottonwood Springs fault to form a pull-apart basin, resulting in deposition of Tertiary Wassuk Group sediments (McIntyre, 1990). Rangefront Quaternary units are significantly modified from House and Adams (2009), and all other geology is modified from McIntyre (1990) and Surpless (*in press*).

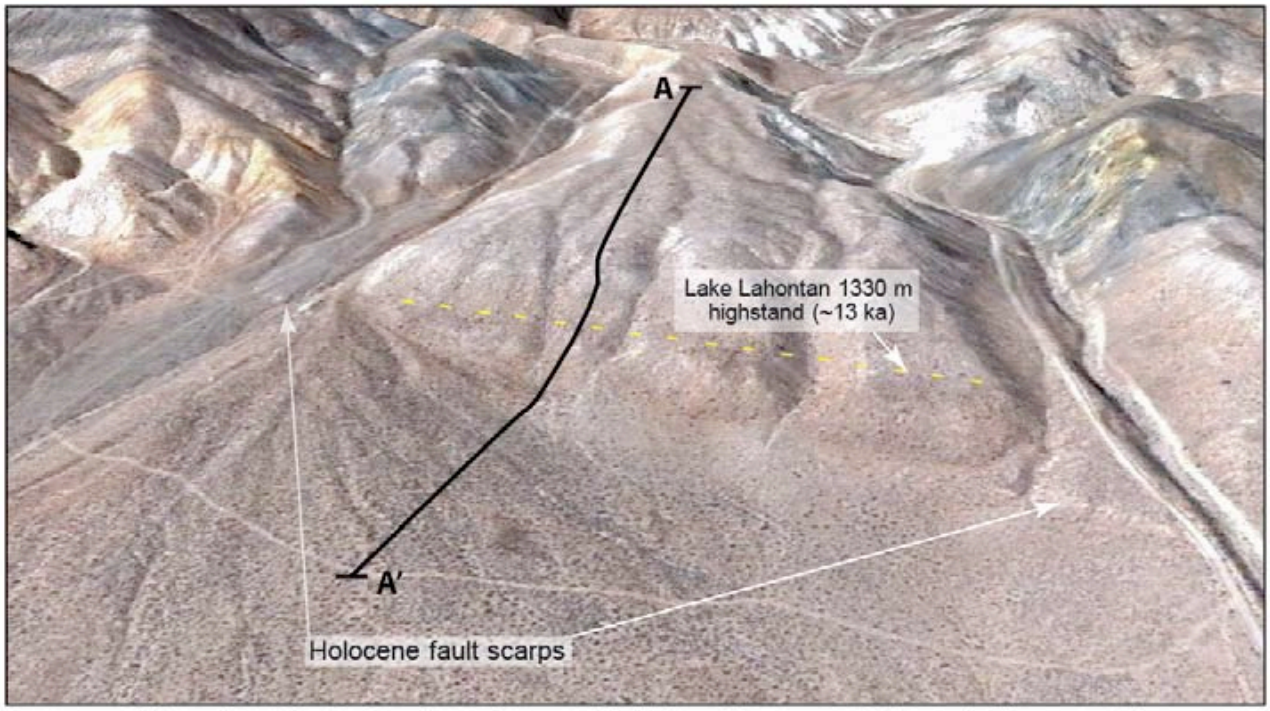

Figure 3a. Oblique view of the abandoned Penrod Canyon alluvial fan and Quaternary fault scarp, looking west. Holocene scarps cut active alluvial surfaces to the NE and SW of the older Quaternary fault scarp, and the degraded wave-cut bench of the Lake Lahontan 1330-m highstand has modified the older scarp. The cross-section A-A' shown in Figure 3b is based on the topographic profile along line of section A-A', shown above.

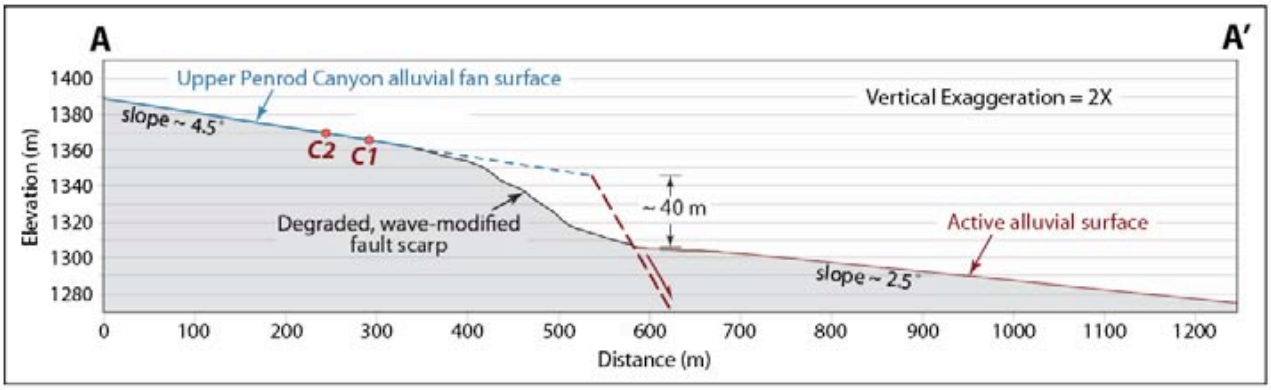

Figure 3b. Cross-section across the Penrod Canyon alluvial fan and degraded Quaternary fault scarp. Samples from two large (>1.5 m diameter) boulders yielded cosmonuclide exposure ages of 91 ka +/-12 ka (C1) and 106 ka +/- 15 ka (C2) using a constant production rate model of Lal (1991) and Stone (2000).

STOP 5 - Ken Adams, Desert Research Institute

Surficial Geology and Holocene Lake-Level Fluctuations of Walker Lake, Nevada

Kenneth D. Adams, Desert Research Institute, Reno, NV
P. Kyle House, Nevada Bureau of Mines and Geology, Reno, NV

Introduction

The purpose of this stop is to present details of recent surficial geologic mapping efforts along the lower Walker River (House and Adams, 2009; www.nbmg.unr.edu/dox/of0913.pdf) that provide a broader context for late Holocene lake-level fluctuations at Walker Lake and other active geologic processes. The material presented on lake levels and sedimentary environments at this stop is largely excerpted from Adams (2007), with the addition of a few new thoughts on maximum Holocene lake levels. We are now near the historic highstand (~1252 m) but evidence for at least three other late Holocene highstands is also found along this part of the river.

Geologic Setting

Walker Lake is located in western Nevada at the terminus of the Walker River, its principal tributary. The Walker River drainage basin has its headwaters at the crest of the Sierra Nevada (~3050-3750 m) and encompasses about 10,500 km^2. Along most of its course, the river flows over an alluvial bed through relatively flat, semiarid basins. Strongly seasonal flow in the river is controlled by melting winter snow that falls on the higher parts of the Sierra. Since the 19th century, the river's flow has been greatly diminished by agricultural withdrawals, in some years to the point where no water reaches the lake.

In the late Pleistocene, Walker Lake was the site of the southernmost arm of Lake Lahontan. It became separated from the rest of the Lahontan system when lake level receded below the sill in northern Mason Valley (~1310 m) shortly after about 13 ka (Thompson et al., 1986; Adams and Wesnousky, 1998). Walker Lake desiccated and probably remained a shallow, ephemeral playa lake until the late Holocene, when the lake abruptly flooded (Benson and Thompson, 1987). This history strongly suggests that the Walker River was flowing into the Carson Sink for much of the time from shortly after the Lahontan highstand to the late Holocene. During the late Holocene, the level of Walker Lake has fluctuated in response to climate changes, as well as to the occasional shifting of Walker River flow to the Carson Sink and back again (Benson and Thompson, 1987; King, 1993; King, 1996; Adams, 2003a). Preliminary work along the paleochannel through which the river was diverted indicates that the Walker River was flowing toward the Carson Sink during the periods from about 1500 to 1000 and 500 to 300 cal yr B.P. (Adams, 2004). Holocene lake-level fluctuations at Walker Lake, therefore, may not be attributed solely to changes in climate.

Along its lower reaches, Walker River flows south along the axis of a half-graben, bounded on its west by the normal, high angle Wassuk Range front fault zone and on its east by the Gillis Range (Fig. 1) (Link et al., 1985; Demsey, 1987; Wesnousky, 2005). The floor of the half-graben is tilted slightly to the west, which has influenced the locus of deltaic deposition as the lake retreated from its historic highstand (Blair and McPherson, 1994; House and Adams, 2009).

In its lower reaches, the LWR possesses a convex-up long profile with a gradient ranging from about 0.001 to 0.0018. The river has severely incised its bed as a result of lake-level lowering over the last century. Adjacent to the river, the long profile of the valley floor possesses a prominent topographic step just downstream from the general position of the early 20th century delta complex

(Blair and McPherson, 1994). The step probably represents a relatively thick wedge of primarily deltaic sediments that was deposited when lake level was around 1250 m at one or more times in the past.

Site Descriptions

The main types of sedimentary environments recorded in the outcrops and landforms of the LWR include those associated with river, delta, prodelta, and shoreline settings. The modern and ancient deltas along the LWR are shallow-water, Gilbert-type deltas (Gilbert, 1885; Postma, 1990) with foresets ranging in amplitude from 3 + m down to a few tens of centimeters. Deposits along the axial portions of the LWR are generally fine-grained, ranging from sand to clay, with lesser amounts of fine gravel. Small eolian dunes, sand sheets, and alluvial fans and fan deltas shed from the adjacent Wassuk and Gillis ranges are also present (Dohrenwend, 1982; Link et al., 1985; House and Adams, 2009). Table 1 provides brief descriptions of the various fluvial and lacustrine lithofacies found along the LWR, their formative depositional environments, and estimated water depth in which they formed. In the descriptions below, stratigraphic units are designated by the letters A, B, C, D, etc. but are not intended to represent the same units at different sites unless explicitly stated.

Site 1

The most recent incision event probably started when Walker Lake began to recede from its historic highstand in the late 19th century, but may have been as late as about 1925 based on the distribution of historic deltas presented in Blair and McPherson (1994). Site 1 is represented by a fill-cut terrace (T3) composed of fluvial-deltaic sediments (Figs. 2 and 3). The terrace surface here is at an elevation of about 1252 m (4108 ft) and the terrace sediments are a few meters thick at site 1. They are composed of thinly bedded, horizontal mud and sand layers (Stt) that abruptly transition into steeply dipping (10-20°), thinly bedded sands arranged into tabular and trough-cross bedded sets (Sg) with amplitude of at least 3 m (Fig. 3). The foresets have extensive vertical burrows that may be the result of tiger beetles, which live on the margins of many closed basin lakes.

The stratigraphic relations at Site 1 are interpreted as a deltaic topset-foreset transition indicating a lake that reached an elevation of about 1252 m. Detrital charcoal from the topsets yielded a radiocarbon age of 80 + 30 14C yr B.P., which when calibrated (2σ) corresponds to several age intervals. Two of the intervals (140-20 and 0 cal yr B.P.) correspond to the historic period. Based on the calibrated age ranges and an historic map, the topset-foreset transition at Site 1 is interpreted to represent the historic highstand of Walker Lake, which occurred in 1868 (Harding, 1965; Rush, 1970).

Russell (1885) produced a map of Walker Lake as it appeared in 1882, showing both topography and bathymetry. This map was rectified and imported into ArcGIS where the outline of the lake mapped by Russell (1885) was compared to contours generated from a digital elevation model (DEM). Russell's outline at the north end of the lake appears to most closely match a lake surface elevation of about 1250 m, suggesting that Walker Lake was near this elevation in 1882. Because the 1860s was a particularly wet decade in western Nevada (Morrison, 1964), it is not unreasonable to conclude that Walker Lake reached its historic highstand of 1252 m in 1868 and had receded to about 1250 m by the time Russell surveyed the lake in 1882.

Site 2

Terrace T4 is the oldest terrace studied by Adams (2007) and has beach ridges (~1255 m) formed on its surface (Fig. 2). The mode of emplacement and age of Terrace T4 is provided by evidence in exposures at Sites 2a and 2b, located in a large-north-facing amphitheater downstream from Site 1 (Fig. 2). Between Sites 2a and 2b, a tephra (Tm; Unit C) can be continuously traced for

several hundred meters within the strata exposed in the channel wall. At the upstream end of the exposure (Site 2a; Fig. 4a), the tephra is about 5 cm thick, relatively pure, and overlies a 20 cm thick, discontinuous, lens-shaped fluvial unit (St; Unit B) dated to 760 + 44 14C yr B.P. Based on its age, this tephra may be correlative to the one found in a deep water core (WLC84-8) by Benson et al. (1991) who estimated its age at 750 14C yr B.P., thereby providing an absolute depth estimate for those sediments surrounding the tephra in the core. Unit B is separated from underlying Unit A, which is also interpreted as a fluvial unit (St), by what appears to be a poorly developed buried soil at Site 2a (Fig. 4a). Farther downstream within the amphitheater toward Site 2b, the tephra thickens to 50-70 cm and fills broad channel features cut into the top of Unit A. At Site 2b (Fig. 4a), the tephra zone is expressed as thin to medium beds of glass shards intermixed with varying concentrations of silt. This zone is immediately overlain by shallow lacustrine deposits (Srw; Unit D) that include a prominent bed of interference ripples.

The sedimentologic and stratigraphic relationships at Site 2 are interpreted to represent at least two transgressions and one regression. The first transgression is represented by the aggrading muddy fluvial deposits of Unit A which date to around 1613 + 34 14C yr B.P. (Table 1), the age of a charcoal sample from near the base of the section (Fig. 5). The cutting of the large channel feature shown in figure 5 represents a regression that occurred between about 1613 and 760 14C yr B.P. A subsequent transgression is represented by the backfilling of the large channel. Coarse detrital charcoal from the channel fill provided an age of 4750 + 180 14C yr B.P., but the sample was probably reworked from older deposits because of the obvious age inversion (Fig. 5). Remnants of the minor buried soil separating Units A and B confirm that the 1613 14C yr B.P. and the 760 14C yr B.P. transgressions were different events separated by some amount of time.

Sites 2a and 2b also provide evidence for the lake surface elevation at the time the tephra was deposited. At Site 2a, the tephra is relatively thin and immediately overlies sandy fluvial deposits (Unit B) at an elevation of about 1252 m (Fig. 4a). The tephra thickens downstream, fills channel structures eroded into the top of Unit A and is associated with shallow water lacustrine deposits at Site 2b (Fig. 4a), which is at an elevation of about 1251.5 m. The lake continued to rise after deposition of the tephra, depositing shallow water lacustrine Unit D (Srw), and probably transgressed as high as 1255 m, the elevation of sandy beach ridges on the surface of Terrace T4 (Fig. 2).

Late Holocene (?) 1262 m highstand

The study of Adams (2007) only covered lake-level fluctuations up to about 1255 m. Since that time, it has become reasonably clear that one or more lakes transgressed to an elevation of about 1262 m, forming a well-developed sequence of shorelines (1260-1262 m) that can be traced discontinuously around Walker Lake (Fig. 6). These presumably late Holocene shorelines lie stratigraphically above alluvial fans shed from the Wassuk Range after the late Pleistocene Sehoo lake receded from its highstand of about 1330 m. The elevation and development of the 1260-1262 m shoreline complex is likely related to a sill that spills into a relatively small subbasin, herein referred to the Double Spring subbasin, located east of Schurz (Fig. 6). Work is in progress to date this complex of shorelines, which will probably lead to a modification of the late Holocene lake-level record from Adams (2007) (Fig. 7).

Table 1. Facies and paleoenvironmental interpretations along the lower Walker River.

Facies symbol[1]	Facies description	Depositional environment	Estimated water depth
St	Fine to coarse pebbly sand but occasionally finer, trough-cross bedded, climbing ripple-cross lamination, channel structures, bioturbation (roots, burrows), commonly eroded base	Fluvial	Above lake level
Stt	Similar to St but vertically and laterally associated with deltaic foresets, fine to medium bedded	Deltaic topsets	Above or at lake level
Sg	Fine to coarse sand and fine gravel beds dipping lakeward from 10˚-30˚, tabular and trough-cross bedded, burrows, amplitudes vary between 10s of cms (micro-deltas) to a few meters	Deltaic foresets	Top of foresets approximates lake surface; amplitude of foresets approximates near shore water depth
Fb	Fine sand to silt, laminated to thin bedded, wave ripples and wave-ripple lamination depending on depth	Deltaic bottomsets	10s of cms to several meters
Shc	Medium to coarse sand and grit, low-angle cross sets dipping toward basin, planar erosive base, occasional small tufa heads	Beach	0-1 m
Gmb	Coarse sand to fine gravel, tangential to sigmoidal backsets (≤ 2m) dipping away from lake and commonly interfingered with thinly bedded wave-ripple laminated fine sands to silty fine sands (See facies Srw)	Beach ridge	0 to 1-2 m above lake level
Srw	Interbedded silt to coarse sand, parallel to wavy lamination, wave ripples (RI[2] = 4-8), wave ripple laminations, burrows	Nearshore-wave influenced	0-5 m
Fm	Massive to thinly bedded silty clay, occasional thin sand laminae, commonly slightly oxidized	Offshore lacustrine	10-30 + m
Gmm	Matrix-supported sand and gravel with occasional boulders, contains folded mud layers, Wassuk Range source	Subaerial to shallow water debris flow	Above lake level to one to a few meters below
Tm	Tephra and concentrations of glass shards, most likely erupted from Mono Craters[3]	Variable-fluvial, deltaic, offshore	Variable

[1]Symbols modified from Postma (1990)
[2]RI=Ripple index (Reineck and Singh, 1980)
[3]All late Holocene tephras in Walker Lake area probably have a Mono Craters source (e.g., Davis, 1978; Miller, 1985; Sieh and Bursik, 1986; Stine, 1990) and are very difficult to distinguish geochemically (Personal comm., A. Sarna-Wojcicki, 2005).

References

Adams, K. D., 2003a, Age and paleoclimatic significance of late Holocene lakes in the Carson Sink, NV, USA: Quaternary Research, v. 60, p. 294-306.

Adams, K. D., 2004, Late Holocene diversion history of the Walker River: The tale of a river with a split personality: Geological Society of America Abstracts with Programs, v. 36, no. 5, p. 499.

Adams, K. D., 2007, Late Holocene sedimentary environments and lake-level fluctuations at Walker Lake, Nevada, USA: Geological Society of America Bulletin, v. 119, no. 1/2, p. 126-139.

Adams, K. D., and Wesnousky, S. G., 1998, Shoreline processes and the age of the Lake Lahontan highstand in the Jessup embayment, Nevada: Geological Society of America Bulletin, v. 110, no. 10, p. 1318-1332.

Benson, L. V., Meyers, P. A., and Spencer, R. J., 1991, Change in the size of Walker Lake during the past 5000 years: Palaeogeography, Palaeoclimatology, Palaeoecology, v. 81, p. 189-214.

Benson, L. V., and Thompson, R. S., 1987, Lake-level variation in the Lahontan basin for the last 50,000 years: Quaternary Research, v. 28, p. 69-85.

Blair, T. C., and McPherson, J. G., 1994, Historical adjustments by Walker River to lake-level fall over a tectonically tilted half-graben floor, Walker Lake Basin, Nevada: Sedimentary Geology, v. 92, p. 7-16.

Davis, J. O., 1978, Quaternary tephrochronology of the Lake Lahontan area, Nevada and California, University of Nevada, Nevada Archeological Survey Research Paper 7, 137 p.

Demsey, K. A., 1987, Late Quaternary faulting and tectonic geomorphology along the Wassuk Range, west-central Nevada: Geological Society of America Abstracts with Programs., v. 19, no. 7, p. 640.

Dohrenwend, J. C., 1982, Surficial geology, Walker Lake 1° by 2° quadrangle, Nevada-California: U.S. Geological Survey Miscellaneous Field Studies Map MF-1382-C, Scale 1:250,000.

Gierlowski-Kordesch, E. H., and Kelts, K. R., 2000, Preface, *in* Gierlowski-Kordesch, E. H., and Kelts, K. R., eds., Lake Basins Through Space and Time: Tulsa, OK, American Society of Petroleum Geologists, AAPG Studies in Geology #46, p. iii-viii.

Gilbert, G. K., 1885, The topographic features of lake shores: Fifth annual report of the U.S. Geological Survey, p. 69-123.

Harding, S. T., 1965, Recent variations in the water supply of the western Great Basin, Archive Series Report no. 16: Berkeley, California, Water Resources Center Archives, University of California, 225 p.

House, P.K., and Adams, K.D., 2009, Preliminary geologic map of the southern part of the lower Walker River area, Mineral County, NV: Nevada Bureau of Mines and Geology Open-File Report 09-13, 1:24,000-scale.

King, G. Q., 1993, Late Quaternary history of the lower Walker River and its implications for the Lahontan paleolake system: Physical Geography, v. 14, no. 1, p. 81-96.

King, G. Q., 1996, Geomorphology of a dry valley: Adrian Pass, Lahontan basin, Nevada: Association of Pacific Coasts Geographers Yearbook, v. 58, p. 89-114.

Link, M. H., Roberts, M. T., and Newton, M. S., 1985, Walker Lake Basin, Nevada: An example of Late Tertiary (?) to Recent sedimentation in a basin adjacent to an active strike-slip fault, *in* Biddle, K. T., and Christie-Blink, N., eds., Strike-slip deformation, basin formation, and sedimentation: Tulsa, Society of Economic Paleontologists and Mineralogists, p. 105-125.

Miller, C. D., 1985, Holocene eruptions at the Inyo volcanic Chain: Implications for possible eruptions in Long Valley Caldera: Geology, v. 13, p. 14-17.

Morrison, R. B., 1964, Lake Lahontan: Geology of the southern Carson Desert, U.S. Geological Survey Professional Paper 401, 156 p.

Postma, G., 1990, Depositional architecture and facies of river and fan deltas: A synthesis, *in* Colella, A., and Prior, D. B., eds., Coarse-Grained Deltas: Oxford, Blackwell Scientific Publications, p. 13-27.

Reineck, H. E., and Singh, I. B., 1980, Depositional sedimentary environments: Berlin, Germany, Springer-Verlag, 549 p.

Rush, F. E., 1970, Hydrologic regime of Walker Lake, Mineral County, Nevada: U.S. Geological Survey, Hydrologic Investigations Atlas HA-415.

Russell, I. C., 1885, Geological history of Lake Lahontan, a Quaternary lake in northwestern Nevada, U.S. Geological Survey Monograph 11, 288 p.

Sieh, K., and Bursik, M., 1986, Most recent eruption of the Mono Craters, eastern central California: Journal of Geophysical Research, v. 91, no. B12, p. 12,539-12,571.

Stine, S., 1990, Late Holocene fluctuations of Mono Lake, California: Palaeogeography, Palaeoclimatology, Palaeoecology, v. 78, p. 333-381.

Thompson, R. S., Benson, L. V., and Hattori, E. M., 1986, A revised chronology for the last Pleistocene lake cycle in the central Lahontan Basin: Quaternary Research, v. 25, no. 1, p. 1-9.

Tucker, M. E., 2003, Sedimentary rocks in the field, 3rd Ed., The Geological Field Guide Series: West Sussex, England, John Wiley and Sons, 233 p.

Wesnousky, S. G., 2005, Active faulting in the Walker Lane: Tectonics, v. 24, TC3009, doi:10.1029/2004TC001645.

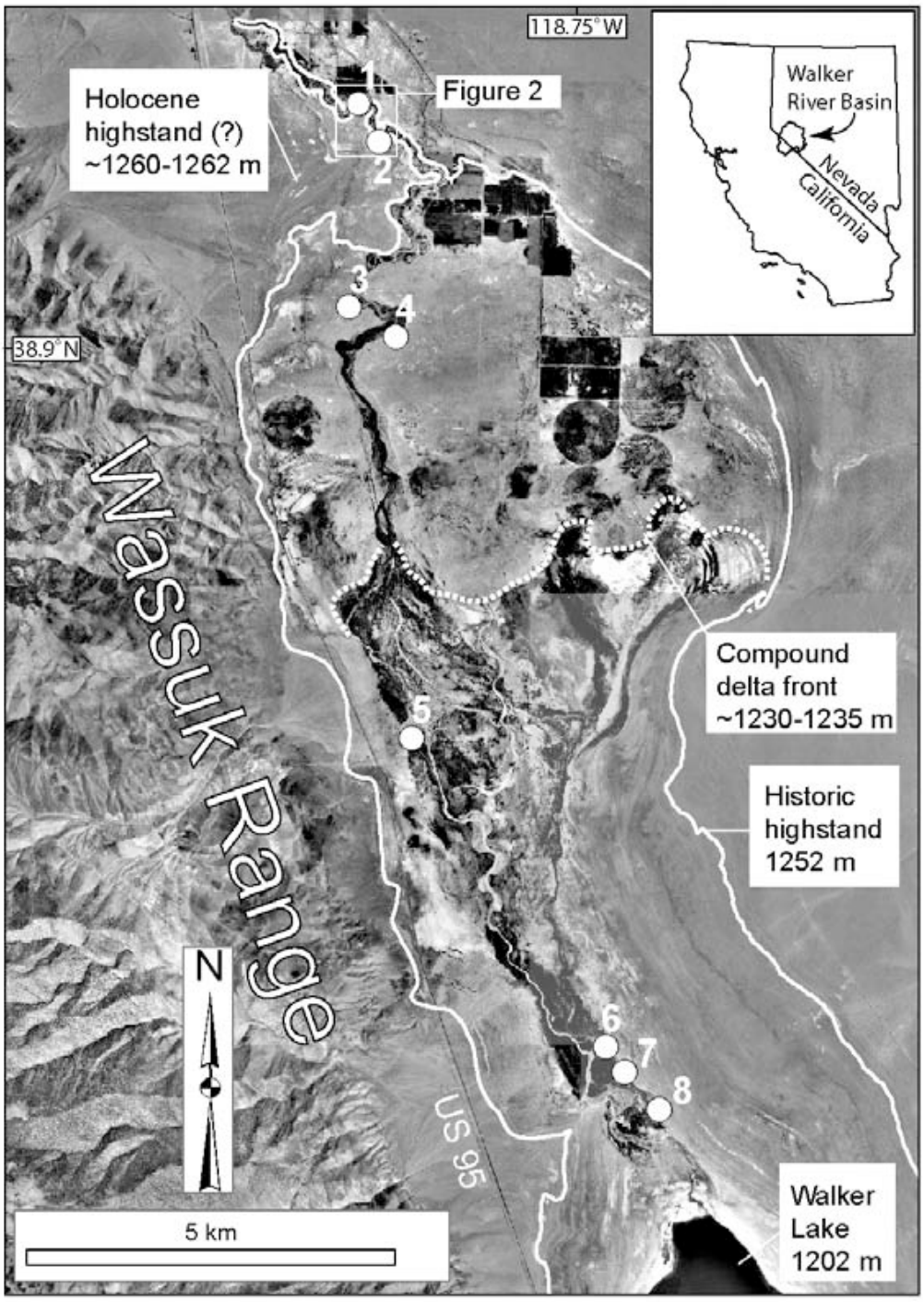

Figure 1. Location map of the lower Walker River system showing features pertinent to this study and site locations for this stop. Walker Lake has declined by about 50 m over the last 100 years or so exposing the former lake bed which is now incised by the river. For descriptions of sites 3-8 see Adams (2007).

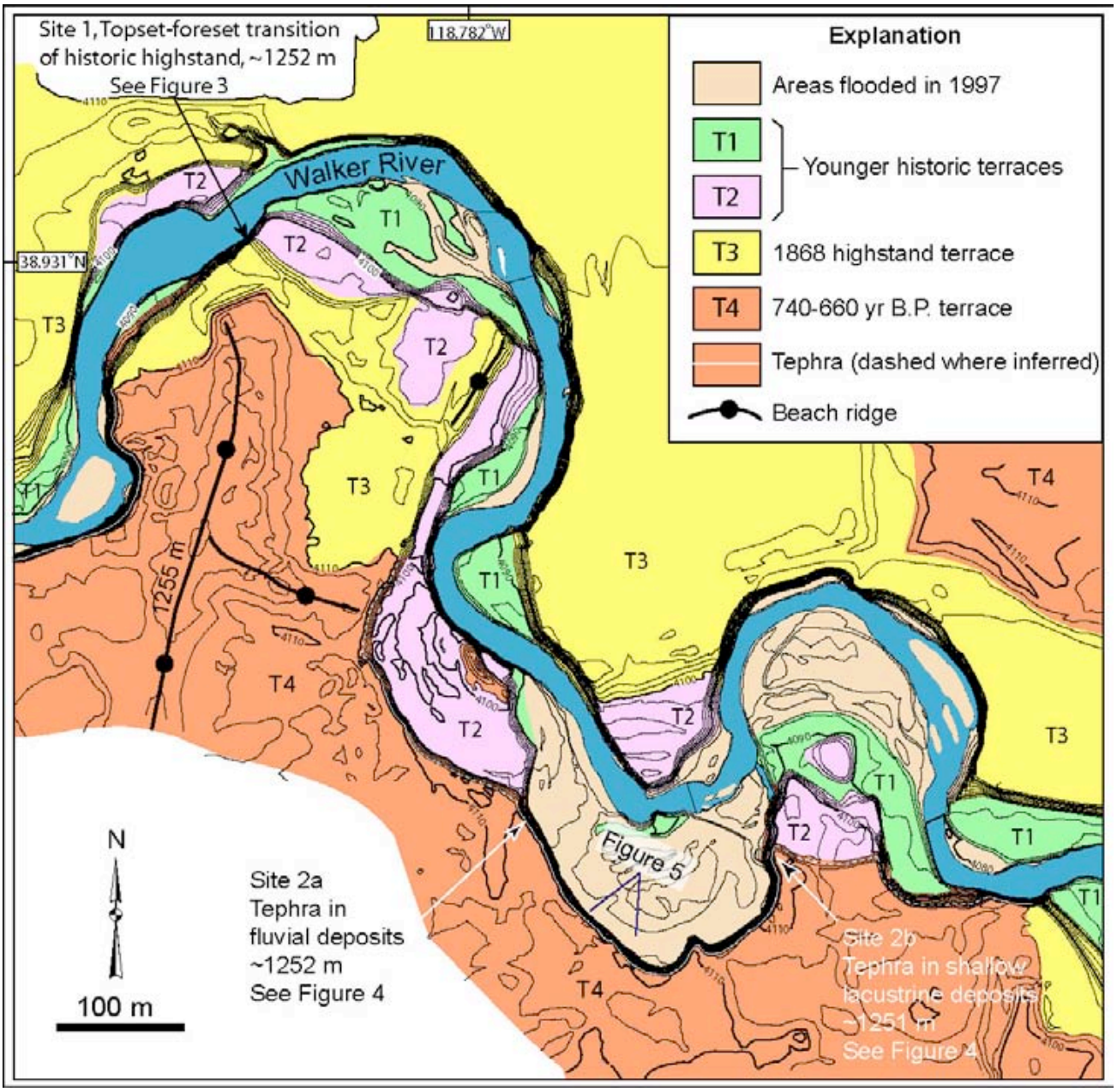

Figure 2. Geologic and geomorphic map of fill and cut terraces formed since 1868, the age of the historic highstand. The locations of Sites 1, 2a, and 2b are also shown. Contour interval is 2 feet.

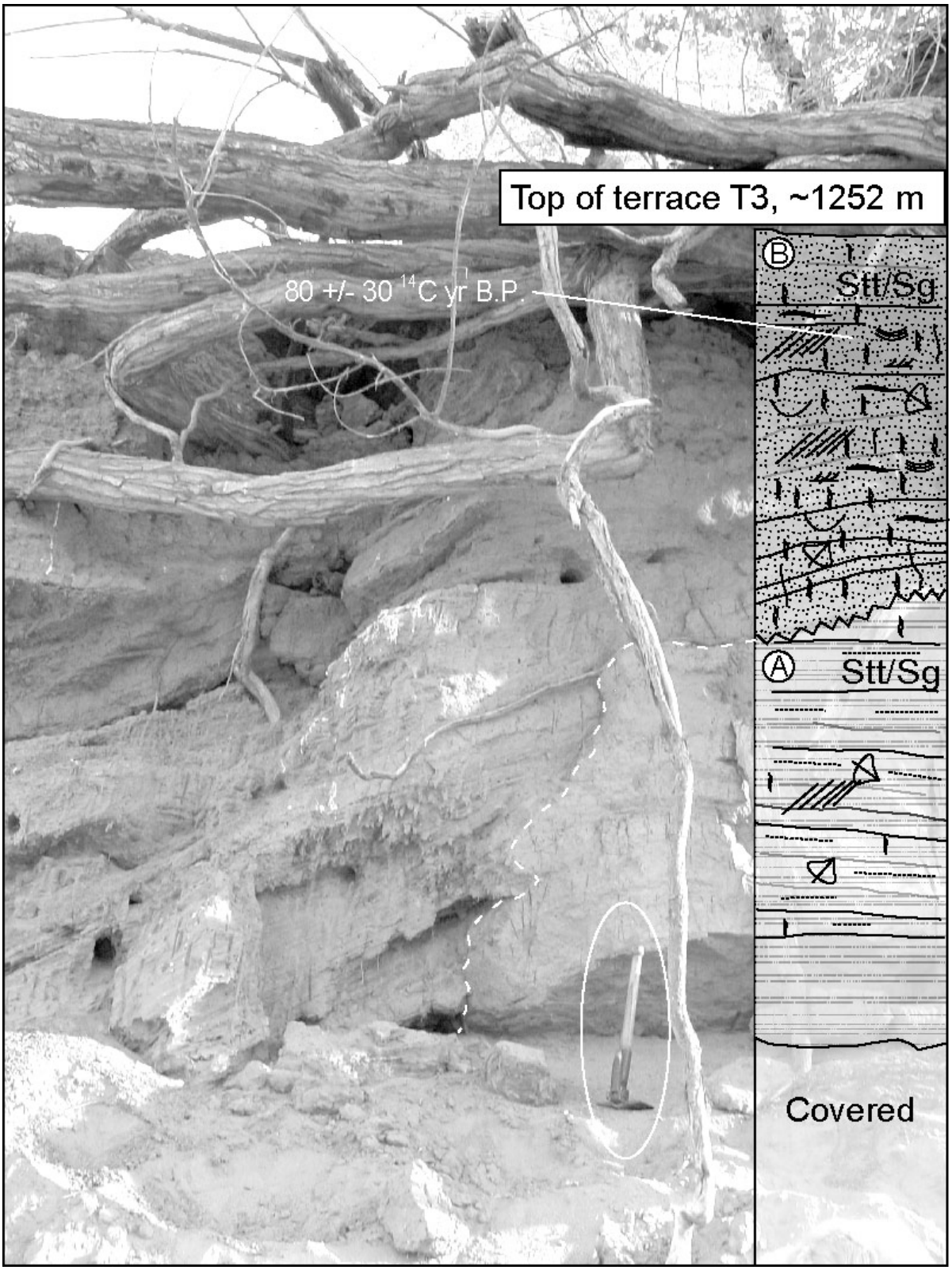

Figure 3. Site 1 represents the topset-foreset transition of the historic highstand at an elevation of about 1252 m. Dashed white line represents the erosional contact between Units A and B. Location of the site is shown in figures 1 and 2 and radiocarbon age is projected from a location about 15 m to the southwest. General facies descriptions are in Table 1 and sedimentary feature symbols are in figure 4b.

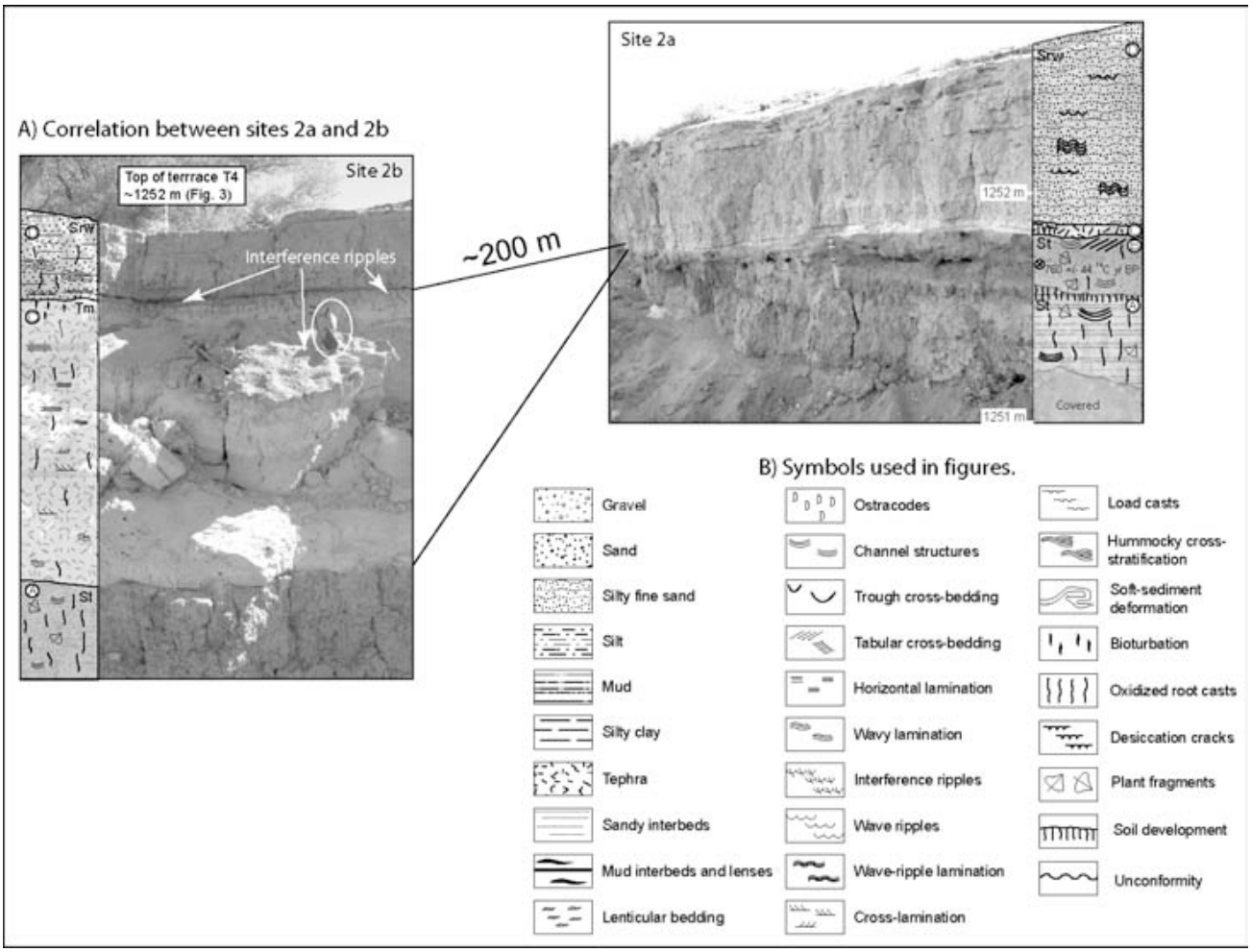

Figure 4a. Photographs of Sites 2a and 2b (Locations in figure 2) showing sedimentary features and their correlation based on tracing Units C (tephra) and D between the two sites. Interference ripples on upper surface of fallen block indicate shallow water (Circled trowel for scale). Facies descriptions are in Table 1. b) Sedimentary symbols used in figures in this paper (after Tucker [2003] and Gierlowski-Kordesch and Kelts [2000]).

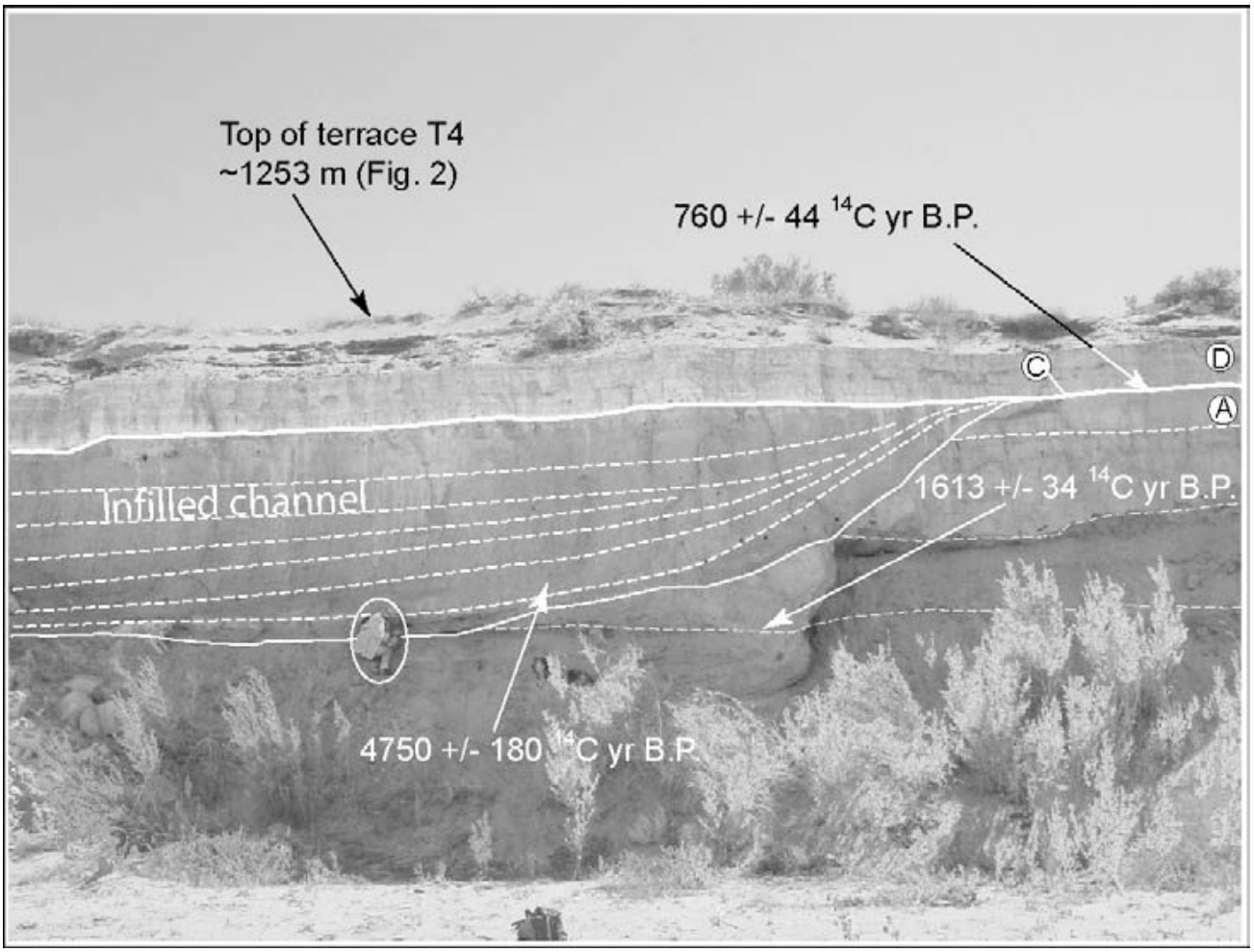

Figure 5. Photograph of large channel feature that was cut after 1613 14C yr B.P. and backfilled before about 760 14C yr B.P. Unit designations are the same as in figure 4a and location is shown in figure 2. Obvious date inversion within channel fill indicates reworking from older deposits. Location of the 760 14C yr B.P. sample projected from a location about 150 m to the northwest (Site 2a).

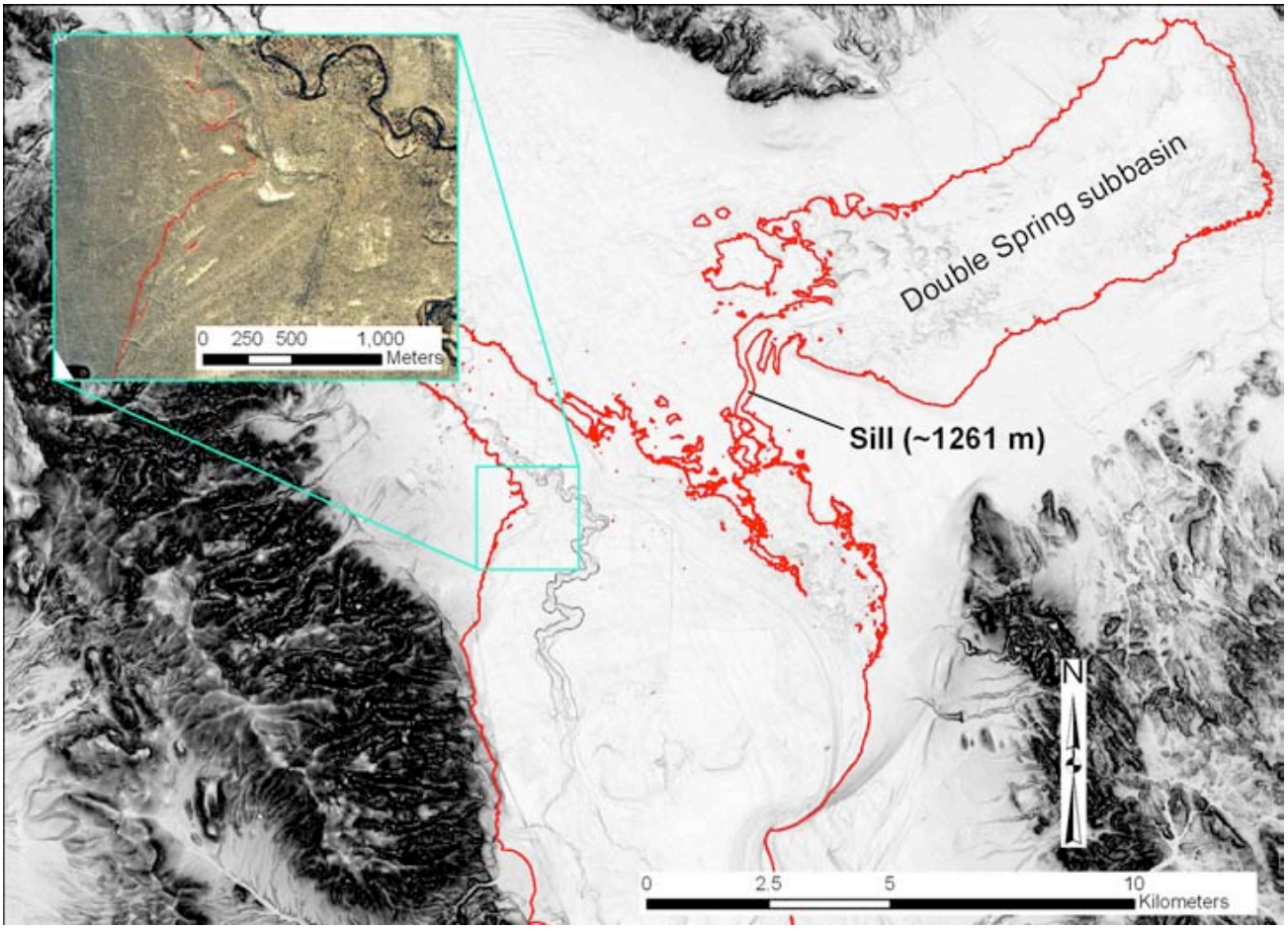

Figure 6. Map of the lower Walker River showing the sill that allowed spill into the Double Spring subbasin, thereby limiting the Holocene (?) highstand to about 1260-1262 m. Red line is the 1262 m contour.

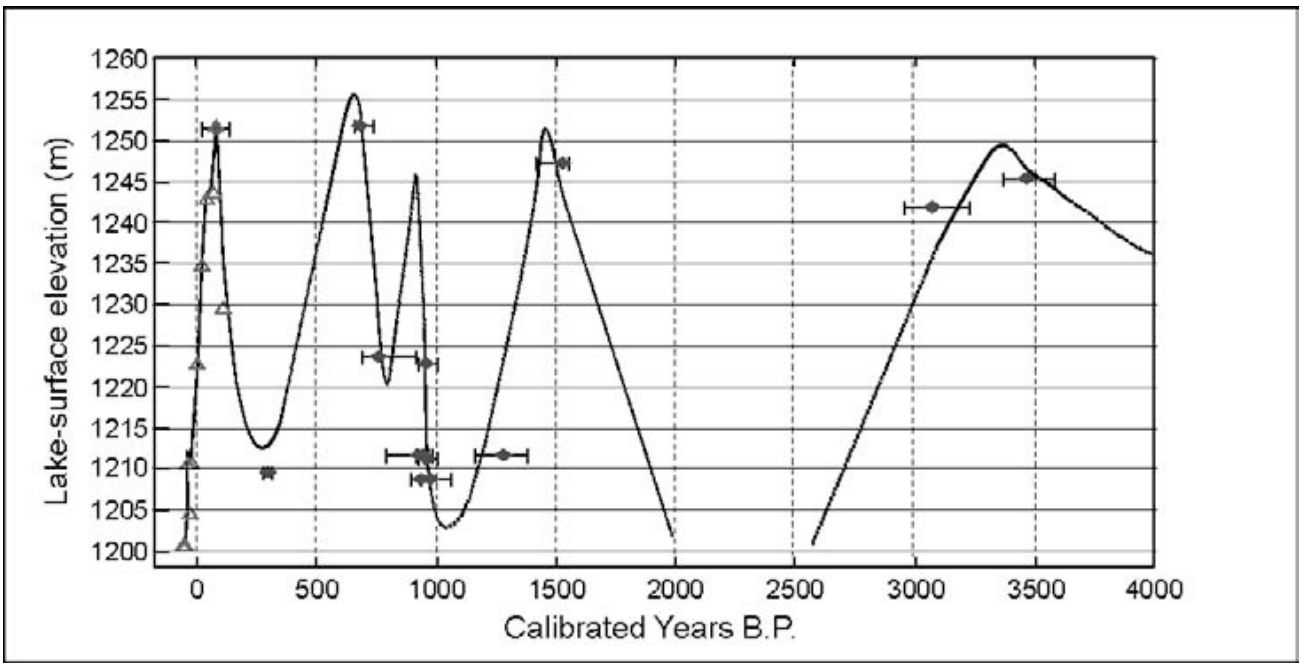

Figure 7. Late Holocene lake-level curve for Walker Lake (Adams, 2007). This curve will probably be modified depending on the age of the 1260-1262 m shoreline complex.

STOP 6- Lake Wellington, Smith Valley

Smith Valley was home to pluvial Lake Wellington. The Lake was not coeval with it's big sister Lake Lahontan. Questions exist regarding its age and genesis. This stop will be at a lacustrine bar deposit that remains well preserved at the northern end of the Valley, where a soil pit has been placed for your viewing pleasure and Heidi Stauffer will present findings arising from her Master's thesis studies some years back.

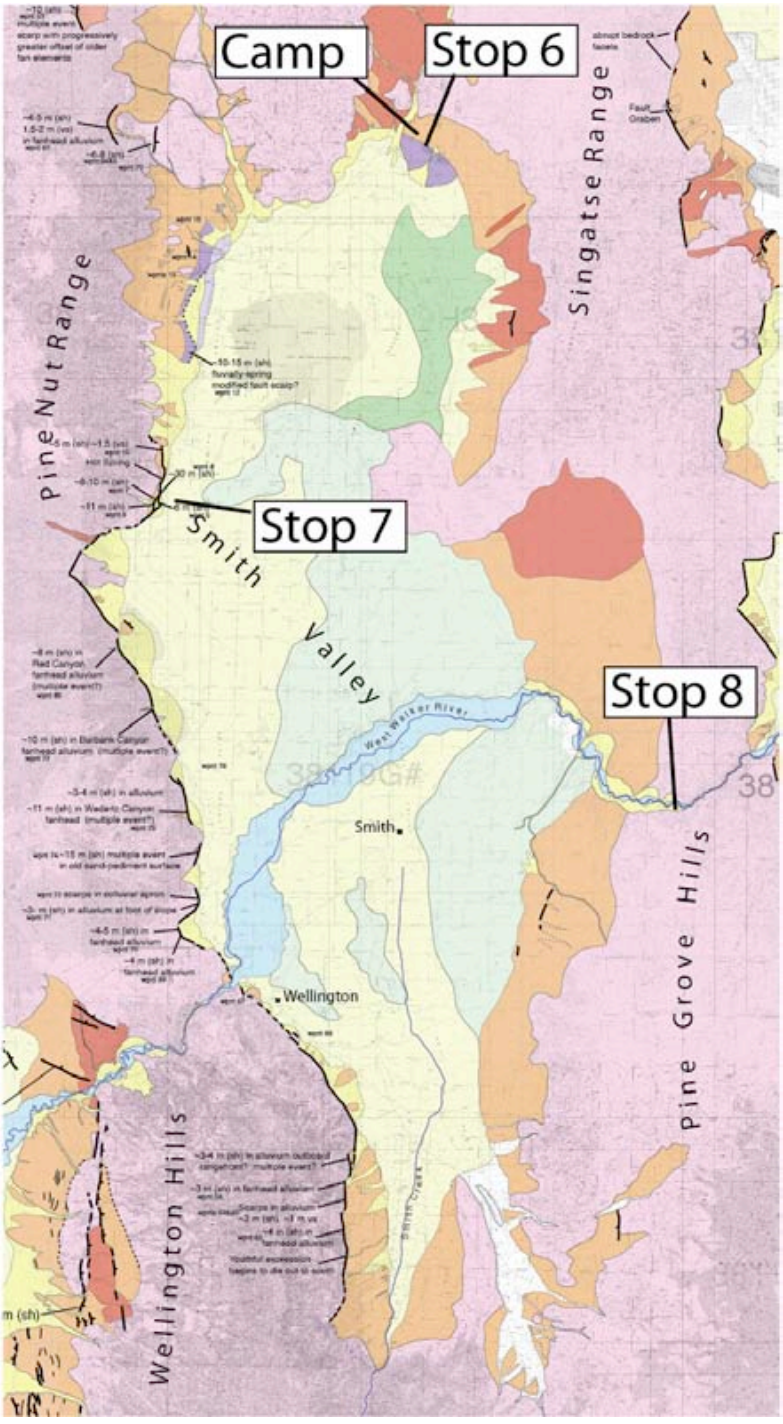

Figure 6-1. Withstanding the simplicity and various errors seen and unseen, this generalized surficial map of Quaternary deposits and Active fault s (solid) line) can give you a little perspective as you gaze around Smith Valley Nevada.

Yellow, Orange, and Red are young, intermediate, and older Quaternary surfaces.

Light yellow and light green are basin-fill and 'basin-fill terrace' deposits.

Dark green is dunes.

Purple are Lacustrine deposits or wave modified features.

The Walker River flows from west to east across the

The soil pit at this stop is brought to you through the efforts of Alexandra Sarmiento (CNS) and Riccardo Civicio (INGV, ITALY). Make sure to say thanks if you see them.

STOP 6- Heidi Stauffer - UCSC

Lake Wellington, Smith Valley Nevada.

Overview:

Smith Valley, in west-central Nevada, was occupied a pluvial lake (Lake Wellington) unconnected to contemporaneous Lake Lahontan, which reached its final highstand of approximately 1,477-m elevation during late Pleistocene time (Mifflin and Wheat, 1979; Stewart and Dohrenwend, 1984). Evidence for Lake Wellington includes abundant lacustrine deposits and shorelines. and Wheat (1979) also suggested that this lake overflowed into neighboring Mason Valley before 35,000 years ago. On the basis of soil development on lacustrine sediment, and a tephra layer within the sequence, the 1477-m highstand of Lake Wellington occurred between 80 and 60 ka (Stauffer, 2003, unpublished Master's thesis).

Deposits and Shorelines:

North of about 38^{o} 50' N and south of about 39^{o} 00' N (see location map), areas of Smith Valley below 1,477 m are covered primarily with deposits of massive and laminated silt and clay, and by minor fine to medium sand (Stewart and Dohrenwend, 1984). These deposits are generally exposed on the valley floor and along the margins of the valley, and are described in detail by Stewart and Dohrenwend (1984). exposures of fine to medium sand were also observed at or less than a few meters below 1,477 m, and a majority of these deposits show either crossbedding or indistinct horizontal lamination (Stauffer, 2003). The deposits range in thickness from less than 1 m to more than 6 m (Stauffer, 2003).

The three measured sections (labeled on map) are well exposed, fairly thick, contain discernible stratigraphy, and are associated with the 1,477 m-highstand by their elevations and proximity to mapped shorelines. #1, #2, and #3 (see location map) are fine-grained exposures and appear to be typical of the deposits of Lake Wellington in grain size and the presence of interbeds of fine to medium sand. Layers with indistinct lamination about 1 mm thick in the clay, and cross-lamination at a scale of a few millimeters in the silt and sand are the only stratification in these exposures (Stauffer, 2003). Exposure #4 is located near the topmost unit of Section #3, and is probably stratigraphically out of place because of faulting along adjacent Smith Valley fault zone. Therefore, it was considered separately from Section #3. Section #3 and Exposure #4 are both at the Artesia Road location (see location map).

Section #1 (see **map**, **figure - 6-2 & 6-3**), measured east of Nordyke Pass, is mostly clay and silt with interbeds of fine to medium sand. The section appears to coarsen upward. Section #1 contains a 1.5-cm-thick tephra layer (see map, figure) located about 220 cm below cross-bedded sand and approximately 250 cm below the poorly sorted pebbly sand of units (Stauffer, 2003). This section also contains at least one distinct layer of fossilized plants within a sequence of silt and clay (see map, figure) and no similar layer was noted in any of the other three sections (Stauffer, 2003). Section #1 is much thicker than the other sections and likely contains a more complete record of deposition. The section is capped by about 0.25 m of poorly sorted gravel containing boulders up to almost 1 m along their long axes. This deposit is part of the alluvial deposit at the top of the section and is interpreted as a debris flow. Its relative resistance to erosion accounts for the preservation of the sedimentary deposits beneath it. The debris flow also appears to have eroded the topmost portion of the post-lacustrine subaerial deposit above Unit 1R (see figure) as well as upper soil horizons (Stauffer, 2003).

Section #2 (see map) is generally fine-grained sediment, ranging from silt at the base to fine sand and silt, silty clay, and silt at the top. The silt and clay layers are generally massive, with faint lamination at a scale of about 1 mm. The silt and fine sand also lack bedding, except for faint cross-lamination at the scale of a few millimeters. The exposure is capped by very well sorted fine-grained sand, mapped as eolian sand by Stewart and Dohrenwend (1984), modern alluvium derived from the bedrock highs to the south, and a thin veneer of subrounded fine gravel and coarse sand. Like Section #1, Section #2 contains layers of fine sand, some showing cross-lamination at a scale of a few millimeters, near or at the top of the lacustrine sequence.

Artesia Road Location - STOP 7 of this trip:

This exposure was originally observed by Marith Reheis of the U.S. Geological Survey (USGS), who noted that lacustrine sediment appeared to be offset by a fault and that a tephra layer is located below the faulted section (Reheis, M., USGS, 1998, oral communication). The trace of the Smith Valley fault zone as mapped by dePolo et al. (1997), is located between the road cut and the range front of the Pine Nut Mountains, and fault scarps can be seen adjacent to the exposure.

**sediments are described in figures (see other attachment)

Coarse-Grained Lacustrine Deposits:

Two additional exposures (Localities A (high shore bar) and D, see map) were not measured but were described. Both contain moderately well to well sorted gravel and sand, showing both imbrication and cross bedding, and are interpreted as beach deposits (Stauffer, 2003). The clasts in both deposits are metamorphic, granitic, and volcanic rocks locally derived from the surrounding mountain ranges.most clasts are around 5 cm in size at Locality D are as large as 20 cm, and individual are well sorted in both deposits, with little fine matrix. The clasts in all layers at Localities A and D show imbrication, and cross-bedding of a few millimeters is common in layers primarily of coarse sand. Possible trough cross-bedding of a few centimeters can be seen in layers of coarse to medium sand in the deposits at Locality A (Stauffer, 2003). the localities do not contain any interbedded fine-grained lacustrine sediment and cannot be correlated to the measured sections, they do provide evidence of deposition at or near the lake shore.

Shorelines:

Four areas at or below 1,477 m with particularly prominent erosional shore features are Localities A and C, in the northern part of Smith Valley, along the eastern margin of the valley (Locality F) and in the area around Nordyke Pass (Locality B), about 10 km north-northeast of the town of Smith (see map-**Figure 6-4**). Shorelines were not observed south of the West Walker River, because deposits from Desert Creek bury evidence of Lake Wellington. On the western margin of the valley, scarps related to the Smith Valley fault zone are abundant, and shorelines there were difficult to confirm in the field. Along most of the length of the West Walker River in Smith Valley, shorelines and lake sediment are generally absent. The origins of small terraces present at Hoye Canyon and at the base of the Wellington Hills are ambiguous, and they were not included in this study. The northern valley margin, along the south end of the Buckskin Range west of the high shore bar (see map), features a conspicuous wave-cut cliff in bedrock, as well as an adjacent bedrock knob showing at least one obvious strandline, previously noted by Mifflin and Wheat (1979) and Stewart and Dohrenwend (1984).

Faults:

Smith Valley is located within the Walker Lane Seismic Belt, a broad zone of predominantly normal faults in western Nevada (see fault map; Stewart, 1988). Many of the faults mapped in Smith Valley and the surrounding mountain ranges offset primarily pre-Quaternary formations, making it difficult to determine whether any Quaternary motion has occurred on these faults. Those

faults with evidence of Quaternary slip show primarily normal offset, characteristic of faults in the Basin and Range (Stewart,

1988). At least three faults mapped in Smith Valley appear to offset Quaternary lacustrine units as mapped by Stewart and Dohrenwend (1984). The Smith Valley fault zone (see fault map) is located at the base of the Pine Nut Mountains, a west-tilted fault block (Moore, 1969; dePolo et al. 1997). The Smith Valley fault zone is the longest of the faults in Smith Valley and offsets alluvium and bedrock within the study area along the base of the Pine Nut Mountains and into the Wellington Hills in the southwest part of the valley. The Smith Valley fault zone exhibits primarily normal motion and has an estimated slip rate of 0.21 to 0.81 mm/yr (fault map; dePolo et al., 1997).

Along the eastern edge of the Buckskin Range (location map), a much smaller normal fault appears to offset primarily bedrock and, at a few localities, Quaternary alluvium (Hudson and Oriel, 1979). On the eastern margin of Smith Valley, the Singatse Range is also considered a west-tilted fault block, with the bounding fault located on the eastern flank of the range, in neighboring Mason Valley (Moore, 1969).

Soil Development

In the 1960s, John Hawley and others of the U.S. Soil Conservation Service made several field excursions to western Nevada, including to Smith Valley, on a reconnaissance investigation of argillic soil development (Hawley, 1969; Hawley, 2001, written communication). They conducted field reconnaissance of soil sites in Smith Valley and described soil profiles mainly of Holocene and Late Pleistocene age. Hawley and others described the soil formed on a gravel bar later identified by Mifflin and Wheat (1979) at Sec. 17, T13N, R24E, which they estimated to be Pleistocene in age (Hawley, 1969). Examination of soil profile development was made at a location in the Nordyke Pass area (Section #1) and at two exposures of gravelly shore deposits including the high shore bar (Locality A) also examined by Mifflin and Wheat, 1979, and correlated with the 1,477-m shoreline **(Fig6-6)**. Both the soil profile at high shore bar and the soil examined at Section #1 have well-developed argillic horizons and significant pedogenic carbonate development (Stauffer, 2003).

Examination of the soil development on the sediment in Section #1 revealed the presence of two soils, indicated by two calcic horizons**(Fig 6-5)**. At the top of the section, a debris flow truncates an alluvial deposit above Unit 1R with a zone of pedogenic silica (Bqm horizon; soil profile #1). The silica horizon directly overlies the upper Bk carbonate horizon between 7 and about 20 cm below the top of the soil and the older, buried carbonate horizon (2Bkb) is developed within the lake sediment of Unit 1R beneath the alluvium (section #1; Stauffer, 2003).

As is true in many desert soil profiles, the morphology of pedogenic carbonate is an indicator of profile development (Birkeland, 1999). Sediment in Section #1 was observed to have significant carbonate development on alluvial deposits and on the underlying lacustrine deposits. The 2Bkb horizon was determined to be 36 cm thick and the carbonate morphology was inferred be at least Stage II, using the criteria in Birkeland et al., 1991 (Stauffer, 2003).

Soil development was also examined at the exposed portion of the high shore bar. The K or carbonate horizon appears to be at least 40 cm thick, but an exact measurement was not obtained because debris from quarrying activities conceals the lower portion of the section (Stauffer, 2003). At this locality, the pedogenic carbonate is developed primarily on gravel and coarse sand, and the morphology represents a weak Stage III, based on the field criteria in Birkeland et al. (1991). No profile was described for the soil developed on interpreted beach gravels near the West Walker River, but the carbonate morphology at that location is interpreted to be a Stage II. This similar to the carbonate morphology at Section #1.

Tephra:

Two tephra layers located in lake sediment in Section #1 and Section #3 associated with the final highstand of Lake Wellington were chemically analyzed and correlated to tephra of known age (Stauffer, 2003)(**Figure 6-4**

0. The tephra ages better refine the timing of the final highstand, which was estimated by Mifflin and Wheat (1979) from soil development to be before 35,000 years ago. Microscope study and chemical analyses were conducted on samples from the tephra layers found in both sections and microprobe analyses were done at the U.S. Geological Survey by James Walker. The microprobe results were compared to chemical analyses of other tephra of known ages and origins by Andrei Sarna-Wojcicki.

Sample 99AL617-154 was collected from the tephra layer located in Section #1 (section #1 figure) about 430 cm from the top of the section. The petrographic study for this sample revealed a majority of glass shards, 5 to 10% non-glass particles, including some twinned feldspars, biotite, quartz, and various volcanic and metamorphic minerals (Stauffer, 2003). Sample AL98-51A (PN9811-51A) was collected from a tephra located in Section #3, 150 cm below the top of Unit 3F (section #3 figure). The petrographic analysis for this sample yielded a majority of glass shards, and 10-20% non-glass constituents, including biotite, quartz, volcanic minerals, feldspars, and various metamorphic minerals (Stauffer, 2003).

Sarna-Wojcicki (2003, written communication) examined the chemical results from the microprobe analyses and concluded that sample 99AL617-154 (Section #1) matches well with several samples from cores in Walker Lake with a similarity coefficient (SC) between 0.95 and 0.97, likely derived from a proto-Mono Craters source. In the Walker Lake cores, this tephra layer occurs in the interval between 60 and 80 m below the top of the cores, and corresponds to age estimates between approximately 80,000 and 60,000 years, based on the dating of these cores and sedimentation–rate estimates for Walker Lake (Sarna-Wojcicki, 2003, written communication). In the Mono Basin area, this proto-Mono Craters tephra layer is exposed on the north shore of Mono Lake and on Negit Island, where the layer is interbedded with tephra from a Mammoth Mountain source dated between 100,000 and 50,000 years (Sarna-Wojcicki, 2003, written communication).

Sample AL98-51A (Section #3) does not appear to match well with other known tephra, and comparisons indicate that the closest match with a borderline SC of 0.95 is to a tephra unit with no independent age control in southern Nevada. Of the tephra units with independent age control, the closest match, with a SC of about 0.92, is with a sample from an Owens Lake core where the layer is estimated to be approximately 75,000 years old (Sarna-Wojcicki, 2003, written communication).

Fig 6-2

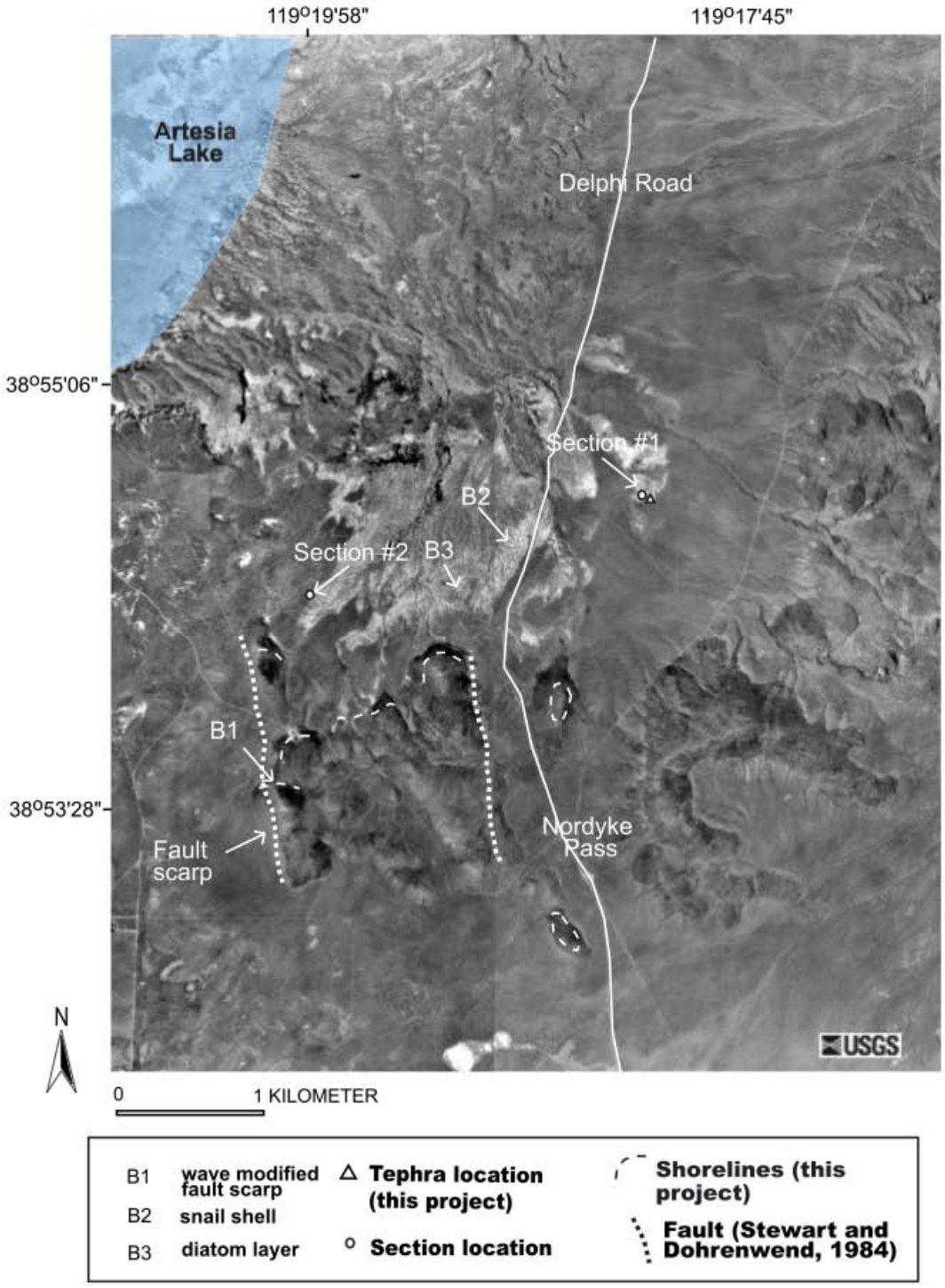

Figure 14. USGS Digital Orthophotoquad showing the Nordyke Pass area, downloaded from Microsoft TerraServer-USA, at http://www.terraserverusa.com/. Photo taken in 1994.

Fig 6-3

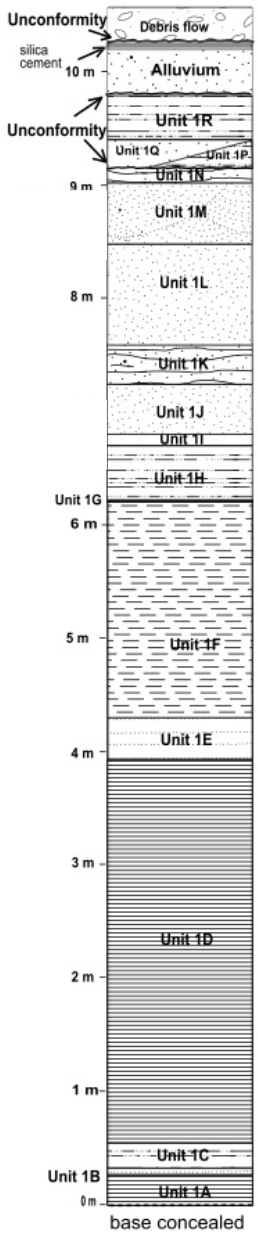

Debris flow yellowish brown to brownish yellow (10YR,5/8 near top; 10YR, 6/8, 6/6 rest of unit), poorly-sorted, ~25% gravel, boulders up to 1 m, base of unit is pinkish white/pinkish gray (7.5YR,8/2, 7/2), silica cement, less than 10% gravel

Alluvium coarse sand and silt, brownish yellow/yellow (10YR,6/6, 7/6), poorly-sorted, < 10% gravel, decreasing upsection, indurated,

Unit 1R silt and clay, pale yellow (2.5Y,7/3), <<5 % gravel, pedogenic carbonate nodules and veins

Unit 1Q sand, pale yellow/light yellowish brown, (2.5Y,7/4, 6/4), moderately sorted, pebble layer, less carbonate than Unit 1R

Unit 1P silt and sand, olive yellow, (2.5Y,6/6), poorly sorted

Unit 1N silt and fine sand, pale yellow, (2.5Y,7/4) moderately sorted, unlaminated, carbonized plants at base of unit, pedogenic carbonate

Unit 1M fine sand, pale yellow (2.5Y,8/3, 7/3) well-sorted, weakly cemented, 2 to 4 cm cross-lamination dipping towards lake center, lithics, quartz, mica, carbonized plants, top 10 cm coarser

Unit 1L silt with more fine sand than unit 1K, pale yellow (2.5Y,8/3, 7/3), possible burrows, carbonized and modern plant roots

Unit 1K silt with some fine sand, pale yellow (2.5Y,8/3,7/3)

Unit 1J fine sand, well-sorted, light gray (2.5Y 7/2), more fines upsection, modern and possible older plant roots and debris

Unit 1I silt and fine sand, light gray/pale yellow (2.5Y7/2, 7/3), subhorizontal lamination, carbonized plants

Unit 1H silt with possible reworked ash, pale yellow (2.5Y,7/3), fairly well consolidated, coarsens above 7.5 cm

Unit 1G tephra, wispy, thin, but continuous, white to gray, 1.5 cm thick

Unit 1F clay, tightly packed, horizontal lamination

Unit 1E sand, light yellowish brown (2.5Y,6/3, 6/4 (dry)), possible very faint cross-lamination,loose to moderately compacted

Unit 1D clayey silt, pale yellow, (2.5Y, 7/3 (dry)) no visible lamination, tightly compacted

Unit 1C silt, pale yellow (2.5Y,7/3 (dry)), faint thin, horizontal lamination, moderately sorted, loosely to moderately compacted

Unit 1B1 and Unit 1B2 two distinct layers of sand; fining upsection from lower layer 1B1(1.75 cm thick) medium to fine sand light gray (2.5Y,7/2 (dry)) to upper layer 1B2 (2.75 cm thick) fine sand, pale yellow (2.5Y, 7/4 (dry)), moderately to well-sorted, subrounded to rounded grains

Unit 1A silt and clay, light yellowish brown (2.5Y,6/4),faint lamination, well-sorted, moderately to tightly compacted, iron stained, mica, quartz, pyrite

Figure 18. Stratigraphy at Section #1 (Fig. 9). All colors from Munsell Color (1992) for moist sediment, unless otherwise specified.

Fig 6-4

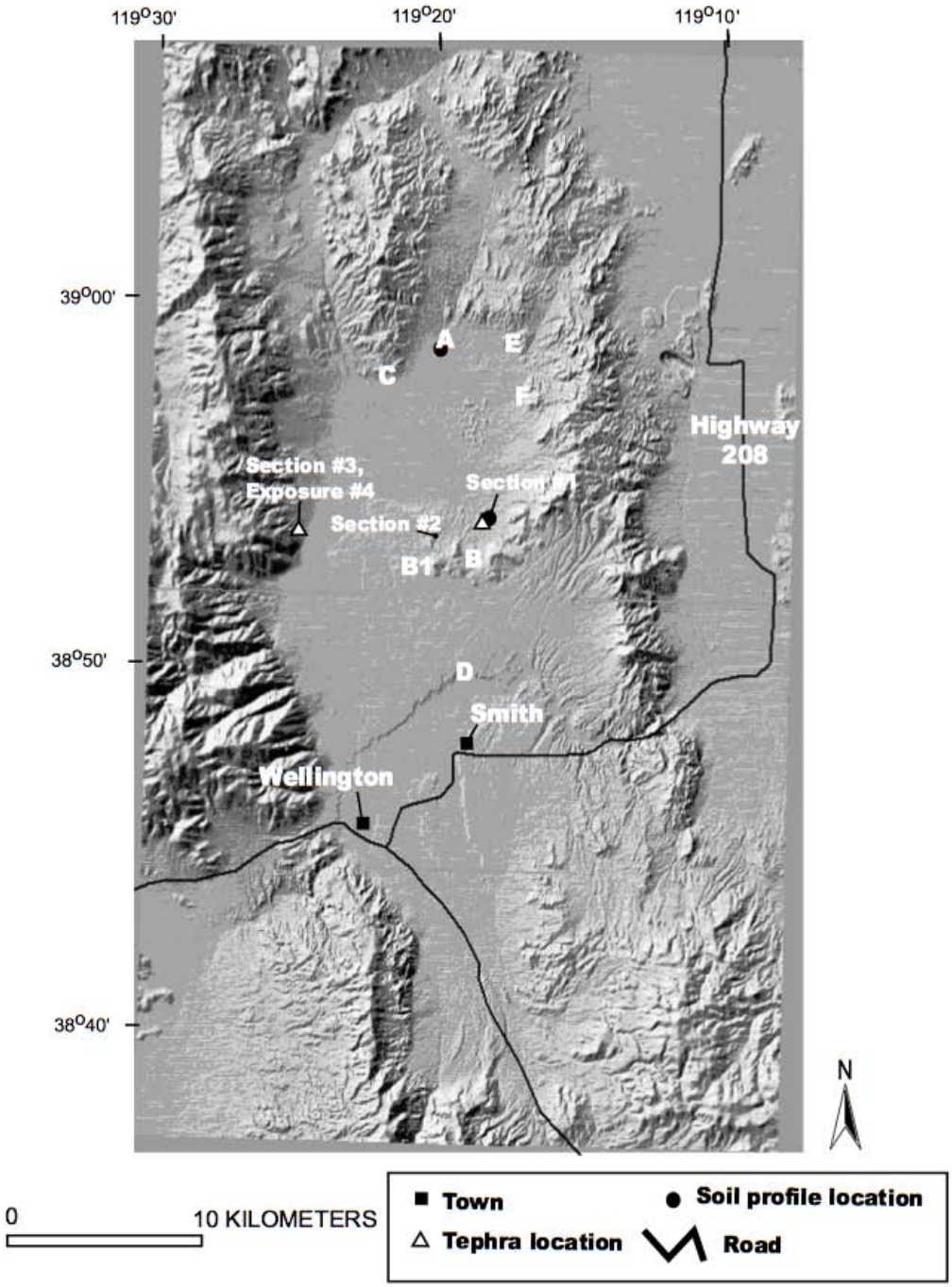

Figure 9. DEM shaded relief map showing localities studied in the course of this project.

Fig 6-5

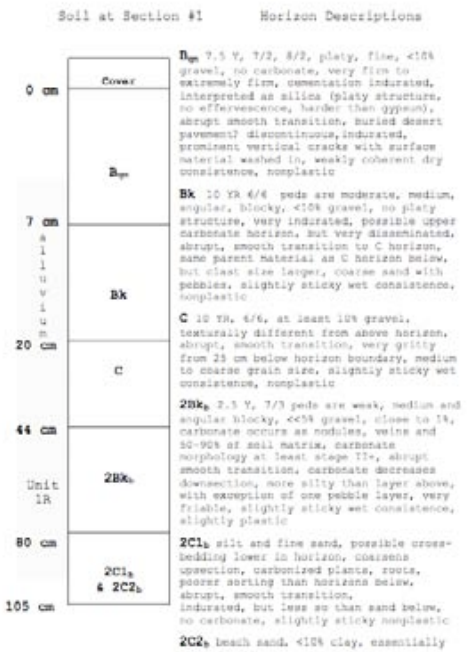
Soil at Section #1
Horizon Descriptions
0 cm
7 cm
20 cm
44 cm
80 cm
105 cm
Cover
Bqm
Bk
C
2Bkb
2C1b & 2C2b
alluvium
Unit 1R
Bqm 7.5 Y, 7/2, 8/2, platy, fine, <10% gravel, no carbonate, very firm to extremely firm, cementation indurated, interpreted as silica (platy structure, no effervescence, harder than gypsum), abrupt smooth transition, buried desert pavement? discontinuous, indurated, prominent vertical cracks with surface material washed in, weakly coherent dry consistence, nonplastic
Bk 10 YR 6/6 peds are moderate, medium, angular, blocky, <10% gravel, no platy structure, very indurated, possible upper carbonate horizon, but very disseminated, abrupt, smooth transition to C horizon, same parent material as C horizon below, but clast size larger, coarse sand with pebbles, slightly sticky wet consistence, nonplastic
C 10 YR, 6/6, at least 10% gravel, texturally different from above horizon, abrupt, smooth transition, very gritty from 25 cm below horizon boundary, medium to coarse grain size, slightly sticky wet consistence, nonplastic
2Bkb 7.5 Y, 7/3 peds are weak, medium and angular blocky, <<5% gravel, close to 1%, carbonate occurs as nodules, veins and 50-90% of soil matrix, carbonate morphology at least stage II+, abrupt smooth transition, carbonate decreases downsection, more silty than layer above, with exception of one pebble layer, very friable, slightly sticky wet consistence, slightly plastic
2C1b silt and fine sand, possible cross-bedding lower in horizon, coarsens upsection, carbonized plants, roots, poorer sorting than horizons below, abrupt, smooth transition, indurated, but less so than sand below, no carbonate, slightly sticky nonplastic
2C2b beach sand, <10% clay, essentially

Fig 6-6

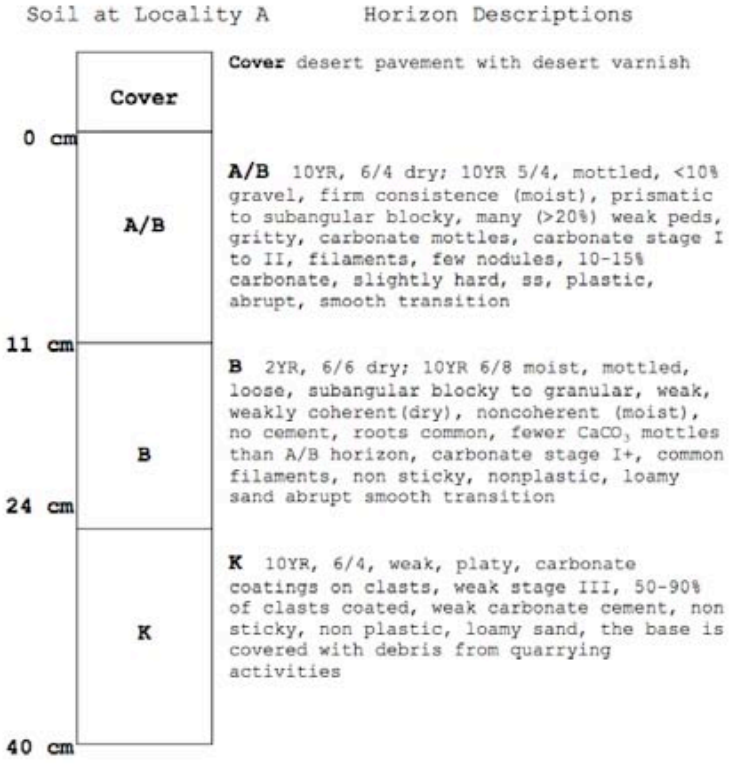
Soil at Locality A
Horizon Descriptions
0 cm
11 cm
24 cm
40 cm
Cover
A/B
B
K
Cover desert pavement with desert varnish
A/B 10YR, 6/4 dry; 10YR 5/4, mottled, <10% gravel, firm consistence (moist), prismatic to subangular blocky, many (>20%) weak peds, gritty, carbonate mottles, carbonate stage I to II, filaments, few nodules, 10-15% carbonate, slightly hard, ss, plastic, abrupt, smooth transition
B 2YR, 6/6 dry; 10YR 6/8 moist, mottled, loose, subangular blocky to granular, weak, weakly coherent(dry), noncoherent (moist), no cement, roots common, fewer CaCO3 mottles than A/B horizon, carbonate stage I+, common filaments, non sticky, nonplastic, loamy sand abrupt smooth transition
K 10YR, 6/4, weak, platy, carbonate coatings on clasts, weak stage III, 50-90% of clasts coated, weak carbonate cement, non sticky, non plastic, loamy sand, the base is covered with debris from quarrying activities

STOP 7- Artesia Road Fan, Smith Valley Nevada.

The location is shown in **Figure 6-1**, and briefly discussed in the preceding Stop 6 section by Heidi. Here you will have a chance to see the Tephra of which she speaks interbedded with lacustrine muds. The lacustrine deposits are in turn overlain by fan deposits. Both the lacustrine and fan deposits are cut by the rangebounding normal fault (**Figure 7-1 & 7-2**). Cosmogenic ages of 3 boulders on the oldest fan element range from about 25 to 50 ka. The fan deposits sit on the lacustrine deposits and are thus younger. The ages would thus most likely appear to place a minimum age on the deposits of Lake Wellington. As well, the fan surfaces are offset vertically 10 to 20 meters by the fault scarp cutting the deposit. Division of the numbers would place the vertical uplift rate somewhere in the range of 0.2 to 0.8 mm/yr. Of course, the reason we're here is to have a little discussion about the methods, assumptions, & uncertainties associated with the estimates, and we'll leave that till we're there.

Figure 7-1. Airphoto of Stop 7 - Artesia Road Fan. Photo: Wesnousky

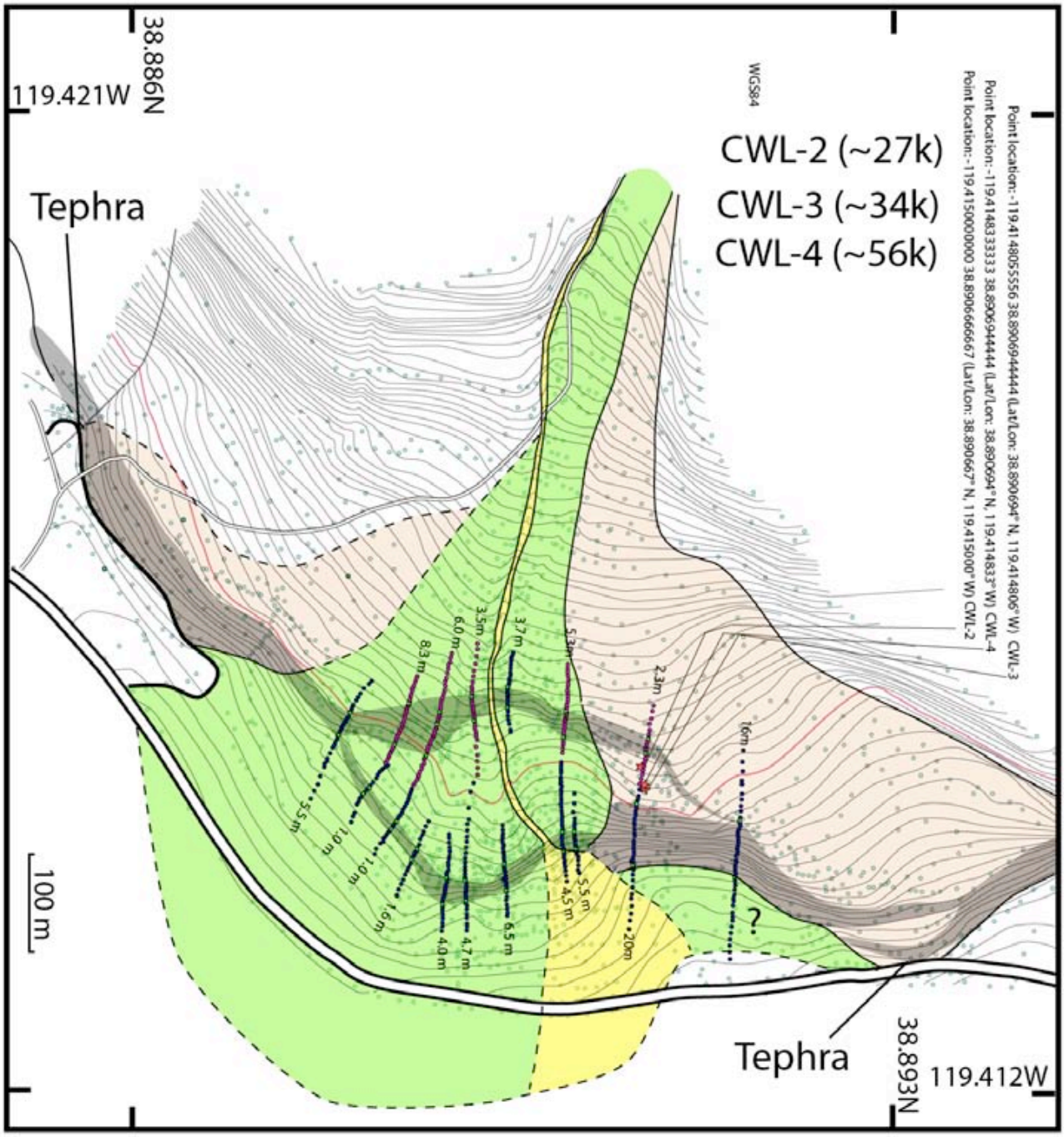

Figure 7-2. Quaternary surficial map of Artesia road fan on 2-m contour base. Red contour is 1477m. Though topo map constructed with GPS it was not referenced to a local benchmark, so absolute elevation may be off a few meters. Fault scarps are shaded. Vertical separations across scarps annotated for respective profiles. Yellow, Green, and Brown units are youngest to oldest fan units. Location of rocks sampled for cosmogenic analysis shown by red stars and annotations give waypoints of respective samples. Location of Tephra discussed by Heidi came from upper left sample locality on edge of gravel pit. The same tephra may also be observed in road cut at lower right of map. Map: Wesnousky

Figure 7-3. Satellite image of map area in Photo -2 extracted from Google Earth.

Day 3 - Sept 19 - Sunday - The Path to be taken...

The tough part about Day 3 is getting up. But assuming you do, we'll head down to the south end of Smith Valley and the outlet of Lake Wellington to look at what appear to be beach gravel deposits and discuss just why Lake Wellington happened. Then you'll haver the opportunity to head north up to Carson City and have Jim Brune show you some precarious rocks that are of quite some interest to those wanting to cite high-level radioactive waste repositories and facilities in our country.

From Camp 3, we'll make it down to stop 8

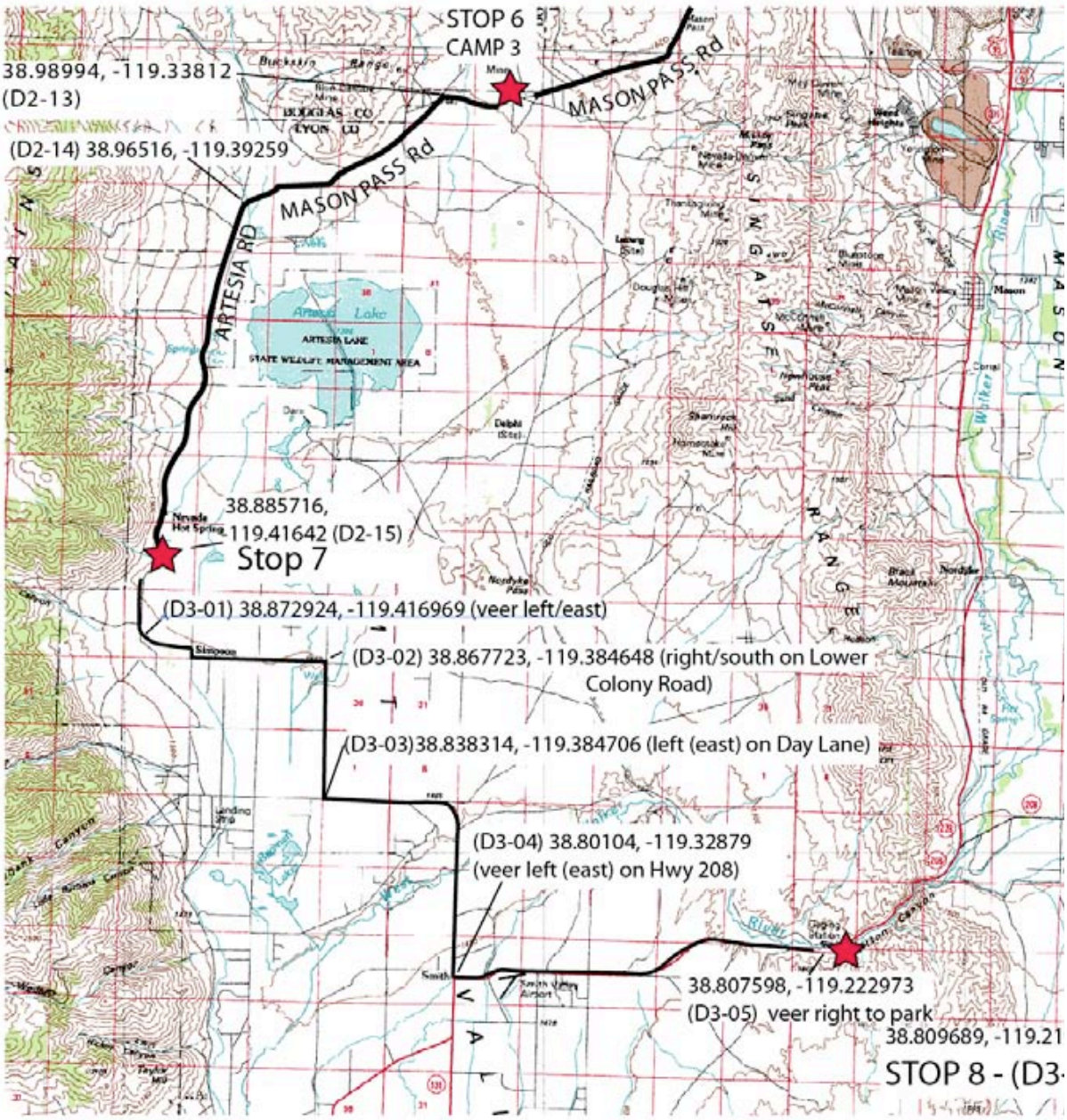

After Stop 8, this is the path...

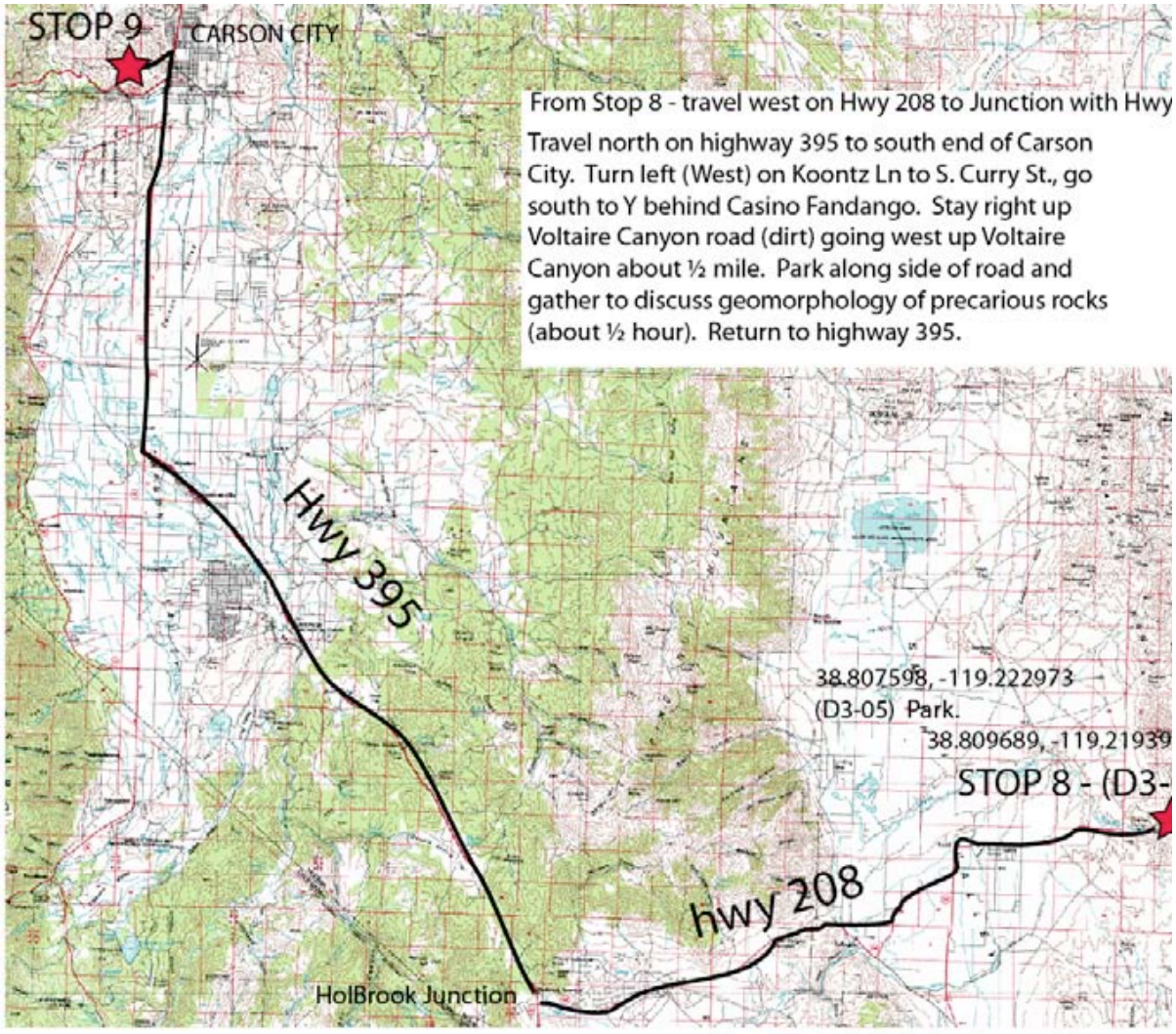

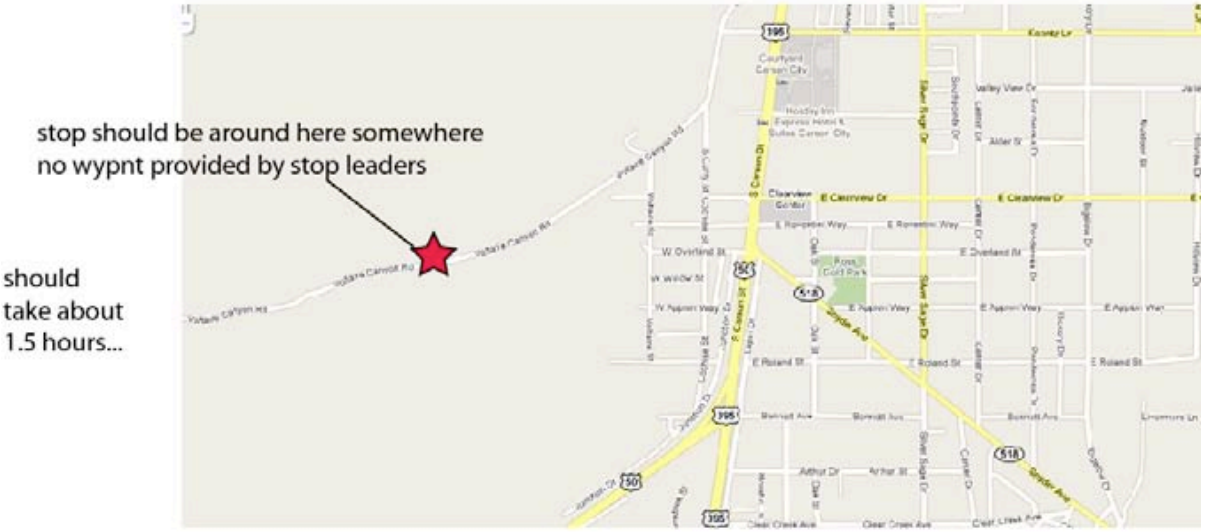

STOP 8 - outlet and genesis of Lake Wellington...

Stop 8 is at the mouth of Wilson Canyon where the Walker River exits Smith Valley (**Figure 8-1**). We'll park in a lot along the road behind that ridge in the Figure, and then take a little stroll up to that cut terrace with rounded gravels. Funny thing, each the terrace with rounded gravel, the cemented 'beach rock' and the horizontal surface with rounded gravel labeled in the Figure sit at the about same elevation of ~1480m.

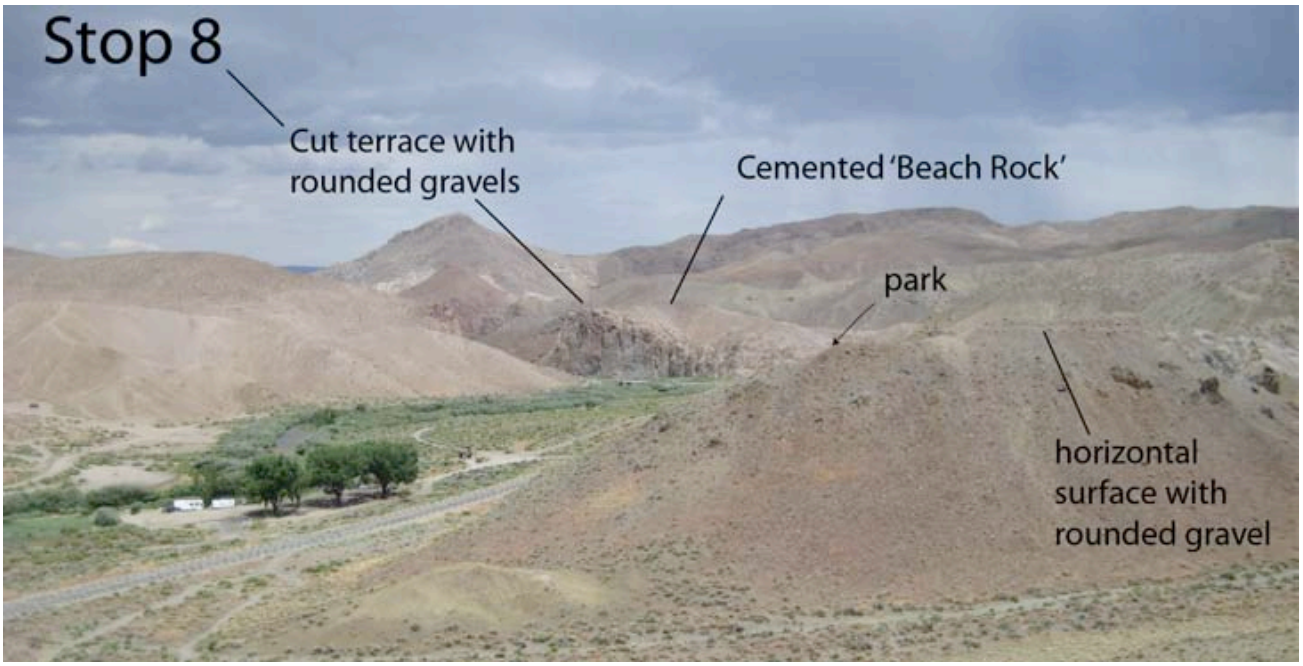

Figure 8-1 (top) . Stop 8. View eastward toward Wilson Canyon.

Figure 8-2 (bottom) Figure 8-2. Carbonate cemented rounded gravels ('Beach Rock') found in and around the entrance to Wilson Canyon are identical to those commonly seen around the edge of Lake Lahontan and other pluvial lakes in the Great Basin which are commonly attributed to wave action at the edge of alkaline lakes..

After hiking up to the terrace with rounded gravel at Stop 8 (**Figure 8-1**), we'll look to the west (Figure 8-3) and then to the east (Figure 8-4). The view west shows a band of rounded gravels along the hills edges, the base of which is at about ~1480 m and commonly shows beach rock like that in Figure 8-2.

The zone of rounded gravel on the far slope in **Figure 8-3** seems for the most part horizontal and contains 'beach rock' at it's base. The elevation of the beach rock is at about the same elevation as the terraces cut into bedrock in both the foreground and distance of **Figure 8-4**. The elevations of the 'beach rock' are at about the same elevation as reported for the highstand of Lake Wellington (1477m).Taken together, the observations would seem to suggest that the features are the result of a relatively long-lived body of water which was Lake Wellington. It's a thought anyway. And if not, there's something else funny going on....

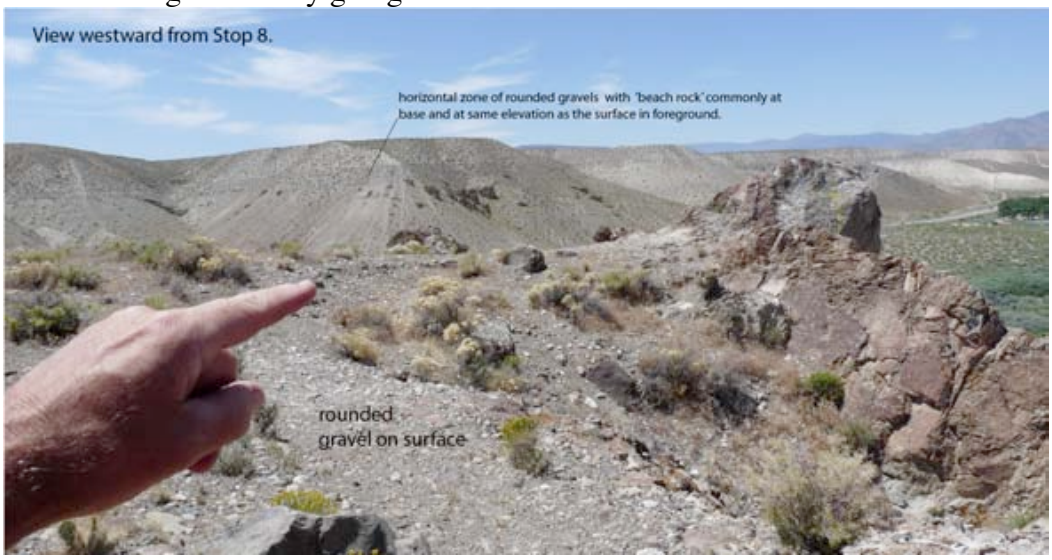

Figure 8-3 (top) Figure 8-4 (bottom).

Near the east end of Wilson Canyon rounded boulder gravel may also be observed perched on a bedrock terrace up the canyon wall (I've yet to go up there) (Figure 8-5). This and the prior

observations contained in Figures 8-1 thru 8-4 lead me to think that any blockage of the canyon to dam the waters of Lake Wellington in Smith Valley must have occurred between the last ridge of Wilson Canyon and the rounded boulder gravel shown in Figure 8-5&6. It would seem a landslide would be the most likely candidate (Figure 8-7). If so, Lake Wellington perhaps should not be attributed to changes in climate, as is generally interpreted for most pluvial lakes of Nevada.

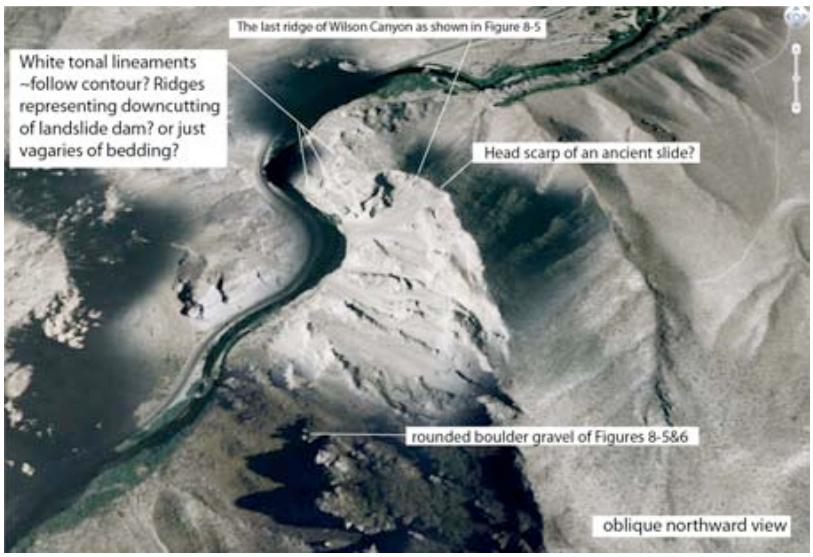

DISCLAIMER: if someone has already made these observations and interpretations, or put forth contradictory interpretations, I apologize for not citing the work. What can I say, it's been more fun puzzling about the lake rather than reading papers, and I thought you might like it too.

Figure 8-5. (upper) Eastward view to last ridge in Wilson Canyon before Walker exits to Mason Valley. Small bedrock terrace on cliff outlined by white circle.

Figure 8-6. (middle) Zoom photo of rounded boulders on small bedrock cliff outlined by white circle in Figure 8-5.

Figure 8-7. (lower) Oblique view (north is up) of east end of Wilson Canyon from Google Earth. The escarpment associated with the last ridge of Wilson Canyon sure looks similar to a lot of landslide headscarps I have seen. Perhaps it was a great landslide at this site that blocked Wilson Canyon and produced Lake Wellington. (Walker River flow is from lower left to upper right in this view).

STOP 8 - Steve Ward, UCSC.

Steve has been using computer modeling to conduct forensic studies of past tsunamis and floods. I asked him if he would take a quick look at Lake Wellington and address a few questions. He made a little model and the comments below are the result of that.

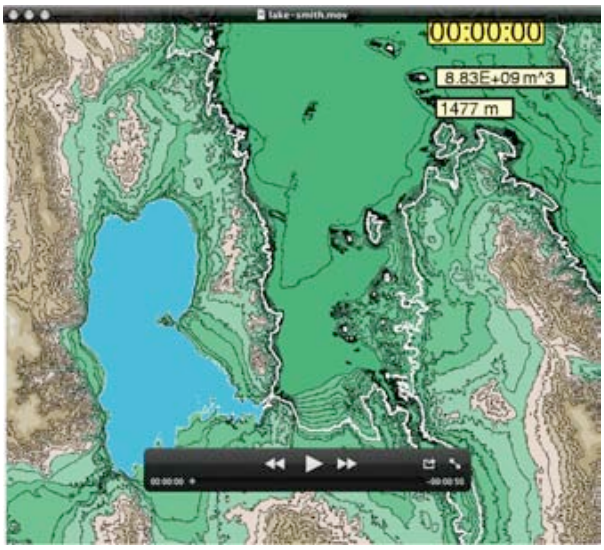

The questions posed to Steve were; Given the West Walker River was dammed to a level of 1477m with todays given topography,

How long would it take to fill up?

Assuming 300 cfs, the average over the last 50 or 60 years or so, it would take about 33 years. Of course, it might have been different back then - but this gives an idea.

How much water was in the Lake?

Given the original lake stood at 1477 m, the canyon was blocked by a dam 77 m high, 225 meters across at the top, and 45 m wide at the bottom, the starting volume of the lake would be 8.8 cubic km.

How long would it take to empty assuming a catastrophic break of the dam?

The simulation shows about 50% of the lake volume drains in the first 7 hours, 75% in 15 hours, 90% in 33 hours, 95% in 70 hours.

During the first 7 hours, The flow rate of 174,000 m^3/s.

For comparison, the nominal rate for Niagara Falls is 2800 m^3/s. So we have 62 times Niagara Falls for 7 hours.

Of course, if the downcutting was gradual, the rates would be less. In that boulders of only about 1 to 1.5 m max are found at the outlet, it seems things are pointing to a less catastrophic ending of the Lake.

Details: This particular basin has a dividing ridge at 1455 m where the north basin becomes cut off from the river to the south. The north basin holds about ½ the lake water. This sim assumes that a channel gets cut so that the northern basin continues to drain. We can change this and isolate the water in the northern basin. Water in southern basin would drain even faster in that case

THIS SIMULATION MAY BE DOWNLOADED FROM STEVE'S HOMEPAGE AT UCSC (ALONG WITH MANY OTHERS) AND A COPY IS PLACED ON THE FOP WEBSITE.

STOP 9 - Jim Brune , Seismo Lab, UNR

Constraints on Ground Accelerations Associated with Normal Faults Provided by Precariously Balanced Rocks

Jim Brune

Introduction

Expanding population centers in extensional regions of the intermountain western United States are exposed to ground shaking from normal faults, *e.g*., Salt Lake City, Utah, Reno, Nevada, and Carson City, Nevada. There are essentially no near-source rock-site strong motion recordings for large earthquakes in this region (none for near-fault rock sites on the hanging-wall of normal faults), and thus hazard maps like the recent USGS-CDMG PSHA maps assume attenuation curves based on data primarily from compressional strike-slip and thrust faulting earthquakes.

Recent evidence from physical and numerical models has indicated that ground motions from normal faults may be much lower than for strike-slip faults with a large fault-normal tectonic stress component. Data from trans-pressional strike-slip earthquakes and thrust faults dominate in the determination of regression curves for ground motions used in the USGS-CDMG PSHA maps. Thus regressions and seismic hazard maps using the current database may severely overestimate the near-fault ground motion for many extensional locations.

One of the main physical reasons for expecting low accelerations for normal faults is the fact that the fault normal component of fault stress must approach zero near the surface since the lithostatic stress approaches zero and the tectonic stress is extensional (Brune and Anooshehpoor, 1998; McGarr *et al*., 2000). As a result, relatively little elastic strain energy can be stored at shallow depth near the fault trace. Preliminary evidence from reconnaissance surveys of precariously balanced rocks provides support for such low ground accelerations. Here describe rocks on the hanging wall of the Genoa fault. where an M~7 earthquake occurred less than ~ 600 years ago on the Genoa fault (Ramelli *et al*., 1999*)*.

Precarious Rocks on the Hanging Wall of the Genoa Fault, Source of an M~7 Earthquake about 600 Years BP

The Genoa fault scarp is one of the most impressive in the western United States and has been documented in numerous studies. The most comprehensive study is the study of Ramelli *et al*. (1999). Four trenches have been placed across the fault and adjacent strands (A-D, Fig. 1), documenting the date of the most recent event as less than~600 years bp. This date is consistent with the very fresh appearance of the fault. Displacements observed from the most recent earthquake in the trenches ranged from 4-6 m, consistent with a very large event. The penultimate (preceding) event has been documented at ~ 2000-2500 years bp. Ramelli *et al*. (1999) demonstrated that scarp profiles on the southern part of the Genoa fault are consistent with two such Holocene ruptures, along with two earlier events (late and earlier Tioga in age).

The Carson Valley is a typical alluvial basin in the Basin and Range except for one factor: a major river (the Carson River), fed by precipitation in the Sierra Nevada, drains the Carson Valley. The action of the Carson River has prevented the accumulation of a sedimentary basin as thick as typical of other basins bounded by similarly active faults. As a result, basement rocks are exposed much closer to the fault on the hanging wall side, resulting in a unique opportunity to use precarious rocks on the hanging wall of a major normal fault. Useful precarious rocks have been found at 5 sites on the hanging wall of the Genoa fault (sites 1-5, Fig. 1). Photographs of rocks at these sites are shown in Fig. 2. Brune (2000) presented photographs of precarious rocks on the footwall of the Carson City fault, a branch of the Genoa fault (site 2 in Fig. 1). Rocks at sites 1 and 2 in Fig. 1, besides being on the footwall of the Carson segment of the Genoa fault zone, are also on the hanging wall of the Jacks Valley segment of the Genoa fault, which experienced about 5.8 m slip

in the 600 bp event (trench C in Fig. 1, Ramelli, *et al*., 1999). Thus sites 1 and 2 provide constraints for solid rock hanging wall ground motions for a large normal faulting earthquake with almost 6 m of slip at a distance of about 5 km. Precarious rocks at site 3 provide ground motion constraints at about 10 km from the main fault trace. Sites 4 and 5 provide constraints at a distance of about 7 and 4 km, respectively. The rocks at these sites will eventually provide important and unique sources of data for 2 large normal faulting earthquakes (and possibly as many as 2 additional events, since the rocks appear to be as much as 10,000 years old. There is a gap in precarious rock sites along the central portion of the Genoa fault (Fig. 1). The width of the sedimentary basin precludes the formation of precarious rocks within ~ 20 km of this segment of the fault

Synthesis of Preliminary Ground Motion Constraints on Normal Faults

Preliminary data from both footwall (Brune, 2000) and hanging wall of major normal fault earthquakes (Carson Valley reconnaissance data) are shown in Fig. 3. The ground motions predicted for M=7.5 (solid lines) and M=7.0 (dashed lines) earthquakes, based on the work of Spudich *et al*. (1999) (red curves) and those of the NGA model of Abrahamson (2005) (blue curves) for normal faults are shown for comparative purposes

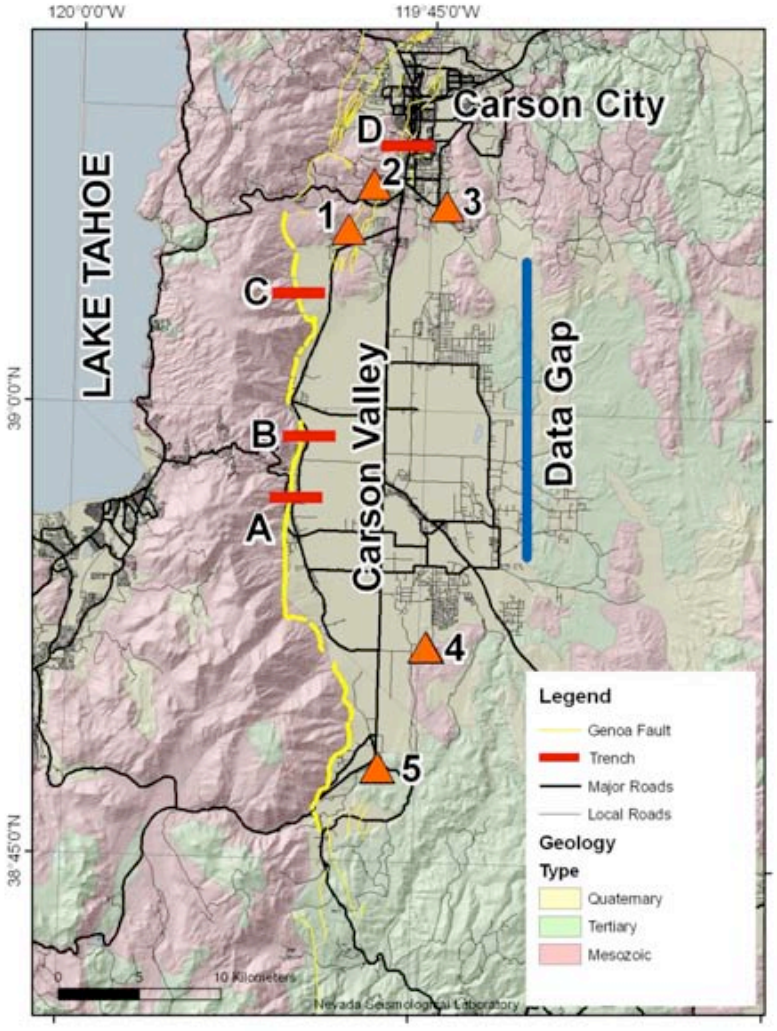

Figure 1: Map of Carson Valley highlighting the locations of the Genoa fault (yellow lineation), precarious rock sites (orange symbols), trench sites from Ramelli *et al*. (1999) (red symbols), and the age of the geologic units. Notice that no precarious rocks exist in the region termed "data gap" due to the widening nature of the valley in this region. Precarious rocks may exist on Mesozoic outcrops at further distances from the center of the fault, though.

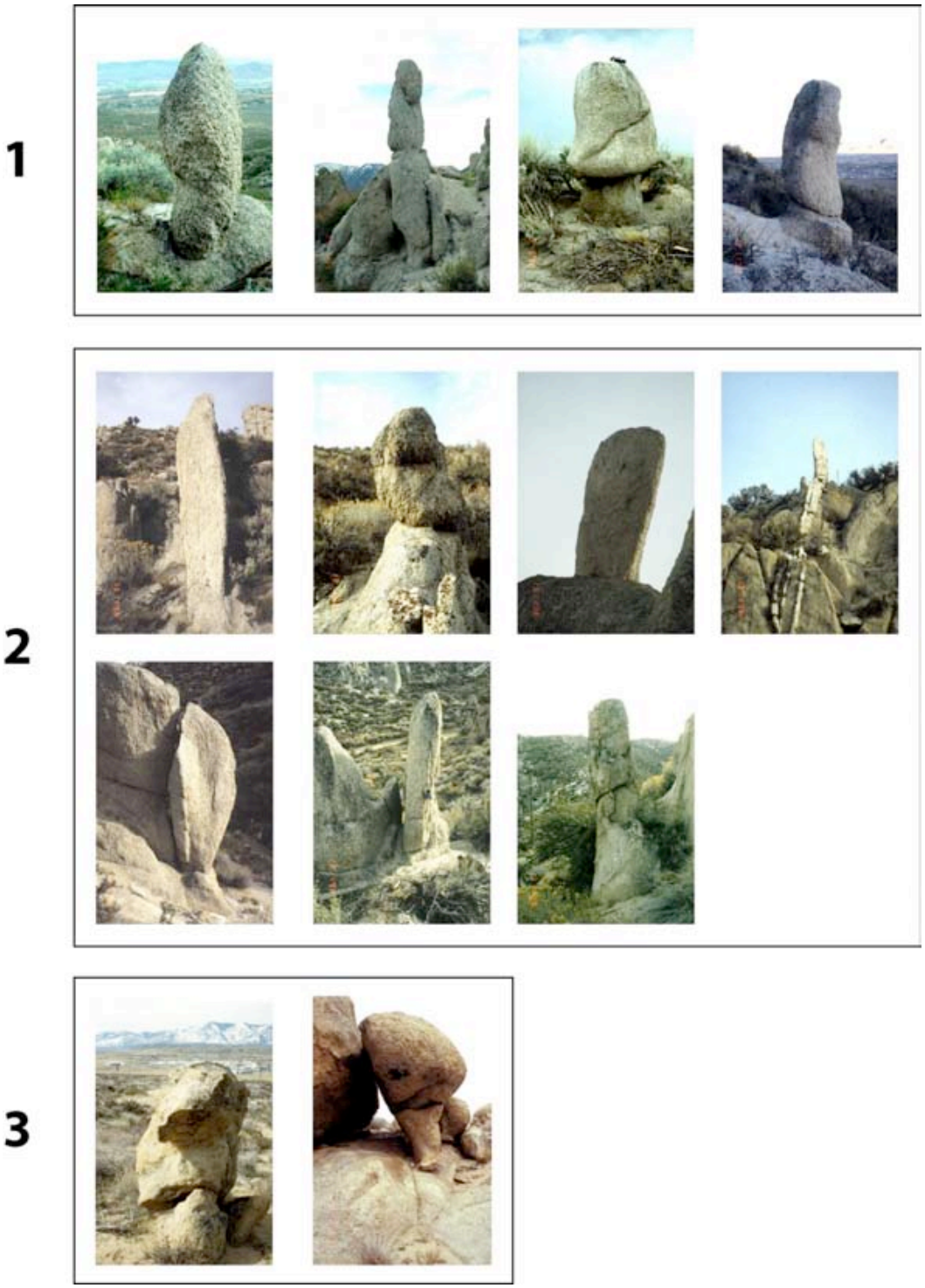

Figure 2: Precarious rocks found on the hanging wall of the Genoa fault. Numbers 1-3 to the left of each box correspond to the same numbers on the map in figure 1.

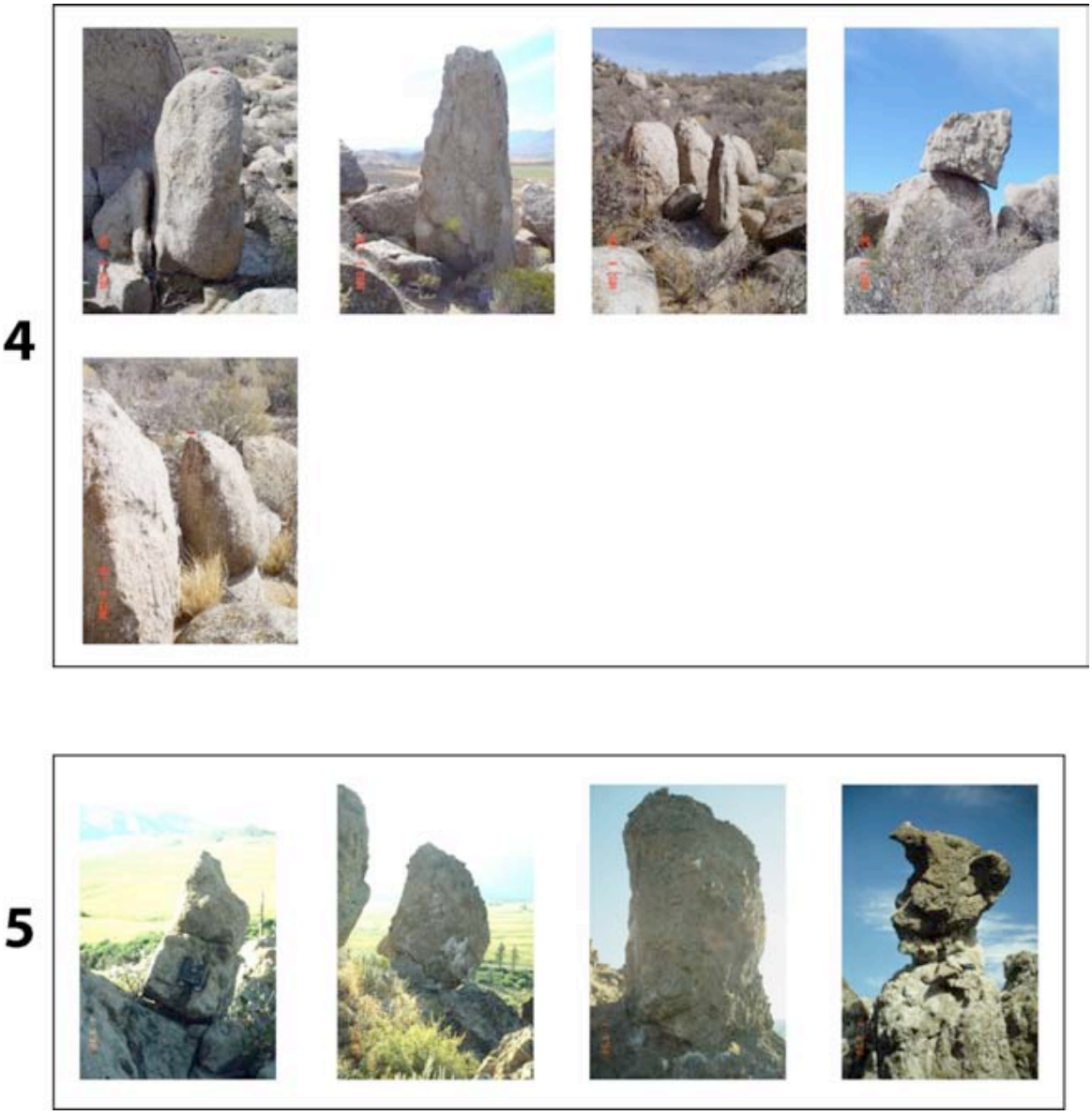

Figure 2-cont.: Precarious rocks found on the hanging wall of the Genoa fault. Numbers 4 and 5 to the left of each box correspond to the same numbers on the map in figure 1.